

AD\_\_

GRANT NUMBER DAMD17-98-1-8176

TITLE: Computer Simulation of Breast Cancer Screening

PRINCIPAL INVESTIGATOR: John M. Boone, Ph.D.

CONTRACTING ORGANIZATION: University of California  
Davis, California 95616

REPORT DATE: July 1999

TYPE OF REPORT: Annual

PREPARED FOR:

U.S. Army Medical Research and Materiel Command  
Fort Detrick, Maryland 21702-5012

DISTRIBUTION STATEMENT: Approved for Public Release;  
Distribution Unlimited

The views, opinions and/or findings contained in this report are those of the author(s) and should not be construed as an official Department of the Army position, policy or decision unless so designated by other documentation.

DTIC QUALITY INSPECTED 4

20001019 065

# REPORT DOCUMENTATION PAGE

*Form Approved*  
OMB No. 0704-0188

Public reporting burden for this collection of information is estimated to average 1 hour per response, including the time for reviewing instructions, searching existing data sources, gathering and maintaining the data needed, and completing and reviewing the collection of information. Send comments regarding this burden estimate or any other aspect of this collection of information, including suggestions for reducing this burden, to Washington Headquarters Services, Directorate for Information Operations and Reports, 1215 Jefferson Davis Highway, Suite 1204, Arlington, VA 22202-4302, and to the Office of Management and Budget, Paperwork Reduction Project (0704-0188), Washington, DC 20503.

|   |   |   |  |
|---|---|---|--|
| 1. AGENCY USE ONLY <i>(Leave blank)</i>   | 2. REPORT DATE<br>July 1999                                 | 3. REPORT TYPE AND DATES COVERED<br>Annual (1 Jul 98 - 30 Jun 99) |  |
| 4. TITLE AND SUBTITLE<br>Computer Simulation of Breast Cancer Screening   |   | 5. FUNDING NUMBERS<br>DAMD17-98-1-8176                            |  |
| 6. AUTHOR(S)<br>John M. Boone, Ph.D.  |   |   |  |
| 7. PERFORMING ORGANIZATION NAME(S) AND ADDRESS(ES)<br>University of California<br>Davis, California 95616<br><br>E*Mail: jmboone@ucdavis.edu  |   | 8. PERFORMING ORGANIZATION<br>REPORT NUMBER                       |  |
| 9. SPONSORING / MONITORING AGENCY NAME(S) AND ADDRESS(ES)<br>U.S. Army Medical Research and Materiel Command<br>Fort Detrick, Maryland 21702-5012   |   | 10. SPONSORING / MONITORING<br>AGENCY REPORT NUMBER               |  |
| 11. SUPPLEMENTARY NOTES   |   |   |  |
| 12a. DISTRIBUTION / AVAILABILITY STATEMENT<br>Approved for Public Release; Distribution Unlimited   |   | 12b. DISTRIBUTION CODE  |  |
| 13. ABSTRACT <i>(Maximum 200 words)</i><br><br>Breast cancer will affect approximately 12.5% of the women in the United States, and currently mammographic screening is considered the best way to reduce mortality from this disease through early detection. There is much controversy concerning the most appropriate screening parameters such as starting age, the screening interval, and the stopping age. Long term multi-center clinical trials are the traditional approach to evaluating the efficacy of a medical test such as mammography, however clinical trials are expensive and lengthy. This grant focuses on the use of computer simulation techniques for evaluating the screening efficacy of mammography. Breast cancer growth rates, incidence rates, multiracial population demographics, death rates, breast cancer prognosis factors, breast density considerations, detection versus diameter probabilities, and other pertinent data have been computer fit and incorporated into a breast cancer screening simulator. The simulator is capable of producing many types of results data, including survival curves, tumor size distributions at detection, and "years of life saved" statistics. We are currently in the process of validating the simulator output with the results from respected clinical trials. Once validated, the screening simulator will be useful for studying ways in which the timing of the mammography examination can be optimized. |   |   |  |
| 14. SUBJECT TERMS<br>Breast Cancer  |   | 15. NUMBER OF PAGES<br>78   |  |
|   |   | 16. PRICE CODE  |  |
| 17. SECURITY CLASSIFICATION<br>OF REPORT<br>Unclassified  | 18. SECURITY CLASSIFICATION<br>OF THIS PAGE<br>Unclassified | 19. SECURITY CLASSIFICATION<br>OF ABSTRACT<br>Unclassified        | 20. LIMITATION OF<br>ABSTRACT<br>Unlimited |

FOREWORD

Opinions, interpretations, conclusions and recommendations are those of the author and are not necessarily endorsed by the U.S. Army.

\_\_\_\_ Where copyrighted material is quoted, permission has been obtained to use such material.

\_\_\_\_ Where material from documents designated for limited distribution is quoted, permission has been obtained to use the material.

\_\_\_\_ Citations of commercial organizations and trade names in this report do not constitute an official Department of Army endorsement or approval of the products or services of these organizations.

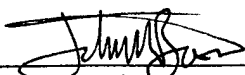
NA In conducting research using animals, the investigator(s) adhered to the "Guide for the Care and Use of Laboratory Animals," prepared by the Committee on Care and use of Laboratory Animals of the Institute of Laboratory Resources, national Research Council (NIH Publication No. 86-23, Revised 1985).

NA For the protection of human subjects, the investigator(s) adhered to policies of applicable Federal Law 45 CFR 46.

NA In conducting research utilizing recombinant DNA technology, the investigator(s) adhered to current guidelines promulgated by the National Institutes of Health.

NA In the conduct of research utilizing recombinant DNA, the investigator(s) adhered to the NIH Guidelines for Research Involving Recombinant DNA Molecules.

NA In the conduct of research involving hazardous organisms, the investigator(s) adhered to the CDC-NIH Guide for Biosafety in Microbiological and Biomedical Laboratories.

  
PI - Signature

AUG 10, 1999

Date

# Table of Contents

DAMD17-98-8176

---

---

## Computer Simulation of Breast Cancer Screening

---

---

| <b>Contents</b>                   | <b>Page</b> |
|-----------------------------------|-------------|
| Report Documentation Form .....   | 1           |
| Foreword.....                     | 2           |
| Table of Contents .....           | 3           |
| Introduction.....                 | 4           |
| Body.....                         | 5           |
| Statement of Work Tasks           |             |
| SOW Task 5.....                   | 5           |
| SOW Task 1.....                   | 7           |
| SOW Task 2.....                   | 8           |
| SOW Task 3.....                   | 11          |
| SOW Task 4.....                   | 12          |
| SOW Task 6.....                   | 12          |
| SOW Task 7.....                   | 12          |
| Key Research Accomplishments..... | 15          |
| Reportable Outcomes.....          | 16          |
| Conclusions.....                  | 17          |
| References.....                   | 18          |
| Figure Captions.....              | 20          |
| Figures.....                      | 27-76       |

## INTRODUCTION

Breast cancer is a devastating disease which will affect one out of every eight women. Although important initial steps towards understanding the molecular biology of breast cancer have been made, a cure is not in sight. It is recognized that the medical prognosis of breast cancer is very much related to the size and stage at which breast cancer is discovered, with better prognosis occurring for breast carcinomas discovered earlier. Consequently, the early detection of breast cancer is a very important aspect towards improving the prognosis of the individuals stricken with the disease.

The early detection strategies for breast cancer include principally mammography and breast self examination. While self examination is economical and is available and important for all women to practice, the smallest palpable lesion that can be found with breast self examination is approximately 10 mm, and the average lesion diameter at detection with BSE is much larger (>20 mm). Mammography has been found to have much greater sensitivity, with routine identification of lesions as small as 2 to 3 mm, and with average detection of lesions of about 11 mm in diameter.

The efficacy of medical screening techniques is traditionally measured using clinical trials. Clinical mammography trials are very expensive, and can focus on only very narrow issues, since the scale (cohort sizes) and cost increase with the number of permutations studied. Clinical trials have been used to measure the effectiveness of mammography, however controversy has ensued concerning certain studies. For example, the Canadian study was criticized<sup>1,2</sup> for employing older mammography technology in its early years, with claims that the results were tainted as a result. Unfortunately, mammography is again about to face a huge change in technology in the next few years, once the digital mammography systems currently facing FDA clearance make it into the clinical screening environment.

The approach being studied in this project is the use of computer simulation techniques to simulate many aspects of a clinical trial. The benefit of this approach is that many factors which affect the clinical trial outcomes can be studied simultaneously. Being only software, the costs of computer simulation are very modest compared to more conventional approaches. Furthermore, much is known about the development of breast cancer, but this knowledge is spread around the literature in different fields – the growth rate of breast cancer, the effectiveness of breast self examination, the population distribution, the death rate, etc. – most of the data necessary for building a breast cancer screening simulator is available in the literature. In this project, we utilize and build upon what is available in the breast cancer literature, with the intention of studying which parameters have the most influence on improving the efficacy of breast cancer screening. While many of the components of the screening simulation model are being built from our own research on mammographic imaging, much of the data are incorporated into the simulation model by computer-fitting published data.

It is hoped that once completed, and after careful and thorough validation, that the breast cancer screening model will help in the optimization of breast cancer screening, by suggesting better timing regimes, custom-tailored to the characteristics specific to each woman in the screening population.

## **BODY**

Most aspects of the breast cancer screening model have been developed in this first year of the grant at least in a preliminary sense, touching on all of the tasks in the Statement of Work (SOW). The following discussion will proceed in the most logical order, which is not necessarily the order of the eight tasks as indicated in the SOW. Therefore, the SOW Task numbers will not be in numerical order.

### ***SOW TASK 5:***

Demographic data concerning the age distribution of women in the US is a key input to the breast cancer screening model. Figure 1 illustrates the US female population projected to July 1, 2000. The distribution of white, black, Asian, and American Indian women is as indicated in the figure. These high-resolution (1-year intervals) population data were downloaded from the US Census Bureau. The age at which breast cancer screening should start is one of the most contentious aspects of breast cancer screening. The debate<sup>3</sup> generally is involved with whether breast cancer screening should start at age 50 or at age 40. One of the reasons why there is so much controversy over this is that the starting age has a profound effect on the number of women to be screened. Figure 2 illustrates the US total female population, and the baby boom is clearly seen as the bump between approximately ages 30 and 54. If screening commences at age 50, then 41.7 million women will need to be screened (assuming no end-of-screening age is set). If screening were to begin at age 40, an additional 23.3 million women would need to be screened, increasing the screening population by 56%. This large increase in the number of women screened of course has a profound economic impact: for insurance payers (including medicare), it represents a large increase in screening costs. For radiologists, clinics, and hospitals, however, screening these women represents an additional source of revenue.

Breast cancer screening seeks to identify women with breast cancer, but breast cancer is in competition with other diseases and occurrences as a potential cause of death for each woman. Consequently, it is necessary to include in the screening model the female death rate, excluding breast cancer as a cause. Figure 3 illustrates the high resolution death statistics available from the US census bureau. This raw data (Figure 3) shows the data for all causes of death, including breast cancer. Other data (not shown) from the National Cancer Institute's SEER (Surveillance, Epidemiology, and End Results) program does provide death rate statistics for all causes excluding breast cancer, but at lower resolution (5 year intervals instead of 1 year intervals). The SEER data also provides the lower resolution death rate from all causes. The ratio of the SEER death rates (excluding and including breast cancer) was calculated, and the 5 year interval data was computer fit using commercially available software (TableCurve 2D, Jandel Scientific, Corta Madera, CA). This computer-generated function modifies the death rate from all causes to the death rate excluding breast cancer. It was used to modify (by multiplication) the high resolution death rate statistics shown in Figure 3, such that they are representative of

death rates by all causes *except* breast cancer. It is necessary to point out that in the screening model, our goal is to identify all women with breast cancer by screening (or competing methods), and those women as identified with breast cancer then represent a separate and unique cohort. Women who do not have breast cancer will face the probability of dying only from non-breast cancer causes (using the death rate statistics corrected to exclude breast cancer as a cause of death). Women who we have identified using the computer model as having breast cancer (whether detected yet or not) not only face death by non-breast cancer causes (as the rest of the population), but also face the additional probability of dying from breast cancer. This latter probability is affected by breast cancer prognosis, which in turn is affected by the current therapies used for treating breast cancer. The issue of prognosis will be discussed later.

The incidence of breast cancer for all races (combined) is shown in Figure 4, and the corresponding figures for white and black women are shown in Figures 5 and 6, respectively. These figures show the raw data (stars, the individual data points), and the computer fit to the data. Because of the multiple bumps in the incidence versus age profile, it was necessary to use multiple fitting functions to each curve to achieve the desired accuracy. Different analytical fits were performed over three age ranges (0-20, 20-68, 68-100), and a hybrid fit function was produced. Incidence data is available for the white and black populations, but not for the Asian or American Indian populations. For these latter two groups, the incidence from the total population (Figure 4) was used, whereas white and black women in the screening model were evaluated using the race-specific incidence data. As above with the death rate statistics, we are interested in the breast cancer incidence amongst women with no-prior breast cancers, and thus the incidence rates used are for breast cancer-free women. The raw data was available from SEER. Incidence refers to the number of women (in this case at a specific age) who are discovered to have breast cancer, but the average size of a breast cancer lesion at detection today is about 11 mm. Obviously, such a lesion has been growing for some period of time. The data of Spratt<sup>4-7</sup> were used to correct the incidence at the time of detection back to the time at which the breast cancer lesion was 2.1 mm. The data of Spratt give the tumor sojourn time for different age groups of women, and the sojourn time was calculated to be the time during which the breast tumor grew from 2.1 mm to 11 mm. Because younger women generally experience more aggressively growing tumors, the sojourn time is shorter for younger women. This data was computer fit, and used to correct the incidence data seen on Figures 4, 5 and 6 to reflect the incidence when women have a 2.1 mm lesion (not a 11 mm lesion). This effectively shifts the incidence curves to the left (back in time) by several years.

A stochastic model was built which draws from the demographic data shown in Figure 1, uses the death rate statistics shown in Figure 3, and applies the cancer incidence data shown in Figures 4, 5 and 6. This model generates a database of women, the size of which is specified by the user. Our model assumes that all women die at age 100, as women over that age number relatively few and their overall influence in the assessment of the breast cancer screening issue is negligible. For the statistics generated in this report, we used database sizes running from 100,000 women to 1,000,000 women. All

rates indicated on Figure 1 were modeled. This model predicts that 1 in 8 women will face breast cancer in her life, similar to the reports of other epidemiological studies.

### ***SOW Task 1***

More than 1000 mammograms from the breast screening clinic at UC Davis were digitized using a high resolution laser digitizer, and were sub-sampled by averaging to smaller, more manageable spatial resolutions (250  $\mu\text{m}$  pixels). Since breast density is known to correlate to increased risk of breast cancer<sup>8,9</sup>, it's inclusion in the screening model is important. Breast density is a low frequency phenomena, and does<sup>8</sup> not require high resolution images for its assessment. Co-investigator Lindfors, the Chief of Mammography at UC Davis, sat down and assessed each of the images for breast density, using her subjective assessment skills based from clinical experience. While we have studied computer determined metrics of breast density<sup>10</sup>, as have others<sup>11,12</sup>, we still consider the radiologist's assessment as the gold standard. We have developed a breast density index (BDI) which spans a range from 0 (least dense) to 100 (most dense) as the quantitative measure of breast density. As a measure of the precision of the radiologist's BDI assessment, Dr. Lindfors studied a subset of 153 mammograms twice, several months apart. Figure 7 illustrates the correlation between these two quasi-independent sessions, indicating excellent precision (less than 5% of the variance  $[1-r^2]$  is associated with radiologist imprecision).

The BDI as a function of patient age is illustrated in Figure 8, and in this figure a cloud-like relationship between breast density and age is seen. The breast density index (BDI) was summed into ten density categories, where category 1=BDI(1-9), 2=BDI(10-19), 3=BDI(20-29), etc. Figure 9 illustrates the distribution of breast density of the screening population at UC Davis. It is well known that women's breasts loose density with age, and the cloud data seen in Figure 8 show this trend somewhat. To better quantify this effect, the data for each age range in five year intervals were assessed using non-parametric statistics (median=50%, 25 percentile and 75 percentile). These data are shown in Figure 10.

For each age interval of 5 years, the BDI data was partitioned into 5 pentiles, from least dense to most dense. For example, for all the women in the 40-45 age range, the 20% (1/5) that had the lowest BDI values were assigned to pentile 1, the next 20% to pentile 2, etc. The median and range of each pentile was then computed, as shown in Figures 11, 12 and 13 for the five pentiles assessed. The median and range data for each pentile was computer fit, and the computer fit profiles are illustrated as the dotted lines in Figures 11, 12 and 13. The computer fit functions were used in generating a model of breast density versus age for the computer simulations. The breast density computer model assumes that a women who has dense breasts when she is young, continues to be in the dense breast category when she gets old. For each women in the simulated data base, the breast density model consists of selecting a pentile category (one of those shown on Figures 11, 12 or 13) at random, and then another floating point random number,  $\xi$ , is chosen on the interval from (-1 to +1). Each women rides the curve of breast density for her assigned

pentile, but where she sits on the curve between the upper and lower bounds is determined by the value of  $\xi$ .

The breast density model was assessed using 100,000 women, and the global BDI versus age data is illustrated in Figure 14. Good agreement between the measured BDI data (solid lines) and the modeled results (dotted lines) is seen. The average BDI for each decade of age for both the original data measured in the 1000 women database at UC Davis is compared with the simulated results in Figure 15. Again, very good agreement exists between the modeled breast density and the original data which is the basis for the model. The mean BDI values are shown with values in Figure 16 for reference.

It is probably not true that every woman maintains the same rank amongst her peers in terms of breast density as she ages (which is what the breast density model assumes), since some women will lose density for example due to weight gain, and some will increase density due to weight loss or if placed on hormone therapy. Nevertheless, the modeled cohort breast density matches the UC Davis population quite well. The purpose of the computer simulation model is not to single out an individual woman, but rather to produce screening simulation results based on large cohorts of simulated women. For these purposes, the breast density model should be adequate.

### ***SOW Task 2***

In order to assess the detectability of breast cancer in women with different breast density, Monte Carlo simulations were used. Simulated spherical breast lesions ranging from 2 mm in diameter to 40 mm in diameter were generated for each of the 1000 digitized mammograms in our database. The measured curves relating optical density to gray scale value (and gray scale to optical density) for the Lumisys 150 digitizer used are shown in Figure 17. The Hurter and Driffield (H & D) curves for the mammography screen-film system used at UC Davis is shown in Figure 18(a), and the inverse curve (relating OD to exposure) is shown in Figure 18(b). These look-up tables were used to "map" the digital mammographic image data back to be linear with units of exposure, as illustrated in Figure 19. The gray scale mammograms were converted to OD using the digitizer response curve, and then were converted to exposure using the inverse H & D curve. Once the images were linear with exposure, the x-ray shadow (it's attenuation) of a spherical breast cancer lesion was calculated and was used to modulate the exposure levels of the image. The lesions were placed randomly over the breast parenchyma regions of the image, and techniques were used to assure that the entire lesion was placed only over breast parenchyma, not over the background areas in the image. The subject contrast of a given lesion (how much it perturbs the exposure level) depends upon the difference in the linear attenuation coefficient between the normal breast parenchyma and the breast cancer lesion itself,  $\Delta\mu$  (Figure 20). The breast composition data as published by Hammerstein<sup>13</sup> were used. The ambient breast composition was assumed to be that of 50% adipose and 50% glandular. As Johns and Yaffe<sup>14</sup> have shown, the attenuation properties of breast cancer are very similar to those of 100% glandular tissue. Therefore, the attenuation coefficients for 100% glandular tissue were used for the simulated spherical breast cancer lesions. To calculate this realistically, the x-ray spectrum used

predominantly at UC Davis, a 26 kVp Mo/Mo x-ray beam, was incorporated (Figure 21) in a polyenergetic model. Using the x-ray spectrum shown in Figure 21, the value of  $\Delta\mu$  was calculated for a range of different lesion diameters and a range of breast thicknesses, as shown in Figure 22. The thickness both of the breast and the lesion affects  $\Delta\mu$  due to spectral hardening influences (“beam hardening”), and that is why the curves seen in Figure 22 are not simply horizontal, which would imply that  $\Delta\mu$  is constant. However, for the typical compressed breast thickness (4 cm), the value of  $\Delta\mu$  is pretty constant over the range of lesion diameters (1 mm <  $\Delta x$  < 10 mm). Therefore, a constant value for  $\Delta\mu$  of 0.16 was used in this simulation.

Once the exposure is modulated by the presence of the simulated lesion, the exposure distribution is remapped to optical density using the H & D curve (Figure 23), and then from the optical density (OD), the film transmittance is calculated. The film transmittance is the signal seen by the mammographer’s eyes, and the transmittance is the relative amount of light coming through the mammogram placed on a viewbox. For each lesion, the transmittance signal under the lesion is averaged, and the image counts in an annular region outside of the circle defining the lesion is averaged as well. The lesion and background areas were made equal. The parameter which is used to assess the lesion detectability is given the symbol  $d$ , and is calculated as shown in Figure 24 as:

$$d = \frac{\overline{T}_{lesion}}{\overline{T}_{bg}}$$

The ratio of the transmittance is taken, since it is thought that the response of the human eye is logarithmic with respect to light intensity. For each lesion size under 20 mm, 500 regions of interest (ROIs) were assessed on each mammogram, 250 containing lesions and 250 not containing lesions. For lesions over 20 mm, 100 regions with and 100 lesions without were assessed. For the placement of a large number of lesions (and non-lesions), the two curves as shown in Figure 25 can be produced (idealized curves are shown in the figure). Using the basics of signal detection theory<sup>15</sup> from the two histograms of normal and lesion ROIs, by setting a specific value of the threshold (Figure 25) the number of true positives (TP), true negatives (TN), false positives (FP) and false negatives (FN) can be determined. For each set of these values, the sensitivity and specificity were calculated:

$$sensitivity = TPF = \frac{TP}{TP + FN}$$

$$specificity = TNF = \frac{TN}{TN + FP}$$

The value of the threshold setting (vertical line shown on Figure 25) was varied in 1000 even intervals, over the pertinent range of  $d$ , and at each threshold value the sensitivity and specificity was calculated. Using this array of data, a receiver operating characteristic (ROC) curve was computed (Figure 26). An ROC curve is a plot of sensitivity (true positive fraction, TPF) as a function of (1-specificity) ([1-TNF]=false positive fraction). Once the ROC was calculated, the area under it,  $A_z$ , was numerically calculated. Figure 26 is representative of the type of ROC curves generated in the computer simulation (it is one). The area under the ROC curve,  $A_z$ , is related to the detectability of the lesion (but it is not the *probability* of detection). For each mammogram, an  $A_z$  value was generated for lesions measuring 2 mm, 4 mm, 6, 8, ...20, 25, 30, ...40 mm in diameter. Since each mammogram has associated with it a breast density index, the  $A_z$  values could be related to the BDI. The  $A_z$  is shown versus the BDI for 14 different lesions sizes in Figure 27. The trends shown quantitatively in this figure are consistent with clinical observation: (1) larger lesions are easier to see than smaller ones (i.e. the  $A_z$  values increase with increasing lesion diameter), and (2) lesions are more difficult to detect in the denser breast ( $A_z$  values decrease with increasing BDI). Figure 28 illustrates the same data in a different way. The mean  $A_z$  value is shown plotted as a function of lesion diameter, and curves for 10 different breast density categories are shown.

We note that the above experiments describe a computer observer experiment, however on a more limited basis these same types of experiments can be performed using human observers. It is not possible to quantity huge numbers with human observes given the constraints of time, but we are planning to perform several computer observer (with a radiologist) ROC studies with the intention of calibrating the computer observer results against a trained human observer.

The  $A_z$  value is a parameter that is *related* to lesion detectability (for example if  $A_z=1.0$ , then the lesion will be quite detectable, and if  $A_z=0.5$ , it will be undetectable except by luck), but it does not represent the probability of detecting a breast cancer lesion when one is there. The  $A_z$  value does describe the general shape of an ROC curve. The probability of detecting a lesion, when one is present, is the sensitivity, the ordinate of the ROC curve. The problem in relating the  $A_z$  value to the sensitivity exists because a radiologist can slide around on his or her ROC curve, trading off increased sensitivity for reduced specificity, or visa versa. We recognized, however, that in mammography there is a way to essentially "calibrate" the  $A_z$  value (that is, an ROC curve based on the standard binormal probability density functions for normal and abnormal patients). In mammography, for most mammographers the positive biopsy rate ranges from about 20% to 30%. If the pre-biopsy follow-up aspects of screening mammography (e.g. ultrasound, additional views, diagnostic examination) are considered part of the examination process, then the positive biopsy rate is equal to the positive predictive value (PPV), where:

$$PPV = \frac{TP}{TP + FP}$$

Whereas the sensitivity and specificity are independent of disease prevalence, the positive predictive value is not. Therefore, to compute the sensitivity from a given  $A_z$  value based on the positive biopsy rate technique that we developed, a knowledge of disease prevalence is needed. Figure 29 shows a plot of the normal,  $N(\xi)$ , and cancer,  $C(\xi)$ , populations, similar to Figure 25 shown previously, except here the area of the cancer population is normalized to the prevalence of the disease in the screening population. In Figure 29, the disease prevalence was taken as 2 cancers per 1000 screens, and the ordinate axis is plotted logarithmically to demonstrate the large range. The curves are actually normal (i.e. Gaussian) in shape, but the logarithmic ordinate changes their usual appearance. Once properly normalized for the disease prevalence or *cancer detection rate* (CDR) as it's called sometimes, the sensitivity can be calculated as a function of  $A_z$ . For example, Figures 30 and 31 show the sensitivity (and specificity) as a function of the positive biopsy rate (i.e. PPV), for  $CDR = 10$  and  $CDR = 8$ , respectively. Higher CDRs result in higher sensitivities for the same positive biopsy rate and  $A_z$  value. This model, we think, is valuable in its own right and we intend to publish it soon. Figures 32 and 33 show the sensitivity as a function of the cancer detection rate, for four different  $A_z$  values. A positive biopsy rate of 10% is shown in Figure 32, and a PBR of 30% is shown in Figure 33. Another way of showing the data is demonstrated in Figures 34 and 35, where the sensitivity is shown plotted as a function of  $A_z$ . Notice that for a realistic cancer detection rate of 5 cancers per 1000 screens (Figure 34), and for a realistic positive biopsy rate of for example 20%, the sensitivity is only 10% at an  $A_z$  value of 0.87. To achieve a sensitivity of 50%, the  $A_z$  value needs to be 0.94.

There is much literature which focuses on determining the sensitivity of mammography, but there is a certain fallacy with such a notion. As demonstrated using a computer observer in Figure 28, the  $A_z$  value changes markedly as the lesion diameter increases. Thus, the sensitivity of mammography depends greatly on the size of the lesion. Once the data in Figure 28 is validated against human detection experiment, we hope to report the lesion size dependency of the sensitivity of mammography.

### ***SOW Task 3***

Computer doubling times were assessed by Spratt<sup>4-7</sup>, and these values were computer fit and are shown in Figure 36. The upper and lower range of doubling times are shown for ductal carcinoma in situ (DCIS), note negative (N-) and node positive (N+) cancers. Longer doubling times of course correspond to more slowly growing cancers. Notice that the implication of Figure 36 is that breast cancers for young women grow at a much faster rate than the same type of cancer for an older women. The tumor doubling times can be converted to growth rates (assuming exponential growth) as illustrate in Figure 37 for tumor onset at age 40 years. Figure 38 shows tumor growth for an age of onset of 60 years. The range of growth rates echos the upper and lower limits of the measured doubling times (from Figure 36). We evaluated a large number of papers (stacks), and find the singular work of the Spratt's (J.A. and J.S.) to be most useful for our purposes here. A search of the literature will nevertheless be continued along these lines.

#### ***SOW Task 4***

Prognosis from breast cancer is highly dependent upon the treatment options that are available. In the 1960s and 1970s, most women with breast cancer underwent radical mastectomy. In more recent years, surgical lump removal perhaps followed by radiation is the preferred treatment in the United States. Tumor suppressing drugs such as tamoxifen are also being more widely used under research protocols. The problem in developing a solid prognosis model for the purposes of building this computer simulation system is that the older data have the longest follow-up and therefore are the most accurate, but it also reflects an era when the clinical management of breast cancer was different. Combining the data from Carter<sup>16</sup> and Lopez and Smart<sup>17</sup>, survival data are shown as a function of years post-detection in Figure 39. The data for four different tumor sizes (at diagnosis), and for ductal carcinoma in situ (CIS) are illustrated. For the four tumor sizes, the data were fit using linear regression with correlation coefficients ( $r$ ) of 0.992, 0.995, 0.993, and 0.989, for the 10, 20, 20-50, and >50 mm data sets. The regression fit lines are shown in Figure 39. The absolute value of the slope of each of these lines is plotted as a function of lesion diameter in Figure 40, and the four data points (plus a zero point) are shown as solid circles. The slope data was computer fit to a function using commercially available curve fitting software, and the best fit function is shown as the solid line in Figure 40. The data shown (i.e. the computer derived fitting function) is capable of relating tumor diameter at the time of detection to the slope of the survival curve, for any arbitrary lesion diameter from 0 mm to 50 (using interpolation) or beyond (using extrapolation). A set of computer generated survival curves, computed as just mentioned, is illustrated in Figure 41 for a range of tumor diameters from 5 mm to 60 mm (in 5 mm increments). While this method of computing prognosis (i.e. survival versus time) is simple, it does very accurately replicate the observed survival data of Carter<sup>16</sup> and Lopez and Smart<sup>17</sup>. We consider this a good starting model for prognosis, and will continue to improve it depending on the discovery of better data in the literature.

#### ***SOW Task 6***

The elements of the breast cancer screening simulation model as described above were combined into a comprehensive pair of routines. The first routine made use of the patient demographics, death rate, breast density, and breast cancer incidence models and was capable of generating databases with various characteristics. At this point, the databases built are similar except for size, and we have constructed data bases ranging from 5,000 simulated women to 1,000,000 simulated women. The smaller databases are useful for debugging purposes.

The second routine reads in a specified database, and applies a user-selectable screening paradigm. Parameters that can be varied include the starting age, stopping age, screening interval, and breast density dependent screening parameters.

#### ***SOW Task 7***

Validation of the model against clinical trial data is just beginning. Figure 42 illustrates the cancer detection rate as reported by two groups as a function of the age categories of

the screened women. Using the same screening parameters as those reported (start at age 50, screening interval of 2 years), the screening model generated the data with the solid circles. We need to emphasize that our approach to peer review reporting of any results from the screening model will be extremely conservative. We make absolutely no claims at this point, and the results discussed below should be considered highly speculative until further, more complete validation can be performed. Given that this is a limited-distribution document, however, we will make some observations, which should be considered as extremely preliminary.

Excellent agreement between the data is seen in Figure 42. The model-derived data were not fit or tweaked in an iterative scheme to match the comparison data, they are a direct output of the screening model, making use of all of the models as described above. We are frankly surprised and extremely encouraged that the preliminary results in terms of this simple parameter, cancer detection rate, are even in the ballpark of clinically reported values.

The frequency distribution of tumor sizes reported by Shetty and Reiman<sup>18</sup> are compared against the results of the computer simulation model described here in Figure 43. The data of Shetty and Reiman were hard to model precisely because of its long acquisition time (1980-1995), which reflects a period in which many screening intervals and start ages were popular.

The number of cancers detected as a function of age in the screening population is illustrated in Figure 44. While the sheer number of cancers represented in the <50 age group is a small (but certainly not negligible) fraction of the total curve, these cancers have a profound effect in reducing years of life per cancer victim (since at this young age women have many more years left of their lives, on average). The total years of life saved are shown in Figure 45. Notice that this curve is shifted left, compared to Figure 44, illustrating that finding a cancer and treating it at an early stage has a greater potential to save more years of life for younger women as compared to older women.

As another example of the types of data that can be generated by the breast cancer screening model, a series of survival curves is shown in Figure 46. The survival curves shown marked improvement for screening at shorter intervals. The survival curve for BSE alone (i.e. no mammographic screening) is also shown in Figure 46. The survival curves shown in this figure are curved (for a large cohort of women), whereas the modeled survival for each individual cancer victim is linear as shown in Figure 41. The difference is a result of the different tumor sizes at detection, and the different ages at detection (which affects growth rate and hence size of tumor at detection).

Figure 47 illustrates the years of life saved *per cancer patient*, as predicted from the screening model. The data on this figure clearly indicate that shorter screening intervals increases the amount of years saved per cancer patient, with a ½ year screening interval saving on average 8.5 years for women age 50, where a screening interval of 3 years results in an average of 5.1 years saved per women aged 50. What is most striking about these results is that they clearly demonstrate that decreased screening interval has a

strong benefit for younger women, which is predicable knowing that younger women experience in general more aggressive tumors. This curve gives quantitative strength to this observation. Another important observation that can be made on Figure 47 is that a 3 year screening interval is equivalent to the ½ year screening interval for women aged 70 and above. If this observation proves to be true after further study, it would imply that the screening interval could be lengthened for older women with no detrimental affect on the outcome (as measured here). However, certainly a broader range of outcome metrics needs to be evaluated before any definitive statements could be made. Nevertheless, by increasing the screening interval in older women, more women could be screened using the same amount of screening resources. This is just an example of the type of result that would be useful in using the screening model to optimize the performance of breast cancer screening in the United States.

## KEY RESEARCH ACCOMPLISHMENTS

At this early phase of the research plan, our key accomplishment is the production of two screening model tools. The first model generates data bases of any number of women (databases having from 5,000 to 1,000,000 have been generated to date), and these women exhibit the proper epidemiological characteristics with respect to breast cancer, as determined by cancer rates, age-versus-incidence, number of cancers in the population, racial distributions, breast density distribution, and so on. The second model reads in the data base generated by the first model, and then applies concepts from fundamental detection theory to simulated breast cancer detection over a range of specified parameters, including start age, screening interval, and end age for mammography, and for different size versus detection distributions for the default competing modality, breast self examination. Preliminary results generated from the computer simulation models are very encouraging.

Another key accomplishment is the recognition that the breast biopsy rate can be used to compute the sensitivity and specificity of mammography, for known incidence (cancer detection rates) and known receiver operating characteristic curve performance (the  $A_z$  value). Since the  $A_z$  value has a definite dependency on tumor size, and on breast density, defining a single pair of sensitivity/specificity values for mammography is probably naïve. A manuscript showing the relationships between CDR, biopsy rate, and  $A_z$ , will be submitted for publication soon.

## **REPORTABLE OUTCOMES**

- (1) JM Boone and KK Lindfors, "Computer simulation of breast cancer screening efficacy", *Medical Physics* 26:1065-1066, 1999 (Abstract)
- (2) JM Boone and KK Lindfors, Symposium Presentation entitled "Computer simulation of breast cancer screening efficacy", presented at the 41<sup>st</sup> annual meeting of the American Association of Physicists in Medicine, Nashville, TN (July 26, 1999).

## CONCLUSIONS

The research is too preliminary to make any definitive conclusions with respect to breast cancer screening, *per se*. However, we can make the intermediate conclusion that our experience with the breast cancer screening model to date has given us a great deal of enthusiasm to pursue our original goals and produce a completely verified and validated screening model. In our next two years, we will concentrate on perfecting and improving each of the individual components of the screening model, and on validating the output results of the model with peer reviewed, high quality clinical trial data.

## REFERENCES

1. C. J. Baines, A. B. Miller, D. B. Kopans, M. Moskowitz, D. E. Sanders, E. A. Sickles, T. To, and C. Wall, "Canadian National Breast Screening Study: assessment of technical quality by external review [see comments].", *AJR.Am.J.Roentgenol.* **155**, 743-7; discussion 748-9 (1990)
2. D. B. Kopans and S. A. Feig, "The Canadian National Breast Screening Study: a critical review.", *AJR.Am.J.Roentgenol.* **161**, 755-760 (1993)
3. D. B. Kopans, "Breast-screening brawl [letter].", *Science* **275**, 1721-1724 (1997)
4. J. A. Spratt, D. von Fournier, J. S. Spratt, and E. E. Weber, "Decelerating growth and human breast cancer.", *Cancer* **71**, 2013-2019 (1993)
5. J. A. Spratt, D. von Fournier, J. S. Spratt, and E. E. Weber, "Mammographic assessment of human breast cancer growth and duration.", *Cancer* **71**, 2020-2026 (1993)
6. J. S. Spratt, J. S. Meyer, and J. A. Spratt, "Rates of growth of human solid neoplasms: Part I.", *J.Surg.Oncol.* **60**, 137-146 (1995)
7. J. S. Spratt, J. S. Meyer, and J. A. Spratt, "Rates of growth of human neoplasms: Part II.", *J.Surg.Oncol.* **61**, 68-83 (1996)
8. N. F. Boyd, J. W. Byng, R. A. Jong, E. K. Fishell, L. E. Little, A. B. Miller, G. A. Lockwood, D. L. Tritchler, and M. J. Yaffe, "Quantitative classification of mammographic densities and breast cancer risk: results from the Canadian National Breast Screening Study.", *J.Natl.Cancer Inst.* **87**, 670-675 (1995)
9. N. F. Boyd, G. A. Lockwood, J. W. Byng, D. L. Tritchler, and M. J. Yaffe, "Mammographic densities and breast cancer risk.", *Cancer Epidemiol.Biomarkers Prev.* **7**, 1133-1144 (1998)
10. J. M. Boone, K. K. Lindfors, C. S. Beatty, and J. A. Seibert, "A breast density index for digital mammograms based on radiologists' ranking.", *J.Digit.Imaging* **11**, 101-115 (1998)
11. C. B. Caldwell, S. J. Stapleton, D. W. Holdsworth, R. A. Jong, W. J. Weiser, G. Cooke, and M. J. Yaffe, "Characterisation of mammographic parenchymal pattern by fractal dimension.", *Phys.Med.Biol.* **35**, 235-247 (1990)
12. J. W. Byng, N. F. Boyd, E. Fishell, R. A. Jong, and M. J. Yaffe, "Automated analysis of mammographic densities.", *Phys.Med.Biol.* **41**, 909-923 (1996)
13. G. R. Hammerstein, D. W. Miller, D. R. White, M. E. Masterson, H. Q. Woodard, and J. S. Laughlin, "Absorbed radiation dose in mammography.", *Radiology* **130**, 485-491 (1979)
14. P. C. Johns and M. J. Yaffe, "X-ray characterisation of normal and neoplastic breast tissues.", *Phys.Med.Biol.* **32**, 675-695 (1987)
15. H. H. Barrett and W. Swindell, *Radiological Imaging, The theory of image formation, detection, and processing*, Academic Press, New York, 1981).
16. C. L. Carter, C. Allen, and D. E. Henson, "Relation of tumor size, lymph node status, and survival in 24, 740 breast cancer cases.", *Cancer* **63**, 181-187 (1989)
17. M. J. Lopez and C. R. Smart, "Twenty-year follow-up of minimal breast cancer from the Breast Cancer Detection Demonstration Project.", *Surg.Oncol.Clin.N.Am.* **6**, 393-401 (1997)

18. M. R. Shetty and H. M. Reiman, Jr., "Tumor size and axillary metastasis, a correlative occurrence in 1244 cases of breast cancer between 1980 and 1995 [see comments].", *Eur.J.Surg.Oncol.* **23**, 139-141 (1997)

## FIGURE CAPTIONS

### Figure 1.

The US female population is shown projected to July 1, 2000. The total population, including the white, black, Asian, and American Indian components of that population are illustrated. The "baby boom" is seen as the distinct hump between the ages of 30 and 60. *Source: US Census Bureau.*

### Figure 2.

One of the reasons why the age in which breast cancer screening should start is controversial is that it has a profound impact on the screening population. As illustrated in this figure, decreasing the age at first screen from 50 to 40 increases the screening population by 23.3 million women, increasing the number of screens by 56%.

### Figure 3.

In the computer simulation of breast cancer screening, factors which compete with breast cancer as a cause of death clearly need to be considered. The US death rate as a function age for four ethnic groups is illustrated. Note that the ordinate is a logarithmic axis, indicating that after approximately age ten, one's probability of dying increases exponentially. *Source: US Census Bureau.*

### Figure 4.

The incidence of breast cancer among breast cancer-free women is illustrated. The raw data are the individual points. To improve the quality of fit to this data, a hybrid computer-fitting technique was used. The curve was split into three discrete regions, and three different fits over the different ranges were used. The end result, the *hybrid fit*, fits the data accurately over the entire age range. This figure shows the breast cancer incidence for all races. *Source: The National Cancer Institute SEER Program.*

### Figure 5.

The breast cancer incidence through white American women is illustrated.

### Figure 6.

The breast cancer incidence for American black women is illustrated.

### Figure 7.

In studying the effects of breast density, it was necessary to produce a metric which quantifies breast density with reasonable precision. In this study, the assessment of an experienced mammographer was used. The mammographer ranked each of 1000 mammograms on an integer scale from 0 to 100, with 100 indicating a very dense breast. To assess the precision of this mammographer's assessment, she assessed the same sub-population of 153 women twice, separated by a period of several months. This plot shows the relationship of the mammographer's breast density index (BDI) between those

two sessions. Given the subjective nature of the assessment, excellent precision was demonstrated.

### **Figure 8.**

The breast density index as determined by the mammographer is shown plotted as a function of the age of the patient. While the data hardly follows any distinct function, there is a trend towards reduced breast density index with increased age.

### **Figure 9.**

The breast density index data was categorized into ten distinct categories (1=least dense, 10= most dense). These data represent the probability density function for breast density of the screening population studied at UC Davis.

### **Figure 10.**

The breast density index is shown as a function of age, and on this plot the median (50<sup>th</sup> percentile), along with the 25<sup>th</sup> and 75<sup>th</sup> percentile ranges are shown. The clear trend indicating a reduction in the BDI as a function of age is seen.

### **Figure 11.**

For each age range spanning five years, the BDI was partitioned into five regions having equal numbers of women in each region ("pentiles"). In order to model the distribution of breast density as a function of age, each pentile as a function of age was parametrized. This figure shows the lowest pentile (pentile 1, top) indicating the trend of the women in the lowest breast density category. Pentile 2 is shown on the lower figure. The median and range of the pentile is shown in each case. The computer fit to the raw data is illustrated as the dotted lines.

### **Figure 12.**

Pentile 3 and pentile 4 data from the UC Davis database are illustrated, with computer fitted results (dotted lines) also shown.

### **Figure 13.**

Pentile 5 from the UC Davis database is illustrated. This pentile has the largest range.

### **Figure 14.**

Using computer-fitting techniques, a computer model was designed to mimic the breast density index versus age profile of the UC Davis database. In this figure, the UC Davis database median, 25<sup>th</sup> and 75<sup>th</sup> percentile are shown as solid lines. The computer model results are shown as the dotted lines. Good agreement between the computer model and the UC Davis breast density index data is illustrated.

### **Figure 15.**

As an additional metric demonstrating the quality of the breast density computer model the original data and simulated data for each decade of age are illustrated on this bar chart. Excellent agreement is demonstrated.

**Figure 16.**

The average breast density index for each decade is indicated on this graph.

**Figure 17.**

The gray scale to optical density (a) and optical density-to-gray scale (b) look up tables as measured for our Lumisys150 film digitizer are illustrated.

**Figure 18.**

The Hurter and Driffield (H & D ) curve showing optical density as a function of exposure is shown in (a). The inverse transform showing the relationship of exposure as a function of optical density for the same curve is shown in (b).

**Figure 19.**

The digitized mammographic images were transformed using the gray scale to optical density look up table, and then were transformed again using the optical density-to-exposure transform look up table, resulting in an image linear with exposure.

**Figure 20.**

Simulated spherical lesions of various diameters were added to the digitized mammograms. This figure illustrates the modeling used in adding the image data to those mammograms. Significant in this figure is the value of  $\Delta\mu$ , which represents the change in linear attenuation coefficient inside the spherical lesions due to the presence of cancer.

**Figure 21.**

In order to accurately model the change in the linear attenuation co-efficient due to the presence of a breast cancer lesion, a 26 kVp molybdenum anode with molybdenum filter x-ray spectrum was used.

**Figure 22.**

This figure illustrates  $\Delta\mu$  arising from a 26 kVp Mo- x-ray spectrum. Curves for 10 lesions diameters (spanning from 1 mm to 10 mm's as indicated) are shown as a function of breast thickness.  $\Delta\mu$  changes as a function of breast thickness due to beam hardening. Because all ten curves converge at a  $\Delta\mu$  of approximately 0.16 at a breast thickness of 4 cm, this value was used for the  $\Delta\mu$  as shown on Figure 20

**Figure 23**

Using the image that was transformed to be linear with exposure, the simulated spherical lesion was added as described previously. The exposure image was then transformed by the H & D curve to optical density, which in turn was transformed through optical transmittance as shown on this figure. It is the optical transmittance, which is observed by the radiologist sitting in front of the light box.

### Figure 24

In order to calculate the detectability of the simulated lesions, the area occupied by the lesion was integrated. A region just outside the lesion of equal area was also integrated, giving rise to  $T_{\text{lesion}}$  and  $T_{\text{bg}}$ , respectively. A decision parameter,  $d$ , was then calculated as the ratio as illustrated on the figure.

### Figure 25

The basic tenants of signal detection theory are shown. Local areas on mammograms may consist of normal areas and lesions, and a likely distribution of these populations is shown. The abscissa is some decision parameter,  $d$ , and for this study  $d$  is defined in Figure 24. By applying some threshold value (vertical line), the data in the two distributions can be placed into the categories true positive (TP), true negative (TN), false positive (FP), and false negative (FN). These categories are shown on the figure for the placement of the threshold value as shown. Using the values of TP, TN, FP, and FN, the quantities *sensitivity* and *specificity* can be calculated. An ROC curve (shown in the next figure) is computed by moving the threshold value across the two distributions laterally, computing sensitivity and specificity at each threshold value. The ROC curve is a plot of sensitivity (ordinate) versus (1-specificity) (abscissa).

### Figure 26

For each mammogram, a total of 500 simulated lesions were placed and their detectability assessed using standard detection theory. As a result of this analysis, a receiver operating characteristic (ROC) curve could be computed for each image. The area under the ROC curve, denoted as  $A_z$ , was then computed for each mammogram. The parameter,  $A_z$ , is related to the detectability of the lesion. Lesions spanning in diameter from 2 mm to 40 mm were studied.

### Figure 27

The average  $A_z$  as a function of breast density index is illustrated on this figure, for lesions spanning the range from 2 mm to 35 mm. As the BDI increases the average  $A_z$  decreases, indicating that lesion detectability is compromised in the denser breast. In addition, larger lesions demonstrate higher  $A_z$  values, indicating, as expected, larger lesions are more detectable than smaller ones.

### Figure 28

This figure shows a different perspective of the data shown in the last figure. The mean  $A_z$  value is shown as a functional lesion diameter for 10 different categories (deciles) of breast density. The most dense 10 percent of breasts illustrate markedly reduced lesion detectability compared to the lower density breasts. These data are consistent with clinical experience.

### Figure 29

This figure illustrates the basic tenants of signal detection theory. The relative frequency of cases ( $N$  = normal cases,  $C$  = cancers), is shown as a function of the decision parameter. This data was used to convert  $A_z$  value to a specific probability of detection,

which is required for modeling purposes. This figure is similar to Figure 25, except that here the disease incidence is accounted for.

### **Figure 30**

Using the computer model relating  $A_z$  to sensitivity (probability of lesion detection), the sensitivity or specificity could be calculated at a given cancer detection rate (CDR) and  $A_z$  value, as a function of positive biopsy rate. This figure shows the results for a CDR = 10 and  $A_z = 0.90$ .

### **Figure 31**

This figure shows the sensitivity or specificity as a function of positive biopsy rate for a CDR of 8.

### **Figure 32**

The sensitivity is illustrated as a function of the cancer detection rate for a positive biopsy rate of 10 percent. Four curves showing a range of  $A_z$  values are illustrated. The sensitivity decreases as the number of cancers in the population decreases. Also, the sensitivity increases as the  $A_z$  value increases, as expected.

### **Figure 33**

This figure is the same as the last figure, except a positive biopsy rate of 30 percent is illustrated. Reduced sensitivity is observed when the positive biopsy rate increases (compare with the last figure).

### **Figure 34**

The sensitivity is shown as a function of  $A_z$  value at a cancer detection rate of 5 per 1,000 for a positive biopsy rate spanning from 5 percent to 50 percent.

### **Figure 35**

The sensitivity as a function of  $A_z$  value is illustrated as in the last figure. As the cancer detection rate increases, the sensitivity increases at the same  $A_z$  value and positive biopsy rate.

### **Figure 36**

The tumor doubling time as a function of age for three different tumor types is illustrated. The three different tumor types are ductile carcinoma in situ, node negative, and node positive breast cancer. The pair of lines for each cancer type represent the range (plus or minus 95 percent) of measured doubling time for this cancer type. Data from Spratt, et al.

### **Figure 37**

The tumor doubling time from the last figure has been converted to a growth rate (tumor diameter versus time) in this figure. These data show tumor growth rates for a woman at age 40.

**Figure 38**

This figure shows tumor growth rates where the tumor started when the woman was age 60. Markedly slower growth rates are observed for older women compared to the last figure.

**Figure 39**

Five sets of prognosis data were evaluated, for ductile carcinoma in situ and tumors discovered at different diameters (as shown). The data for each of the five data sets were fit using linear regression, with correlation coefficients in all cases exceeding 0.98.

**Figure 40**

The absolute value of the slope of the linear regression fit (see last figure) is plotted as a function of the lesion diameter. Computer fitting techniques were used to fit the data points.

**Figure 41**

Using the slope versus lesion diameter fit data from the last figure, survival curves for any lesion diameter could be generated. This model was used to estimate the survival of women based solely on the diameter of the breast cancer lesion at the time of detection.

**Figure 42**

Results generated by the breast cancer screening model (circles) are compared against those reported by others. Here, the cancer detection rate is shown as a function of age. Good agreement is seen.

**Figure 43**

The distribution of tumor size at the time of detection is illustrated in this graph, comparing the work of Shetty and Reiman with the results produced by the computer simulation model. Good agreement is seen.

**Figure 44**

The number of cancers detected is shown as a function of age at cancer detection. These data are generated by the computer simulation model, and are an example of types of data that can be easily computed from such a model.

**Figure 45**

The computer simulation model can also be used to generate results which are not easily measured in a clinical trial. For example, the total years saved in a population due to breast cancer screening can be assessed and in this figure the total years saved is shown as a function of age at cancer detection. The total years saved in the population under age 50 is approximately equal to the number of years saved in the population over 75.

**Figure 46**

Survival curves, as shown in this figure, can also be generated from the computer simulation model. This figure shows the different survival characteristics depending

upon the frequency of mammographic screening (*dt*). For comparison, the survival from breast self-examination (BSE) is also indicated. Decreasing the screening interval demonstrates a measurable improvement in survival, based on these computer simulated results.

### **Figure 47**

In this figure, the years of life saved per cancer patient is plotted as a function of age at cancer detection. The four different curves correspond to four different screening intervals, as indicated. Shorter screening intervals clearly benefits younger women based on this data. Furthermore, it is seen that a screening interval of three years produces the same effect (years of life saved per cancer patient) as a screening interval of six months for women 70 years of age and older. If this result proves to be true, it would have major ramifications for the screening practices of older women.

### **Figure 48**

The number of cancers are shown as a function of the breast density category of the woman. The computer simulation model used a risk ratio of 4.0, and this is reflected in the data shown.

### **Figure 49**

The average years of life saved is illustrated as a function of breast density. Women with increased breast density benefit less from mammographic screening. The breast cancer simulation model demonstrates this fact quantitatively.

### **Figure 50**

The detection rate is shown as a function of screening interval, comparing mammographic detection versus detection by breast self examination (BSE). Mammography has a higher detection rate as the screening interval decreases

U.S. Population on July 1, 2000

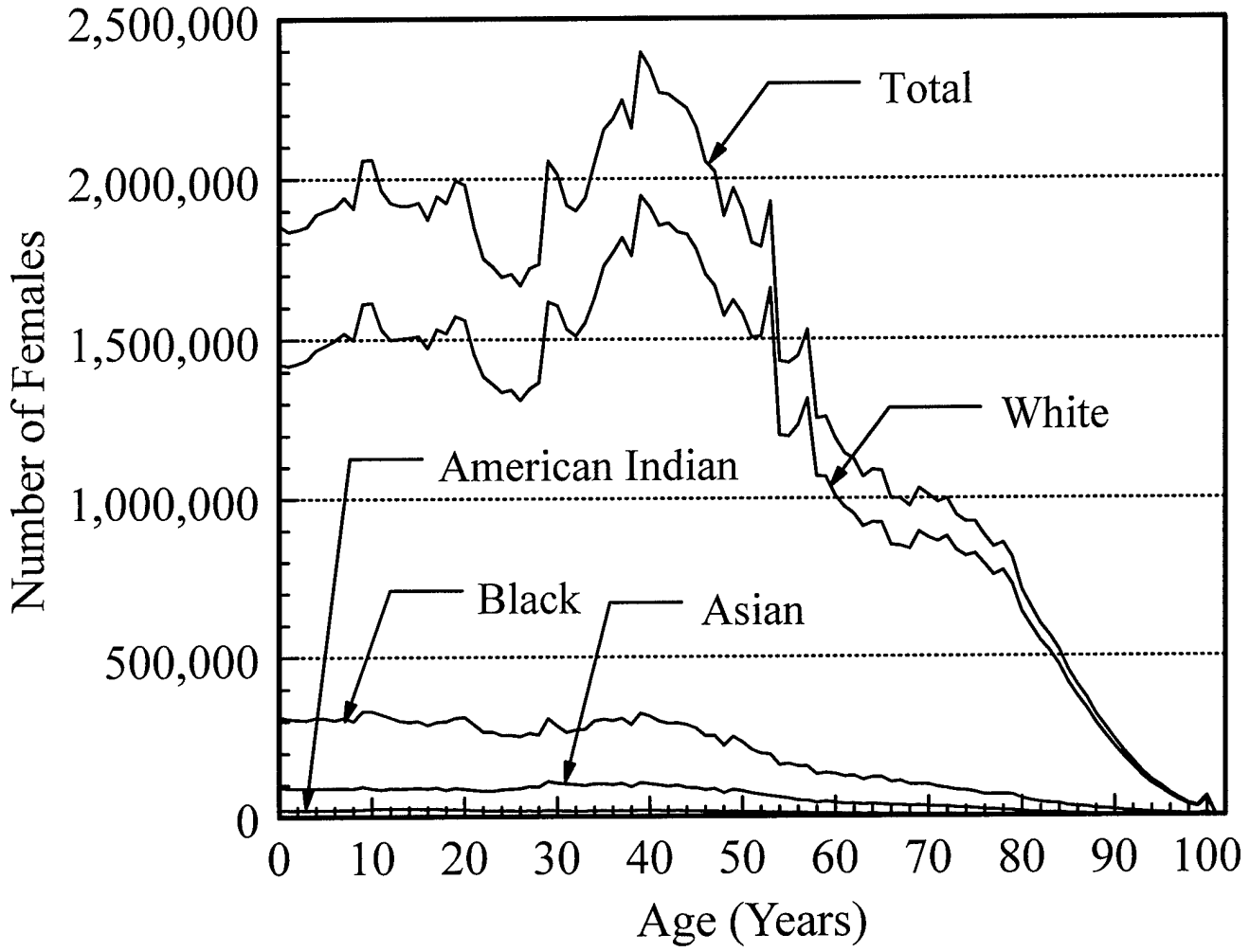


Figure 1

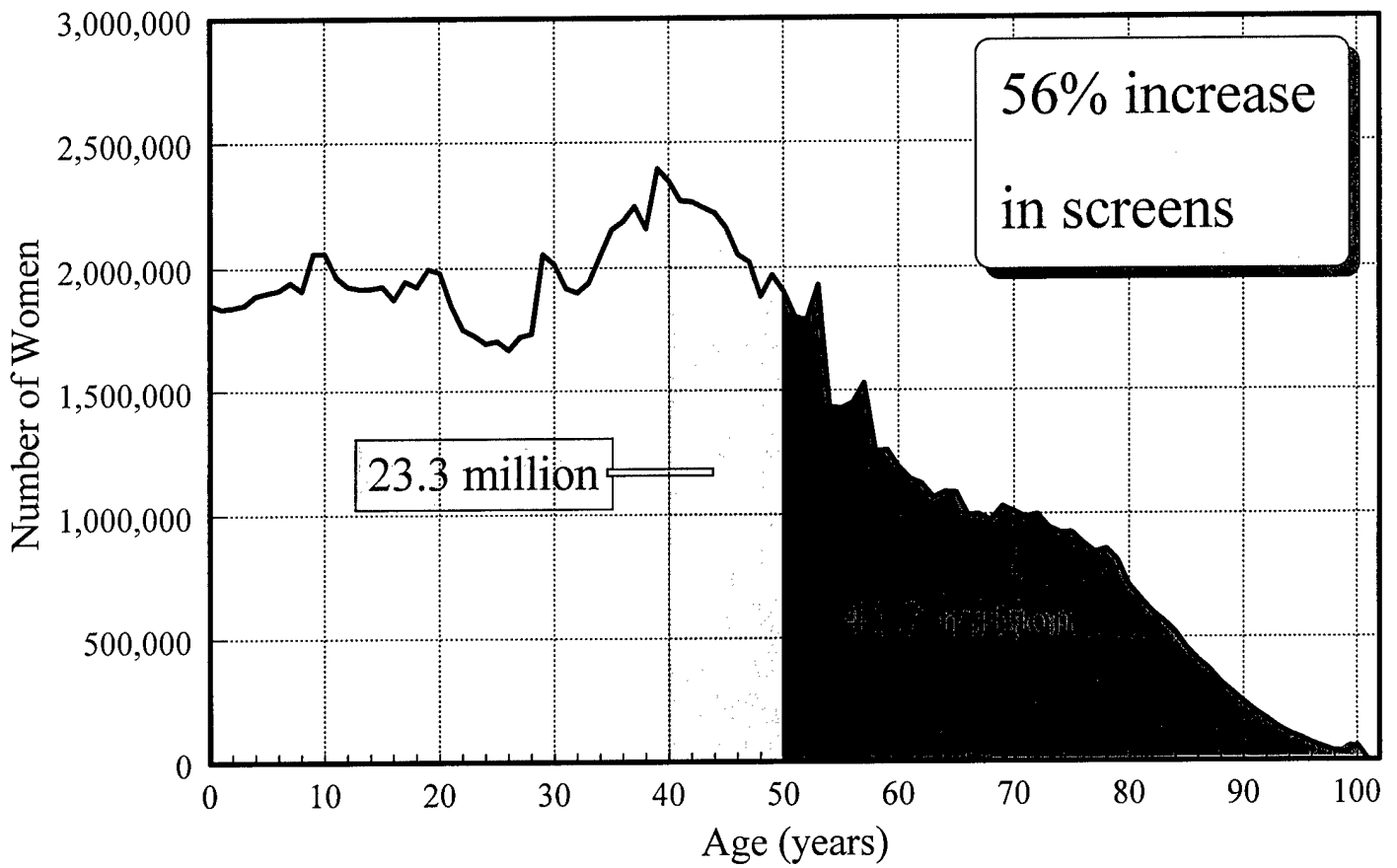


Figure 2

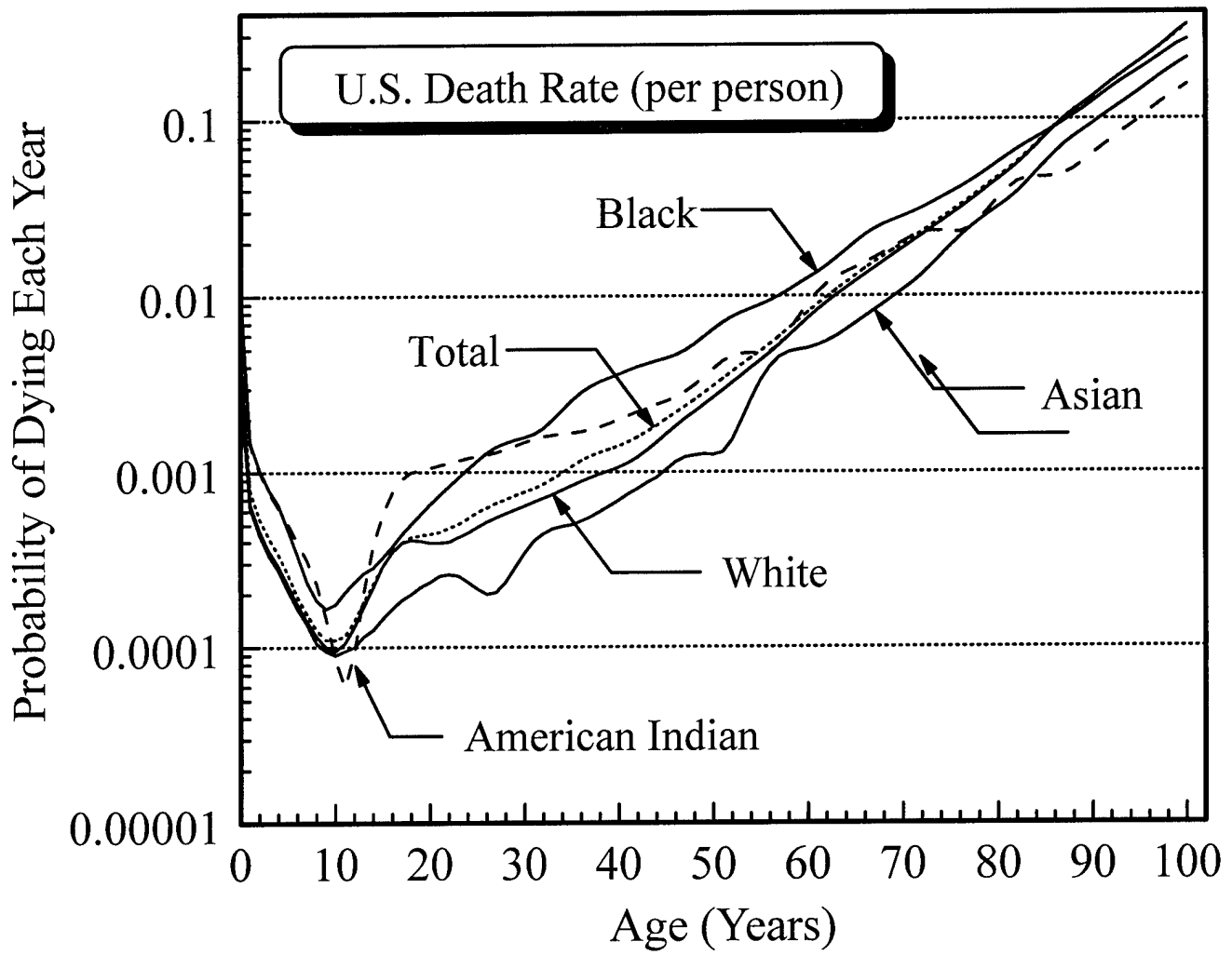


Figure 3

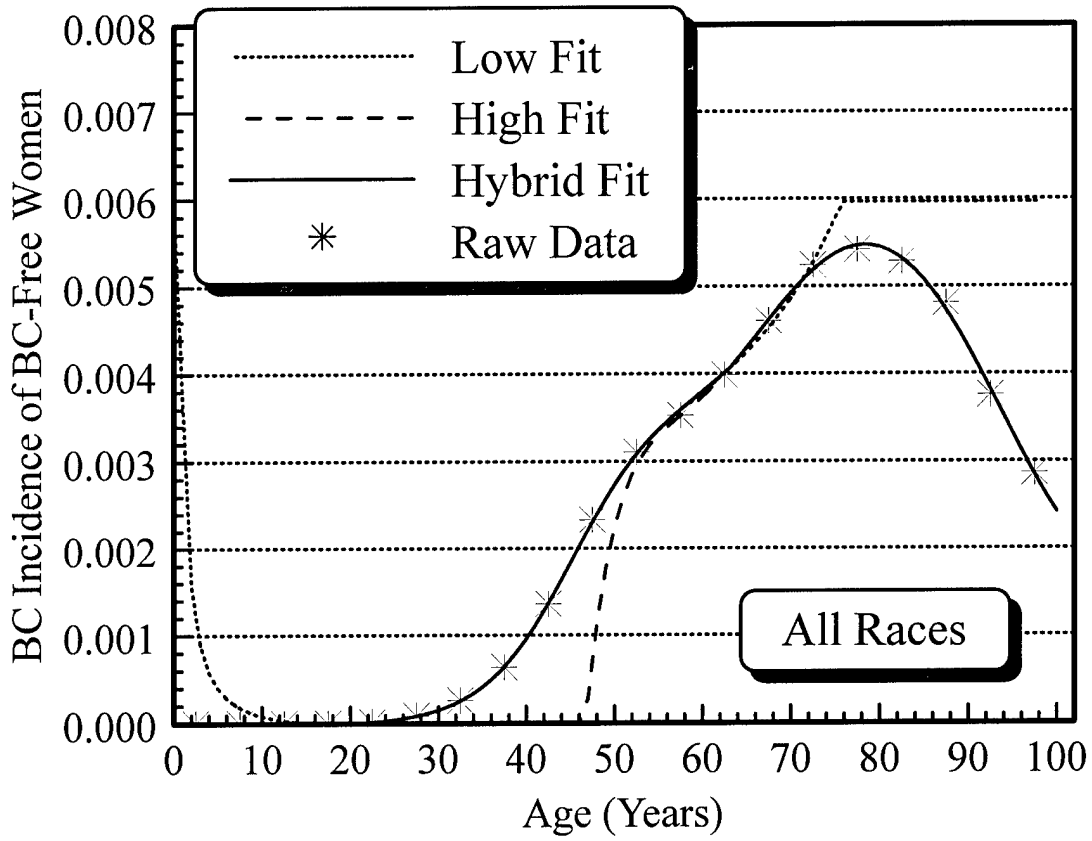


Figure 4

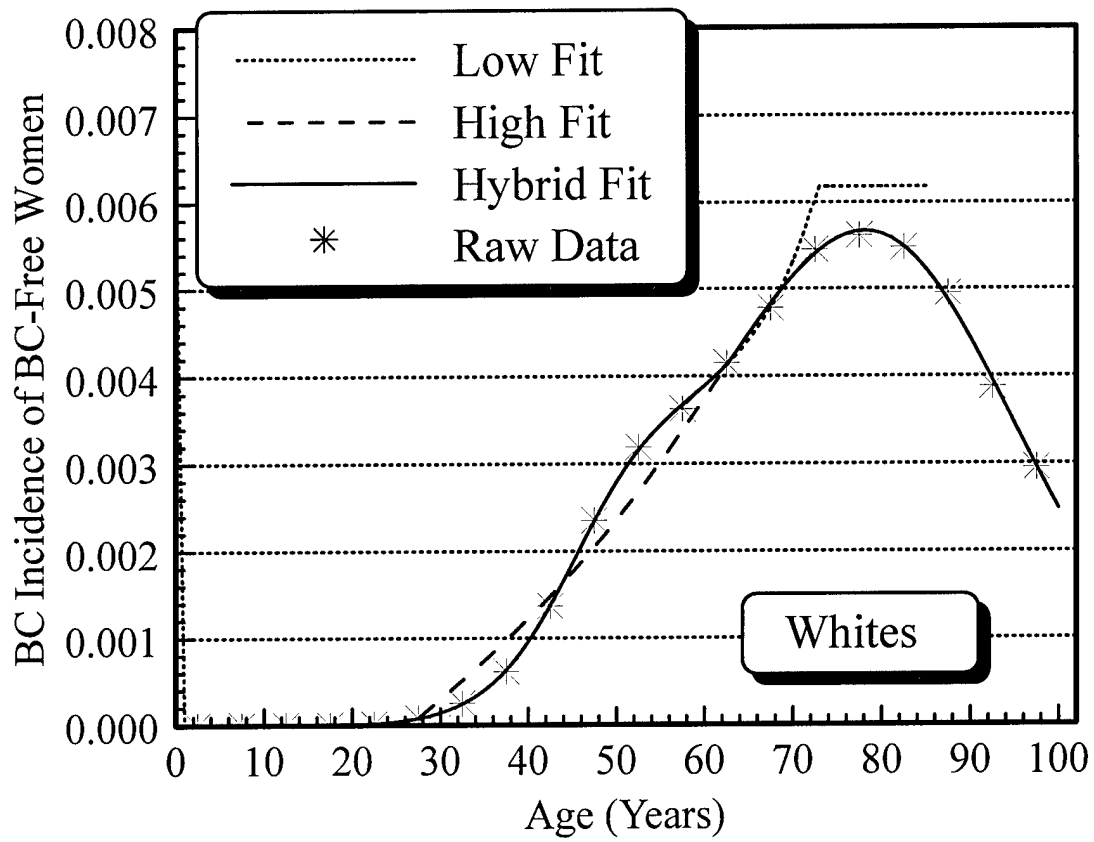


Figure 5

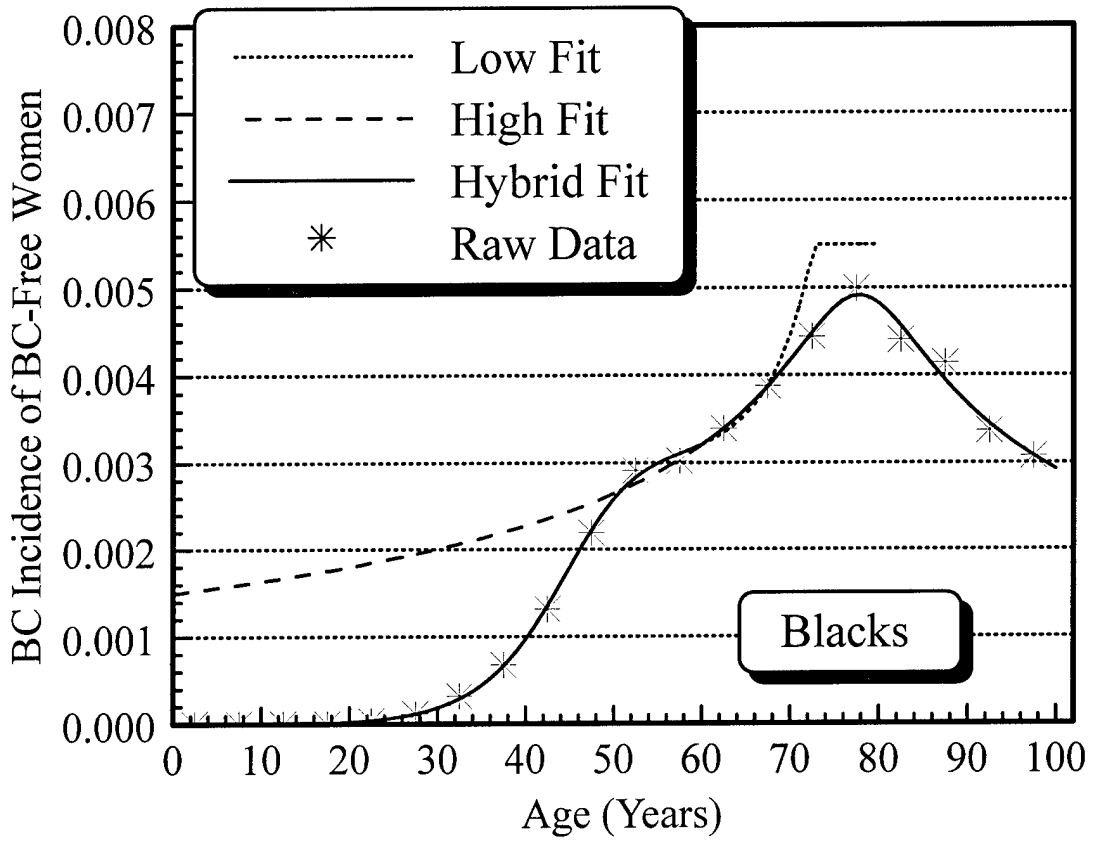


Figure 6

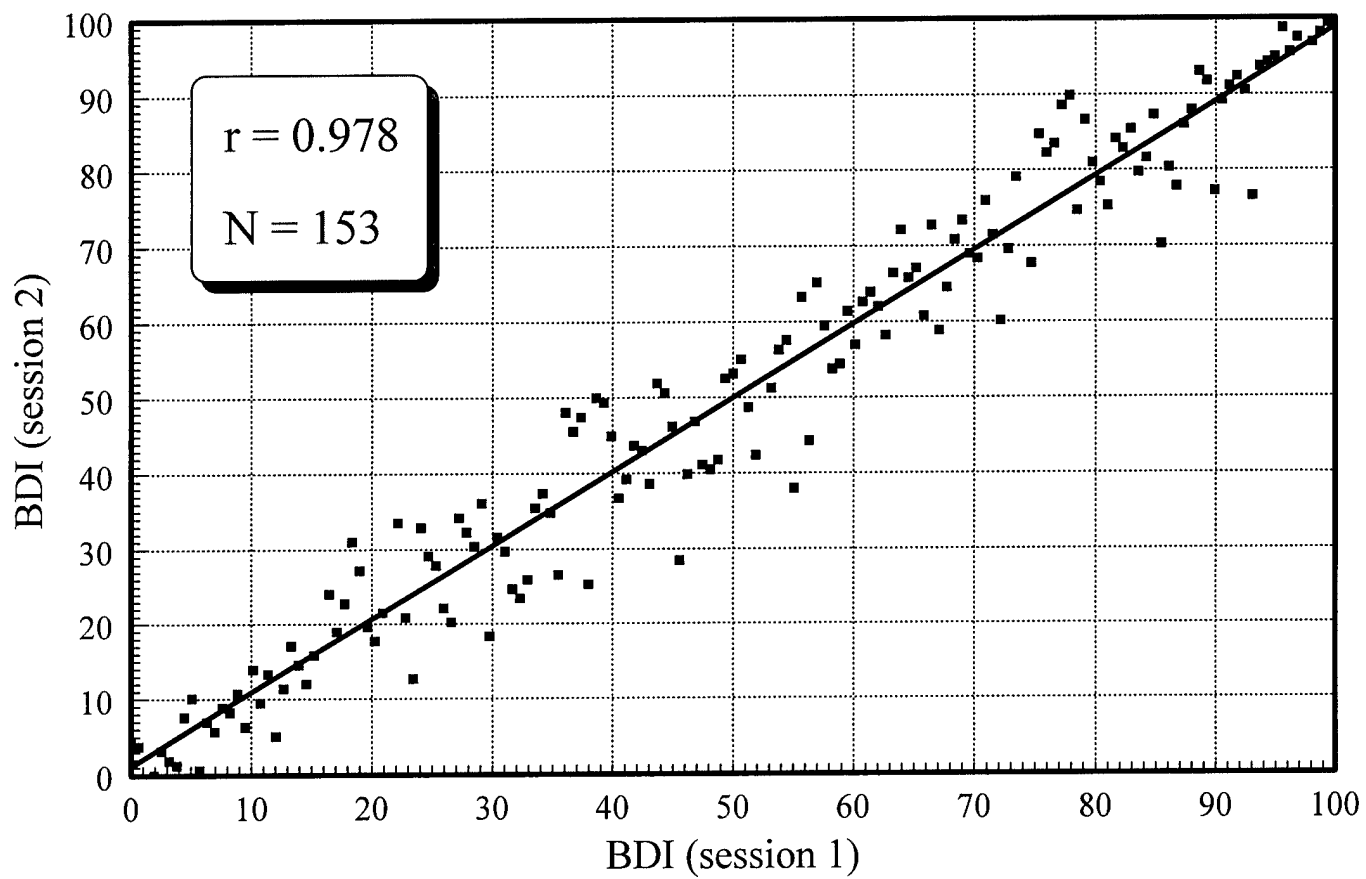


Figure 7

# Breast Density Index

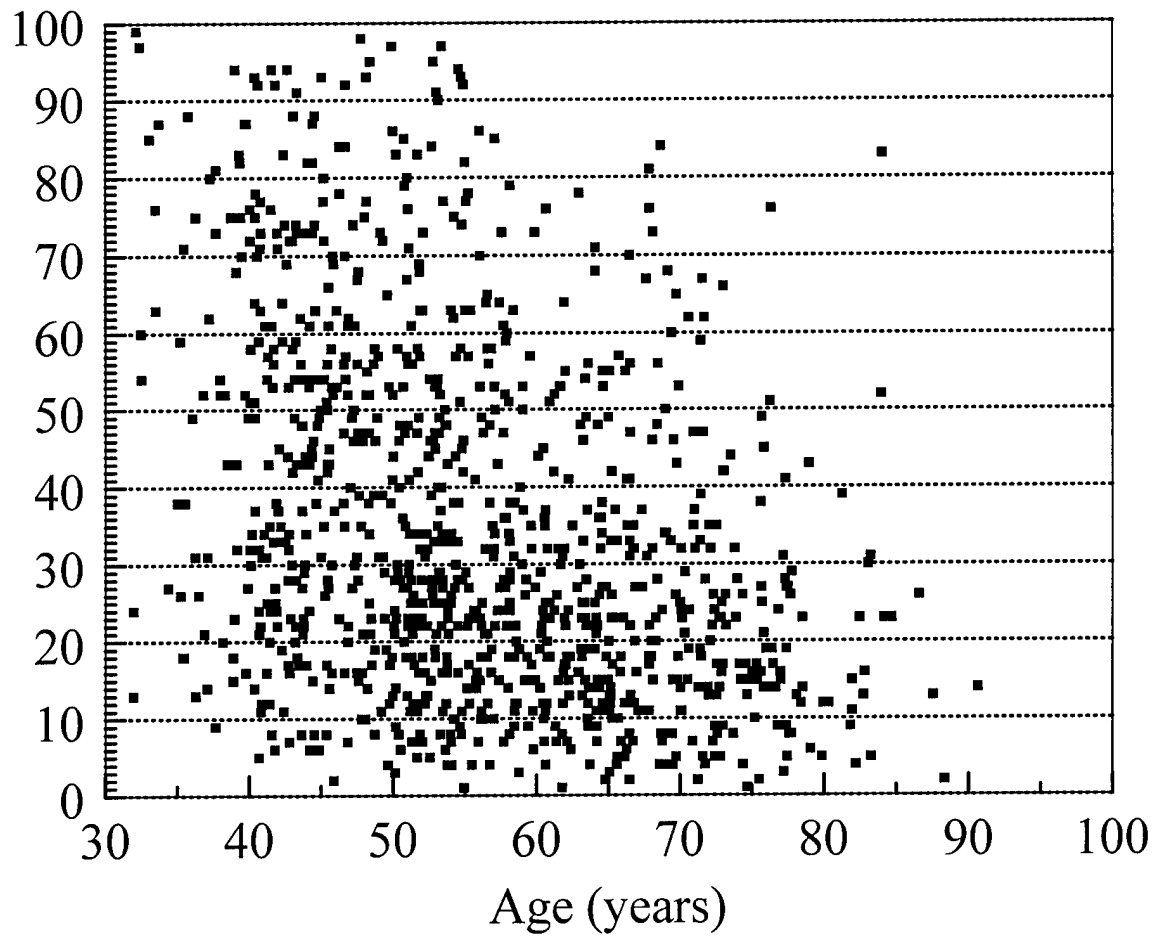


Figure 8

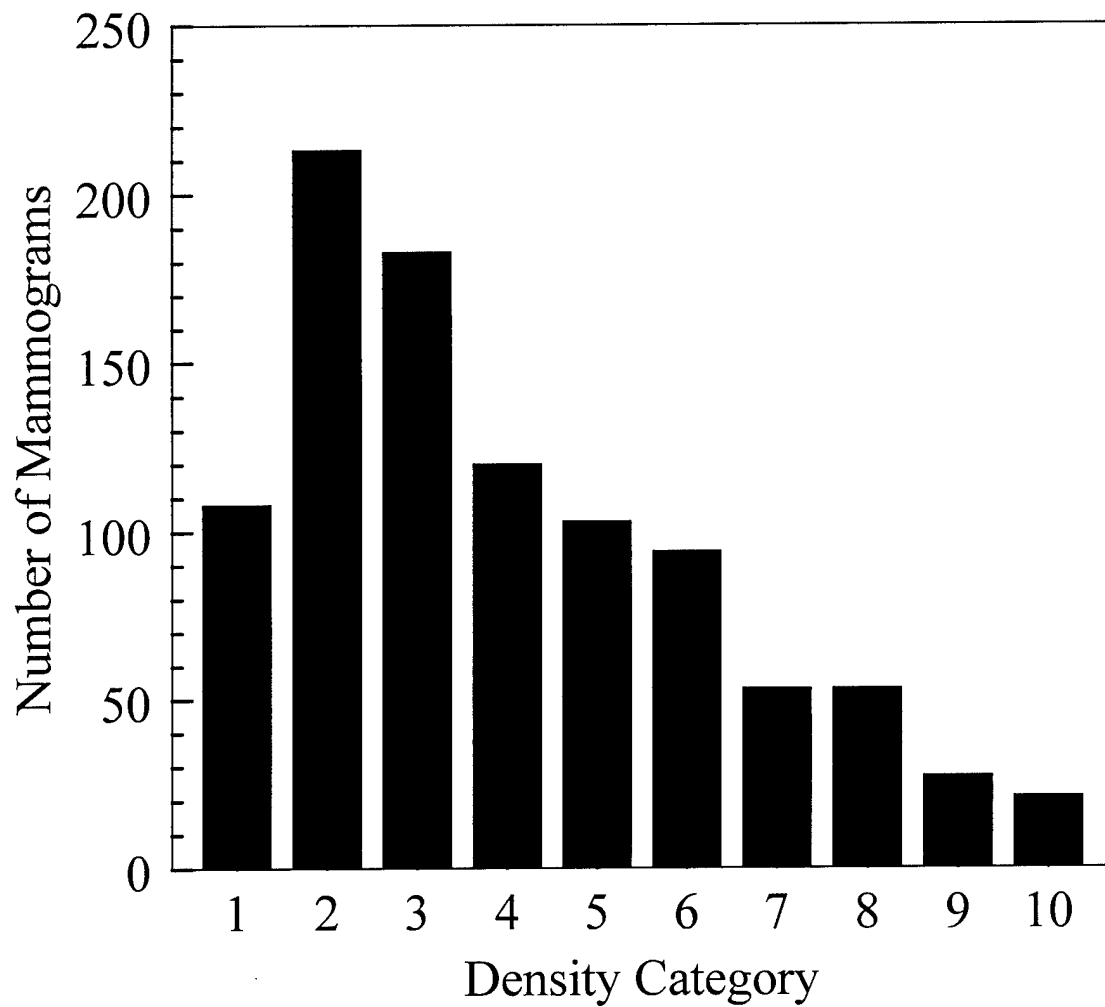


Figure 9

# Breast Density Index

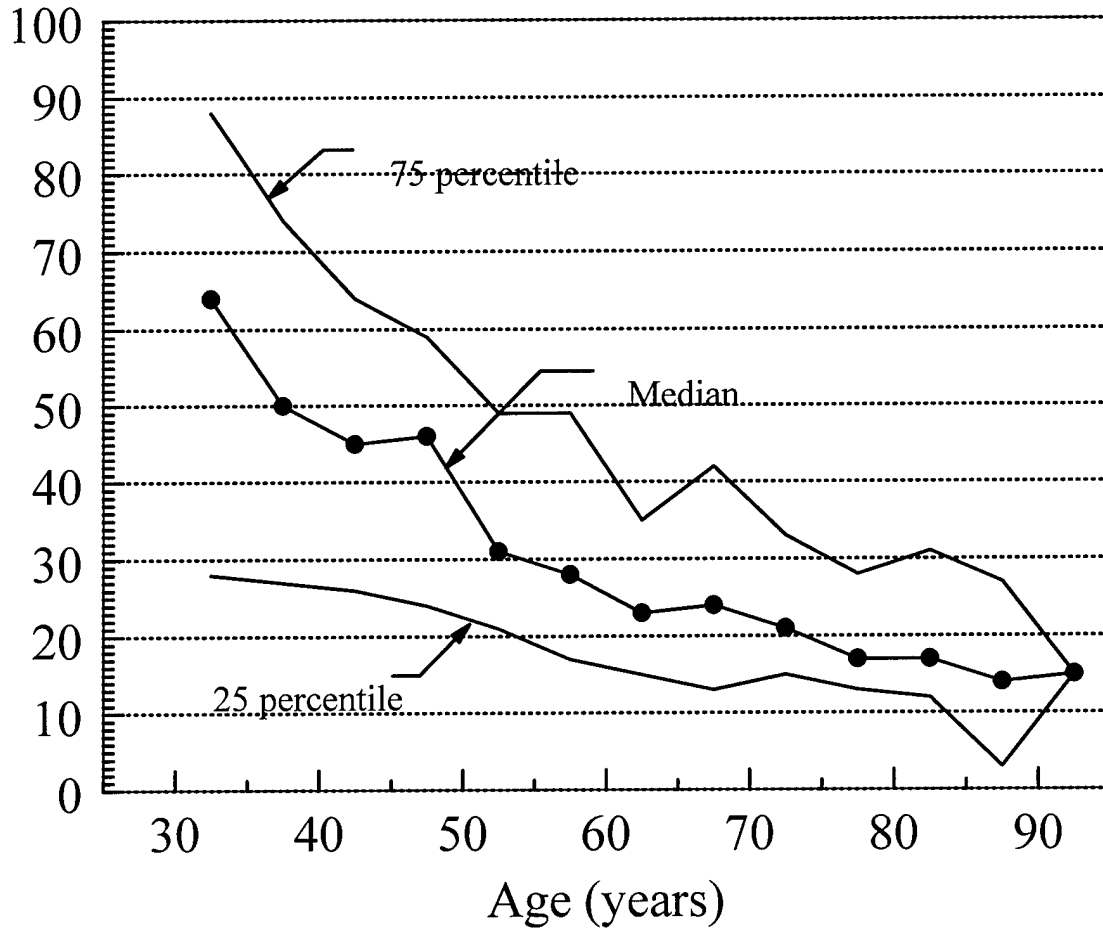


Figure 10

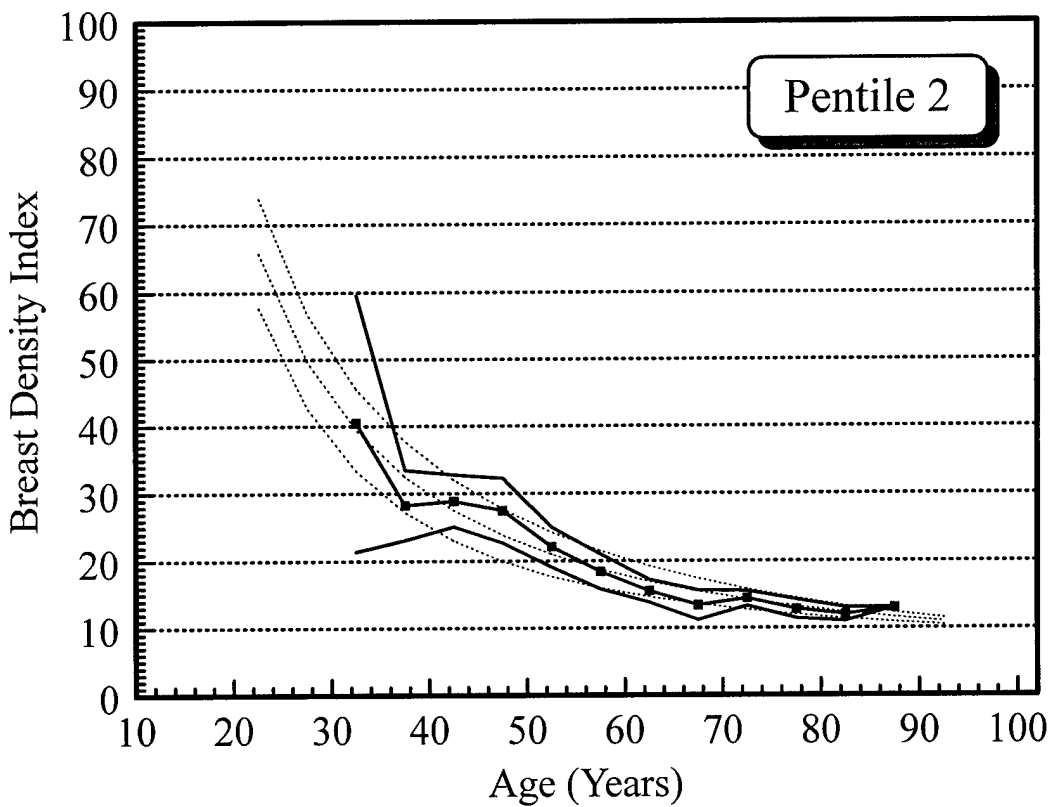
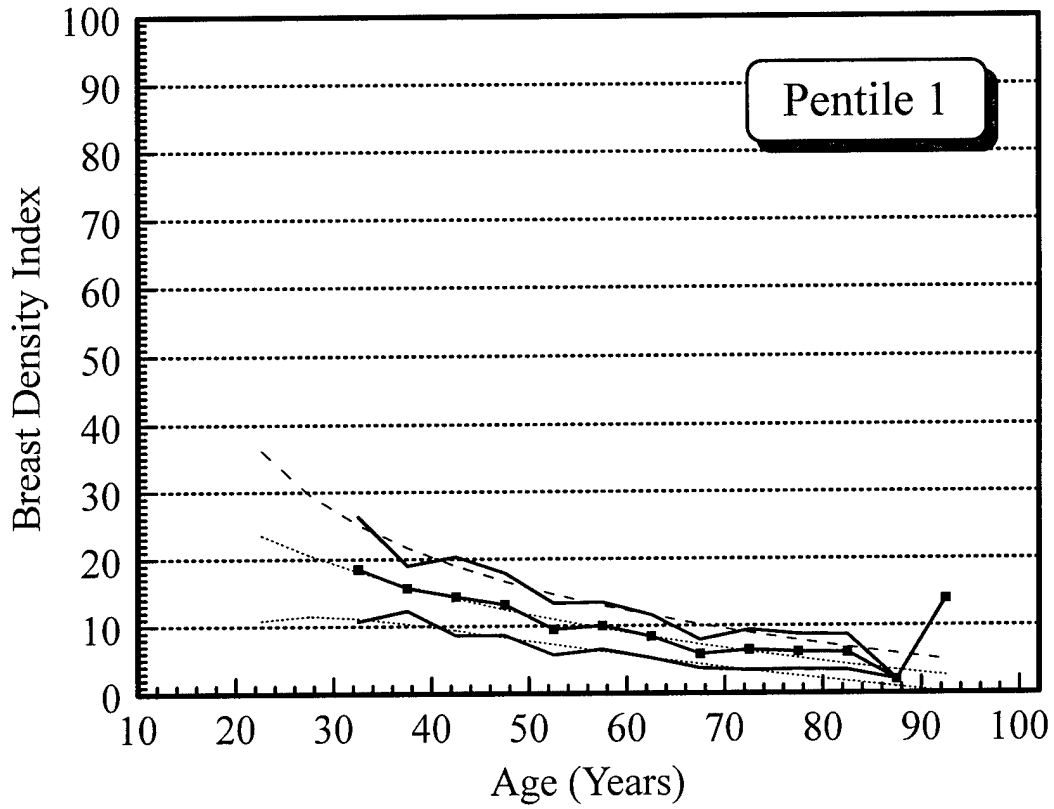


Figure 11

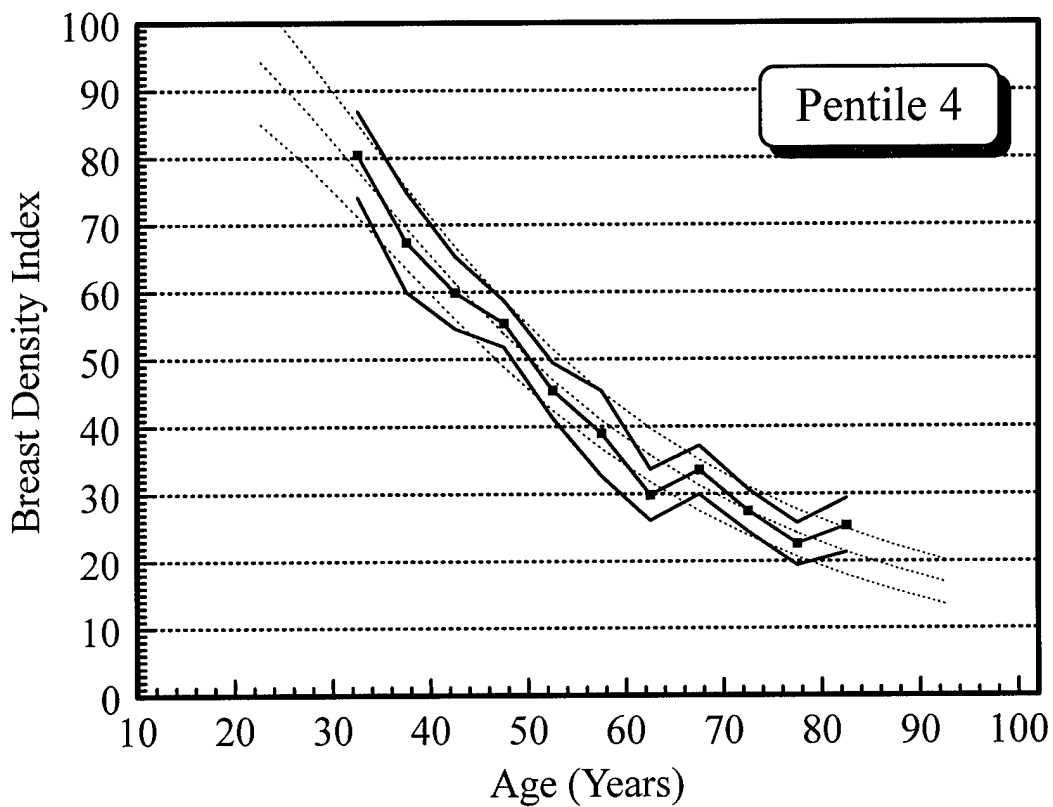
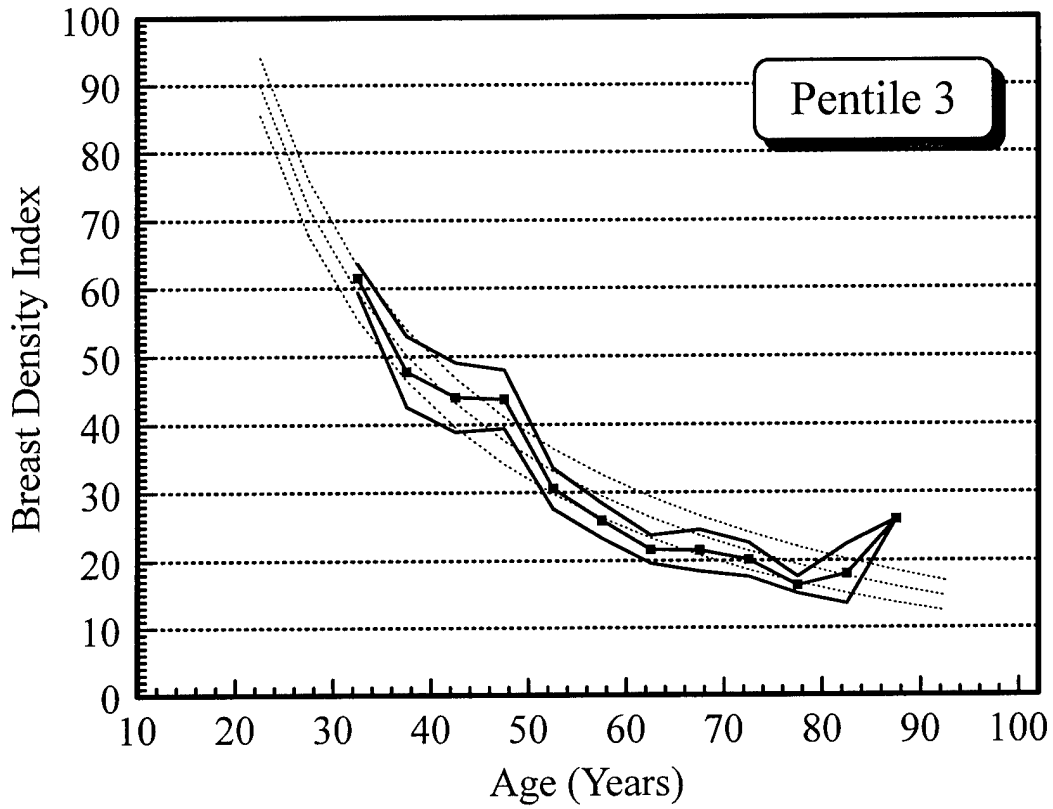


Figure 12

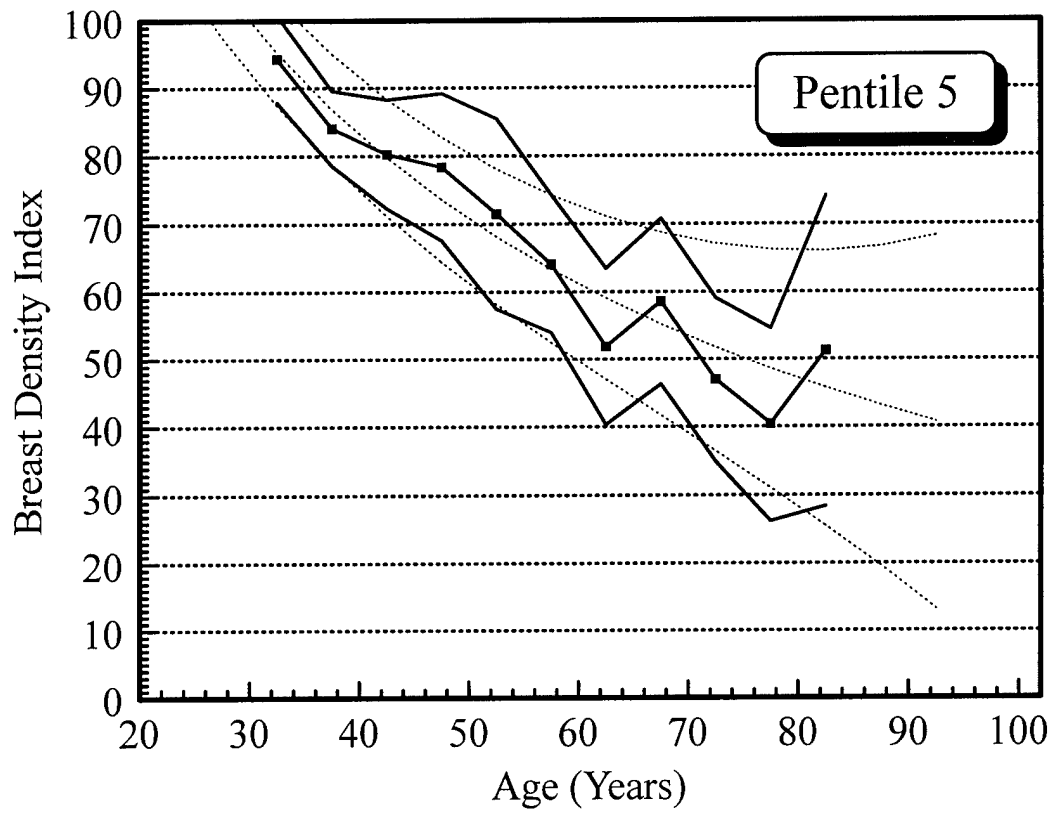


Figure 13

solid lines = original data  
dotted lines = generated data

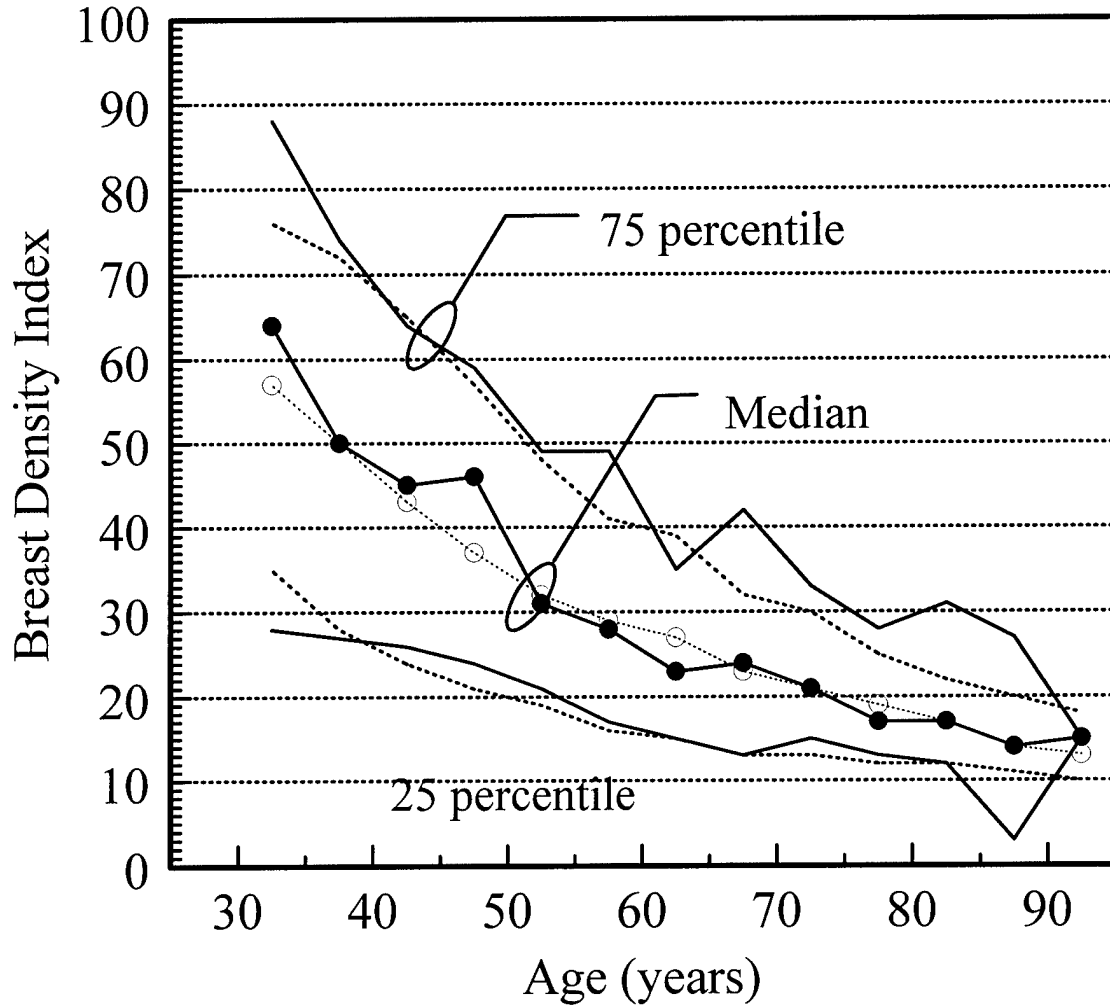


Figure 14

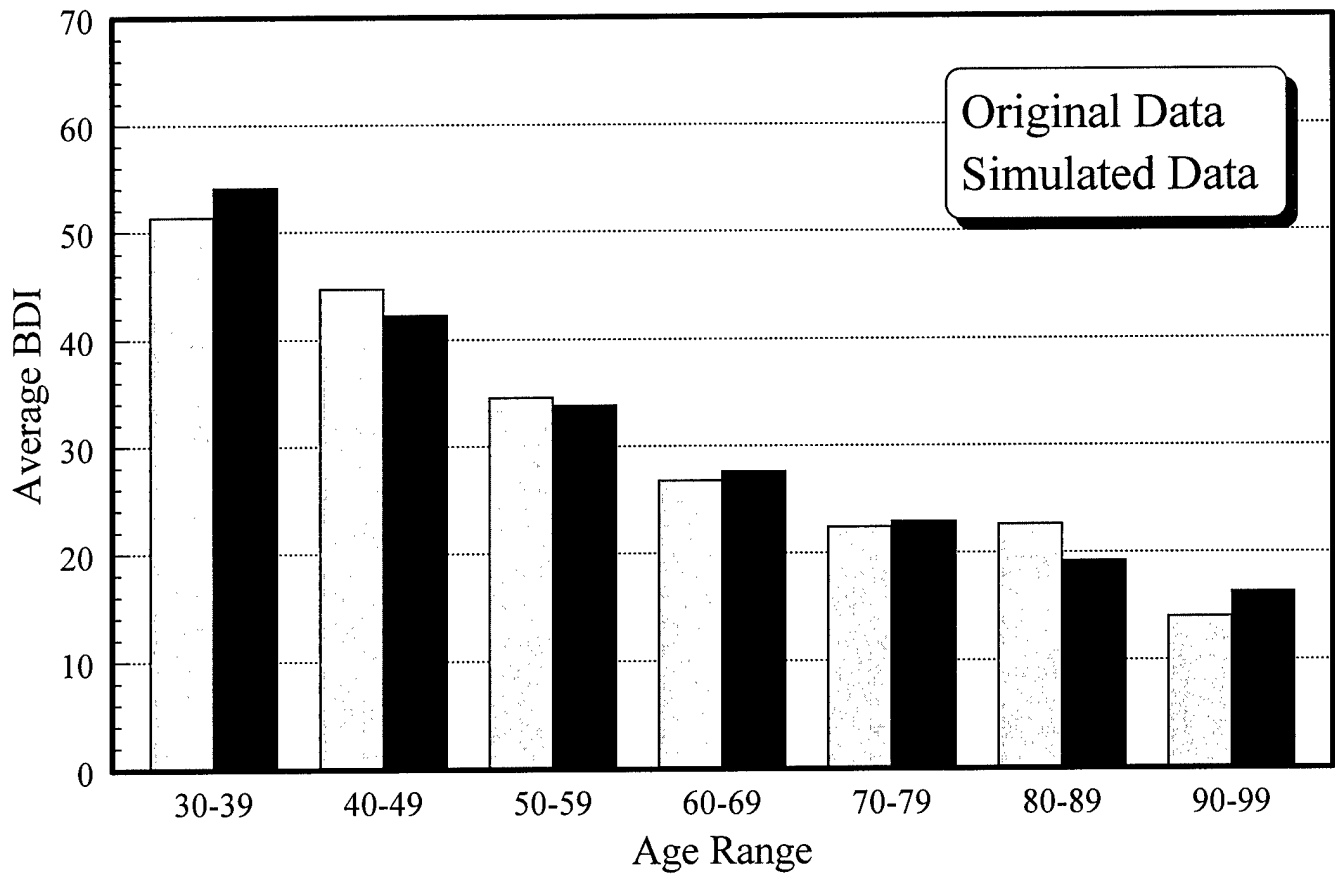


Figure 15

# Breast Density Index

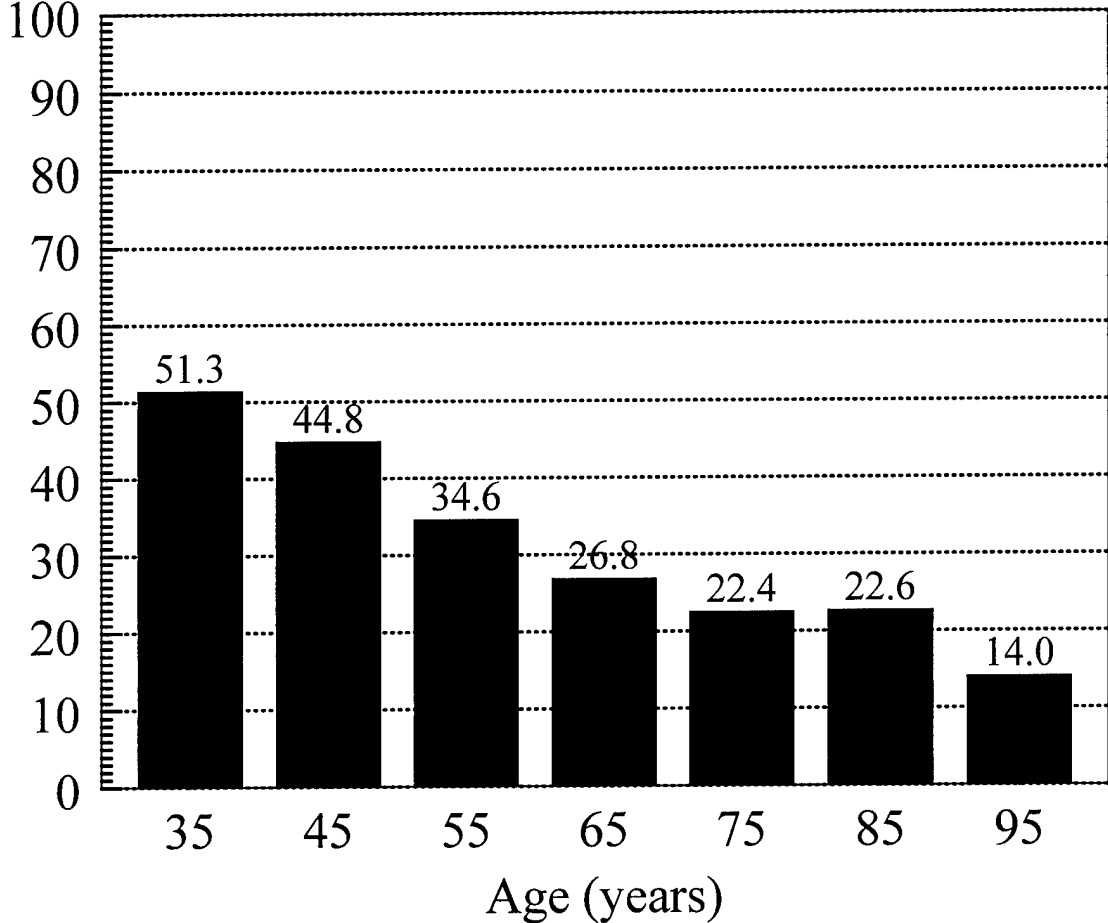
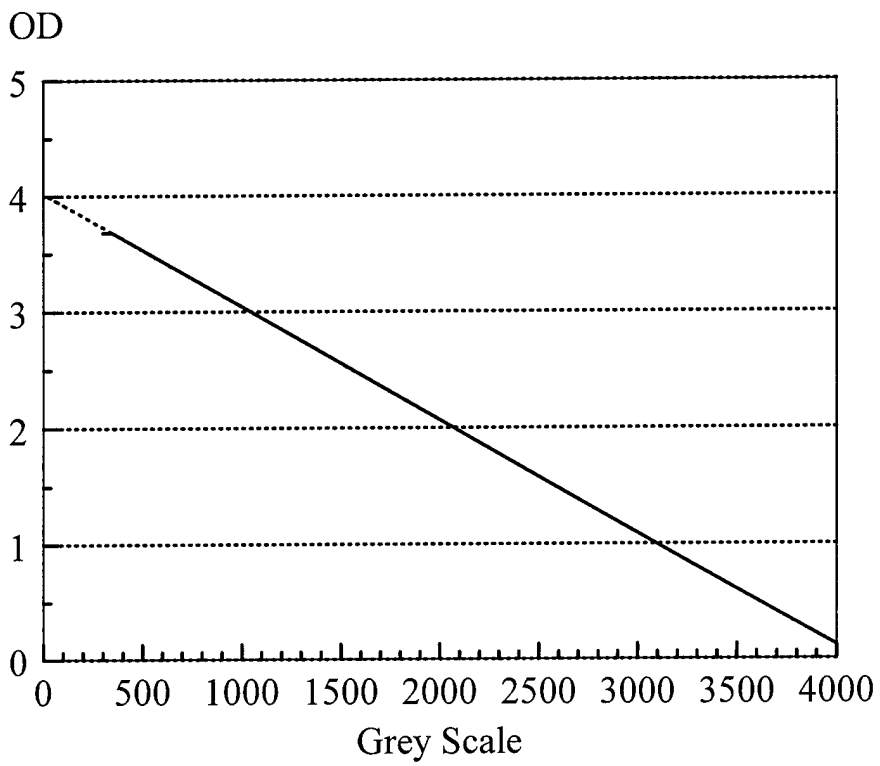
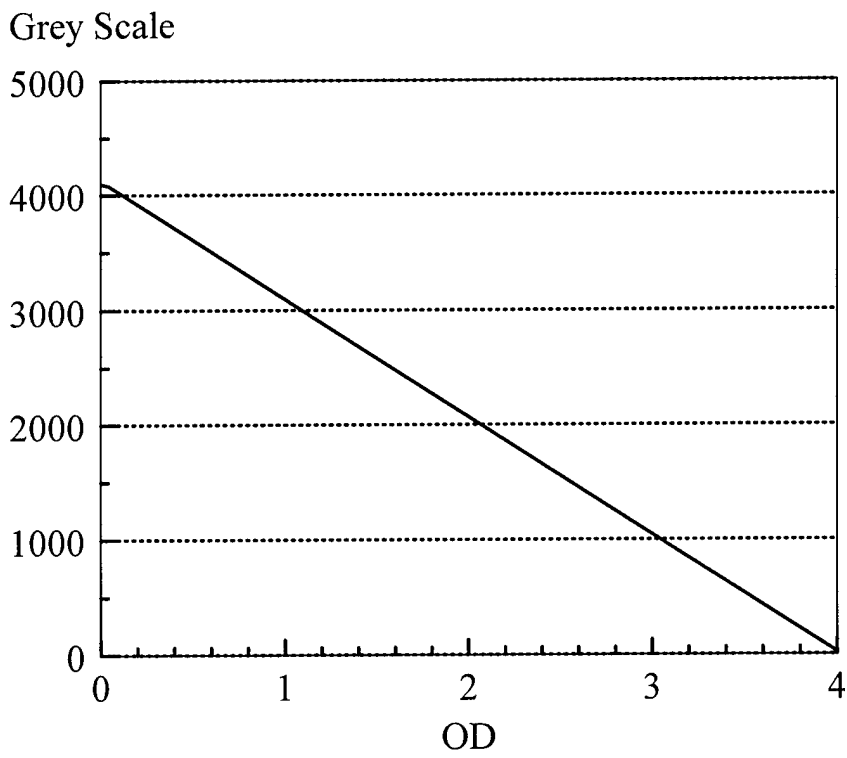


Figure 16

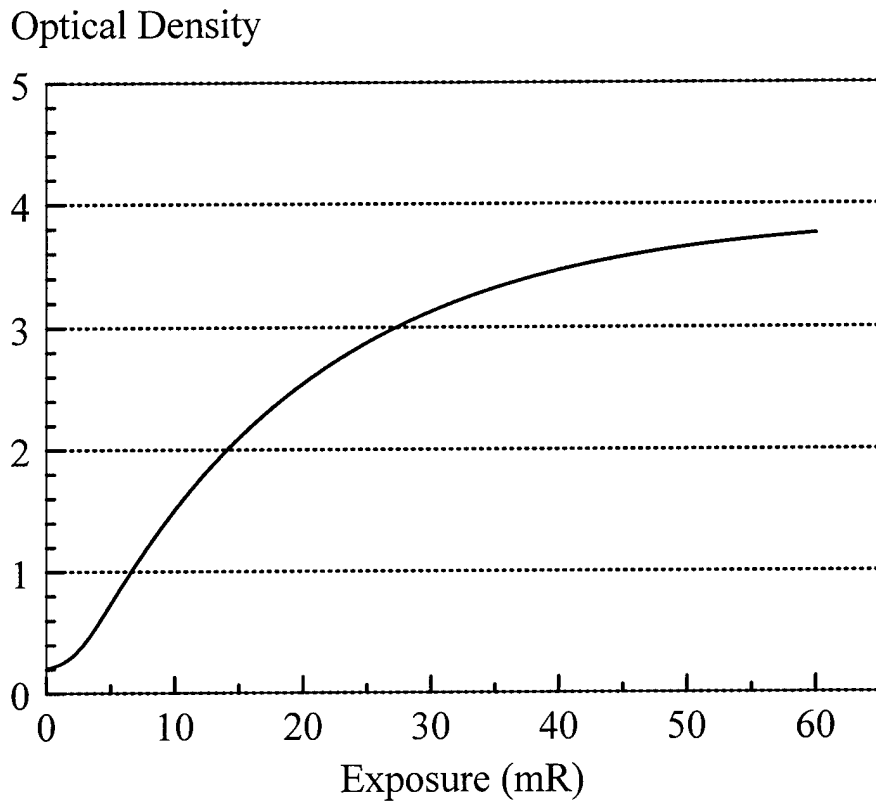


(a)

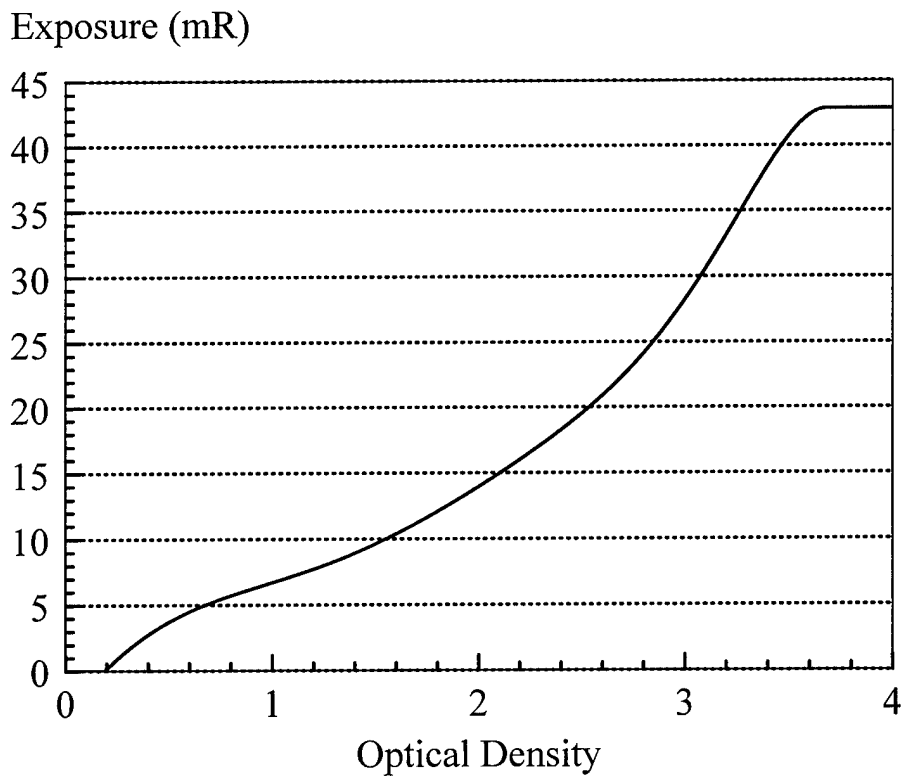


(b)

Figure 17

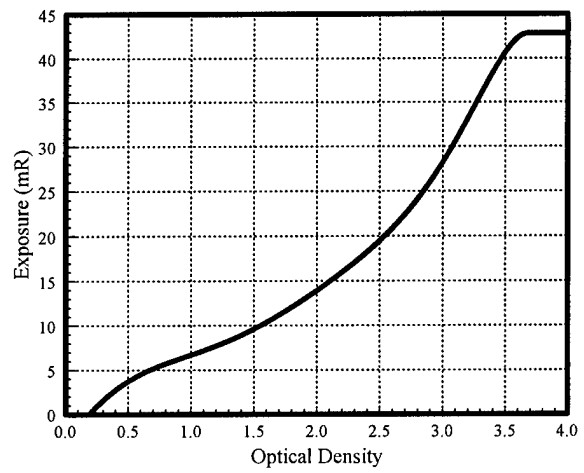
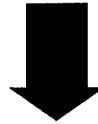
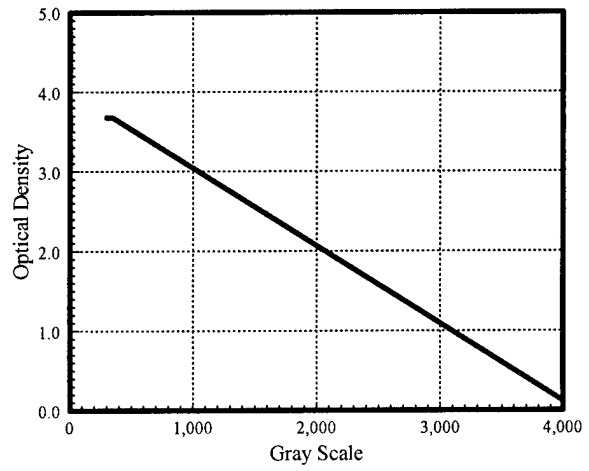
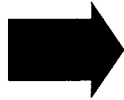
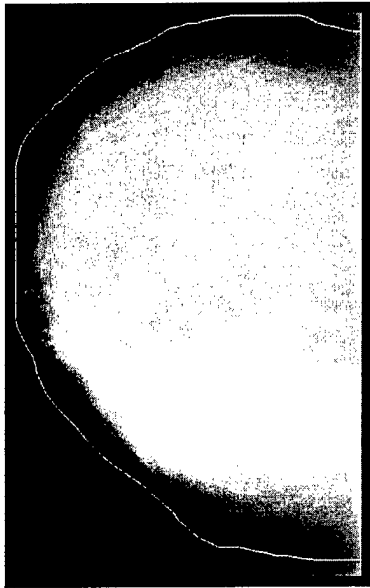


(a)



(b)

Figure 18



exposure



Figure 19

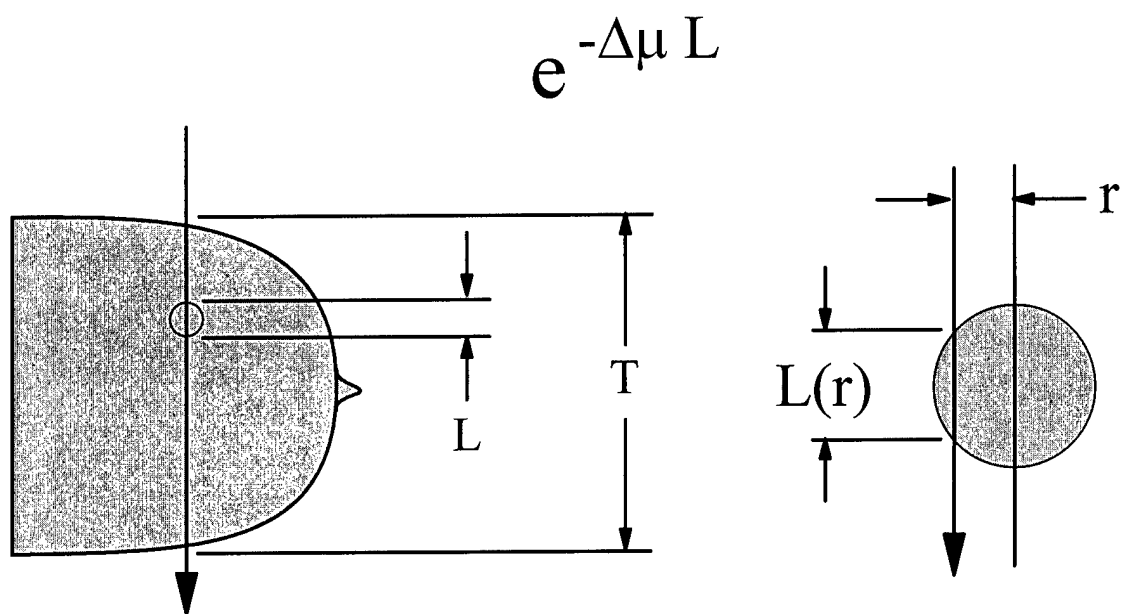


Figure 20

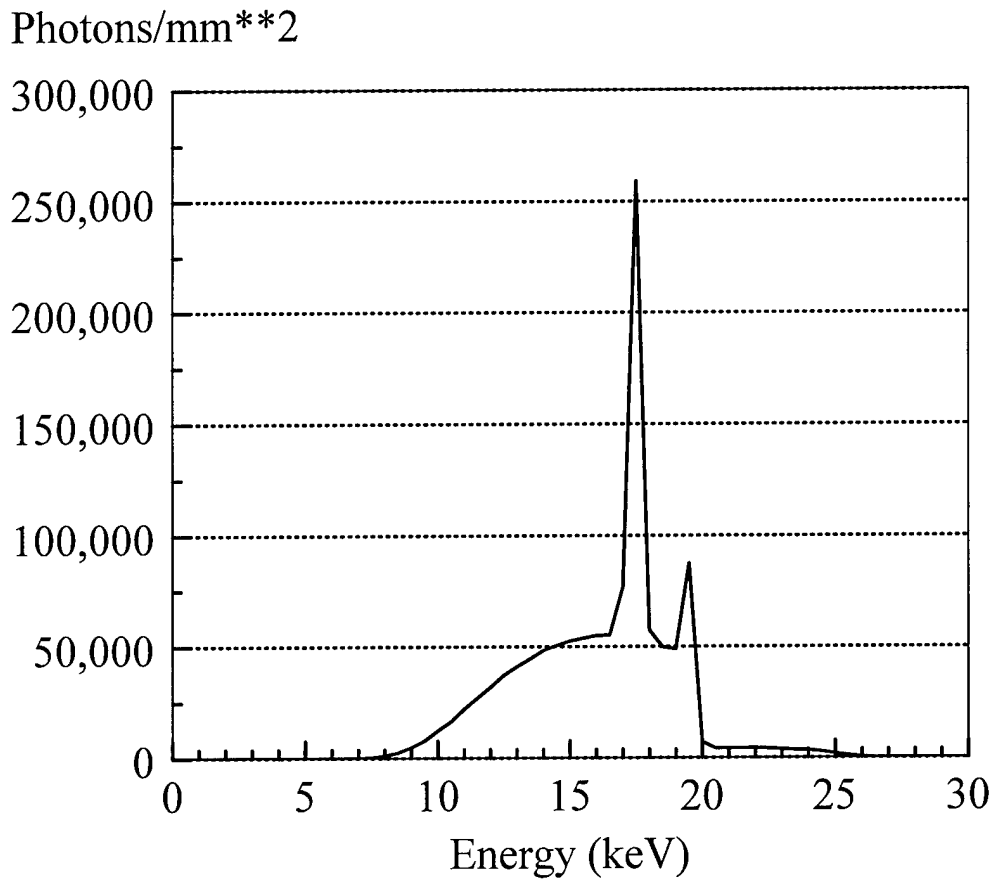


Figure 21

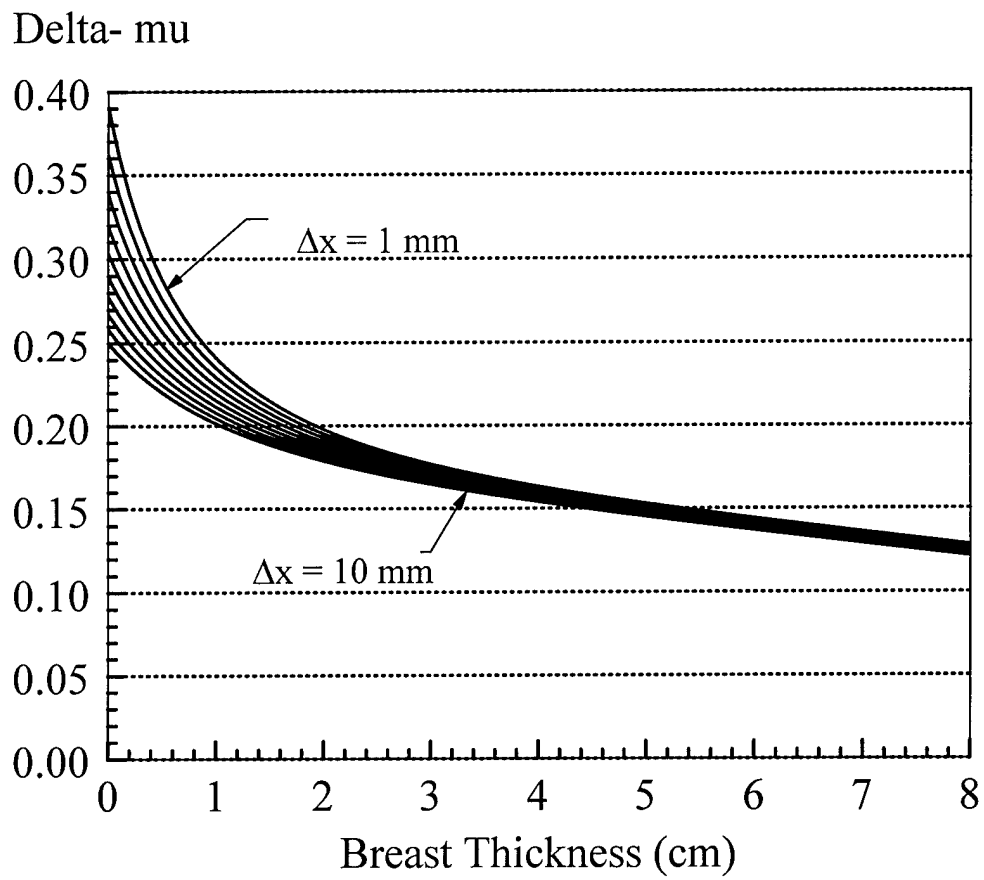
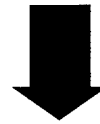
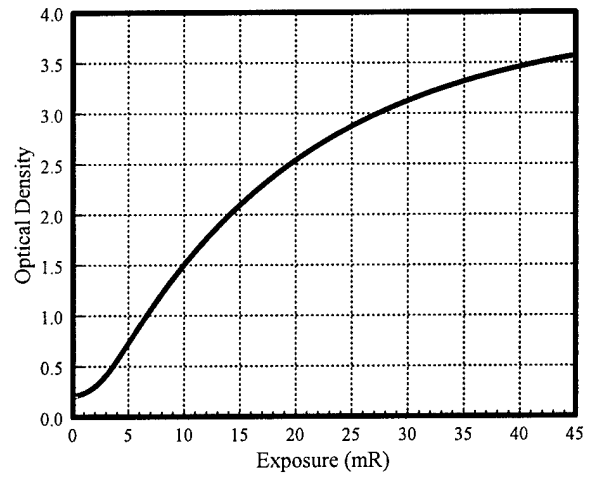
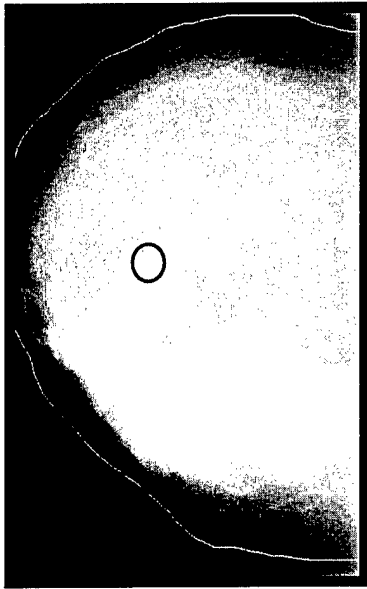


Figure 22

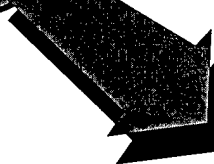
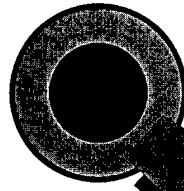


$$T = 10^{-OD}$$

Figure 23

Lesion

Background



$\bar{T}_{\text{lesion}}$

$\bar{T}_{\text{bg}}$

$$d = \frac{\bar{T}_{\text{lesion}}}{\bar{T}_{\text{bg}}}$$

Figure 24

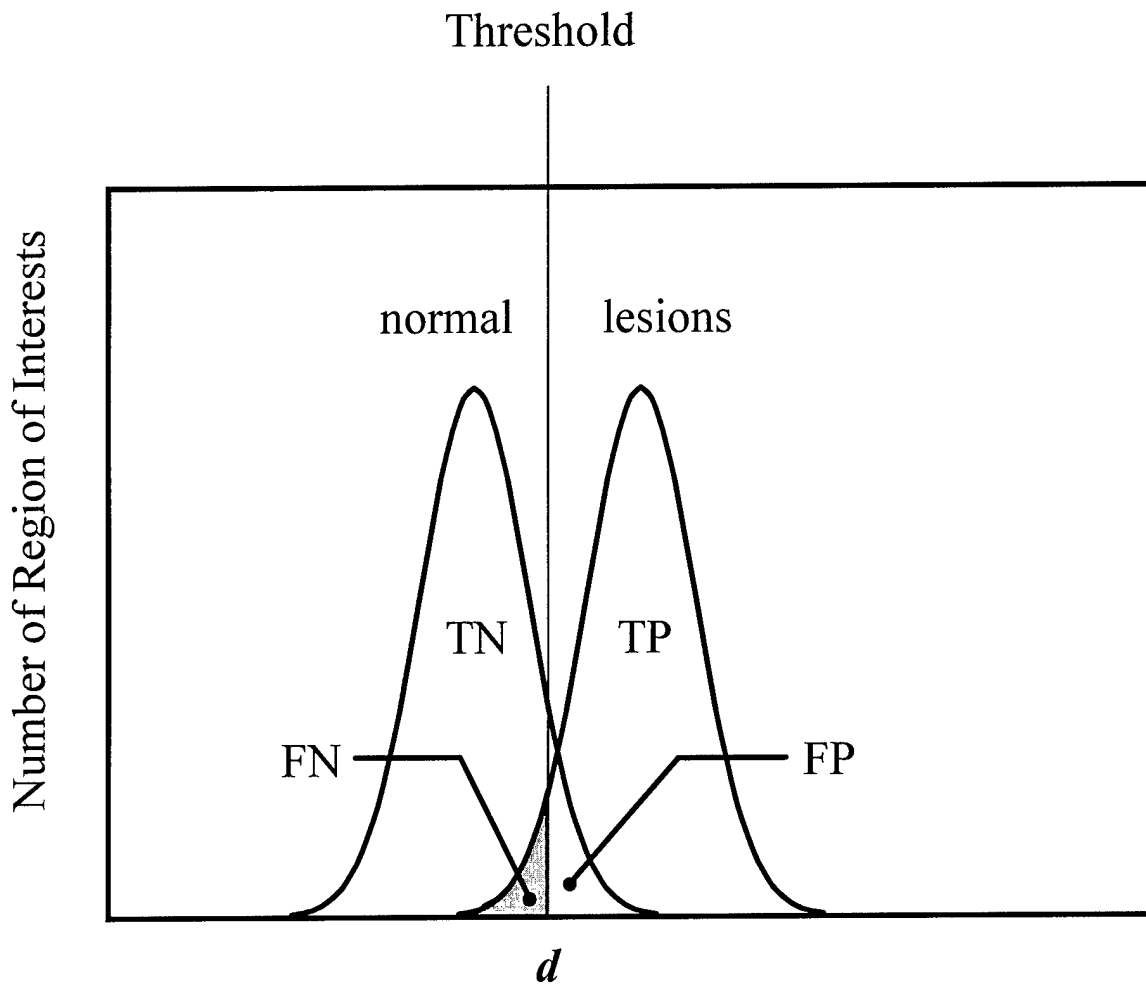


Figure 25

# ROC Curve

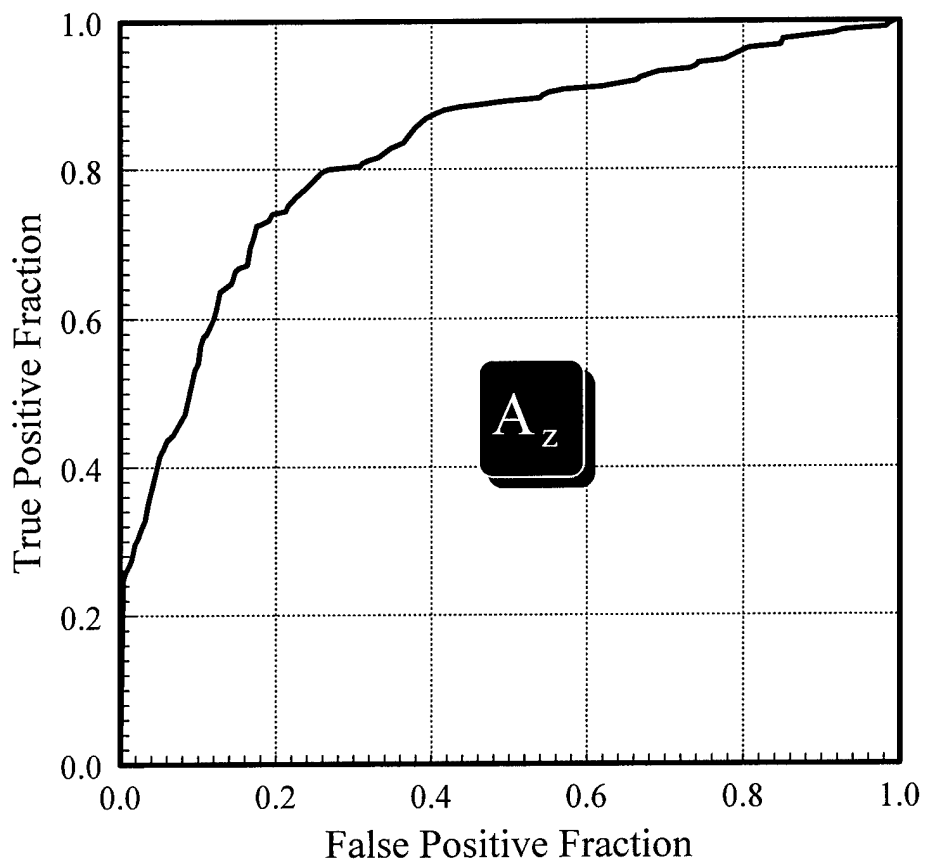


Figure 26

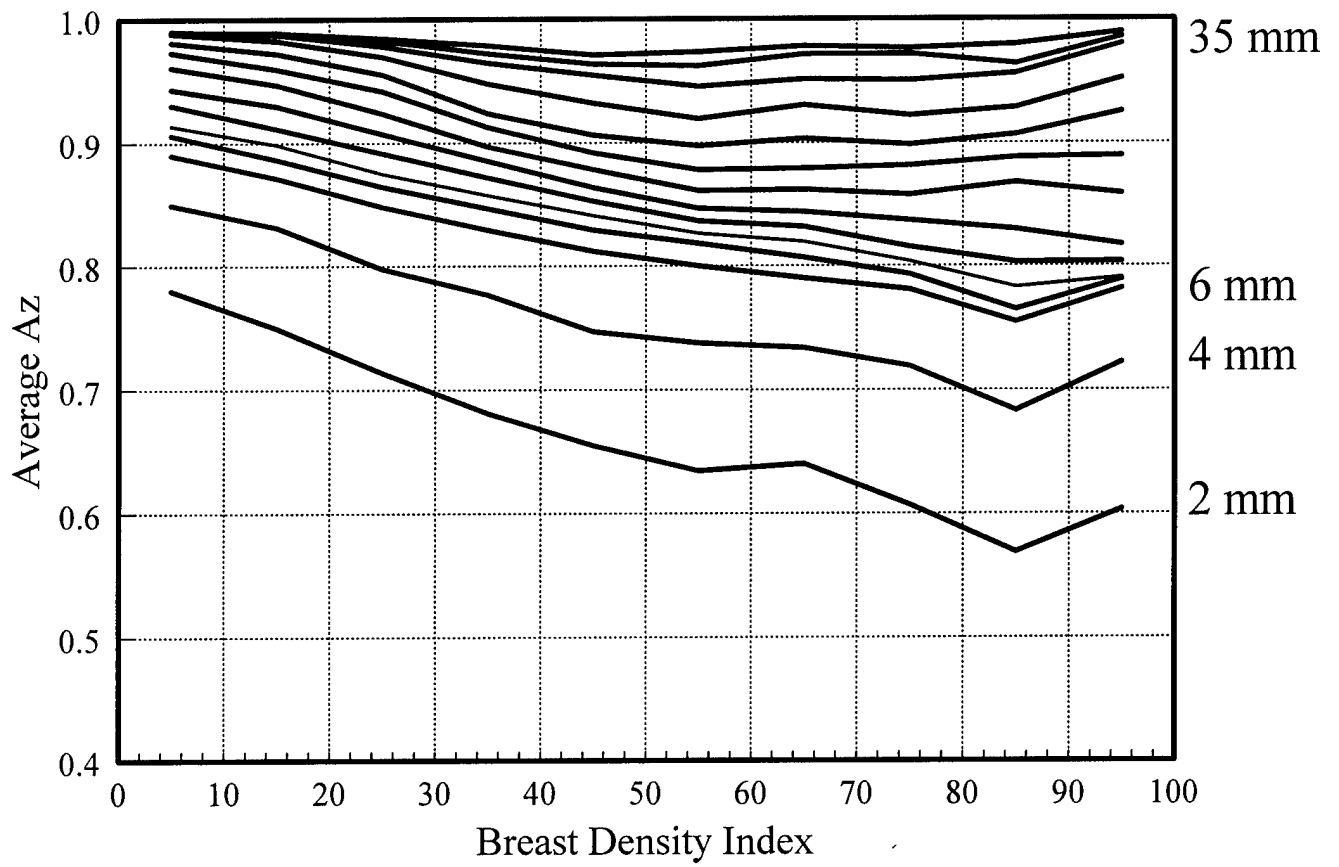


Figure 27

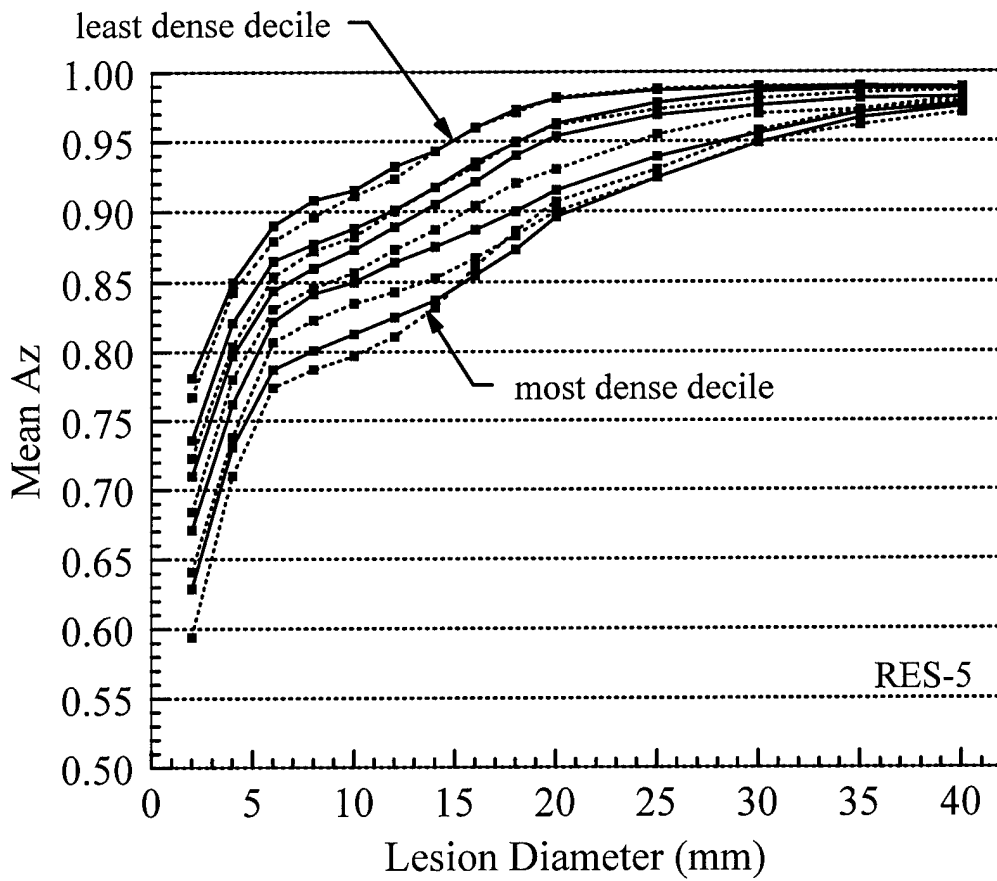


Figure 28

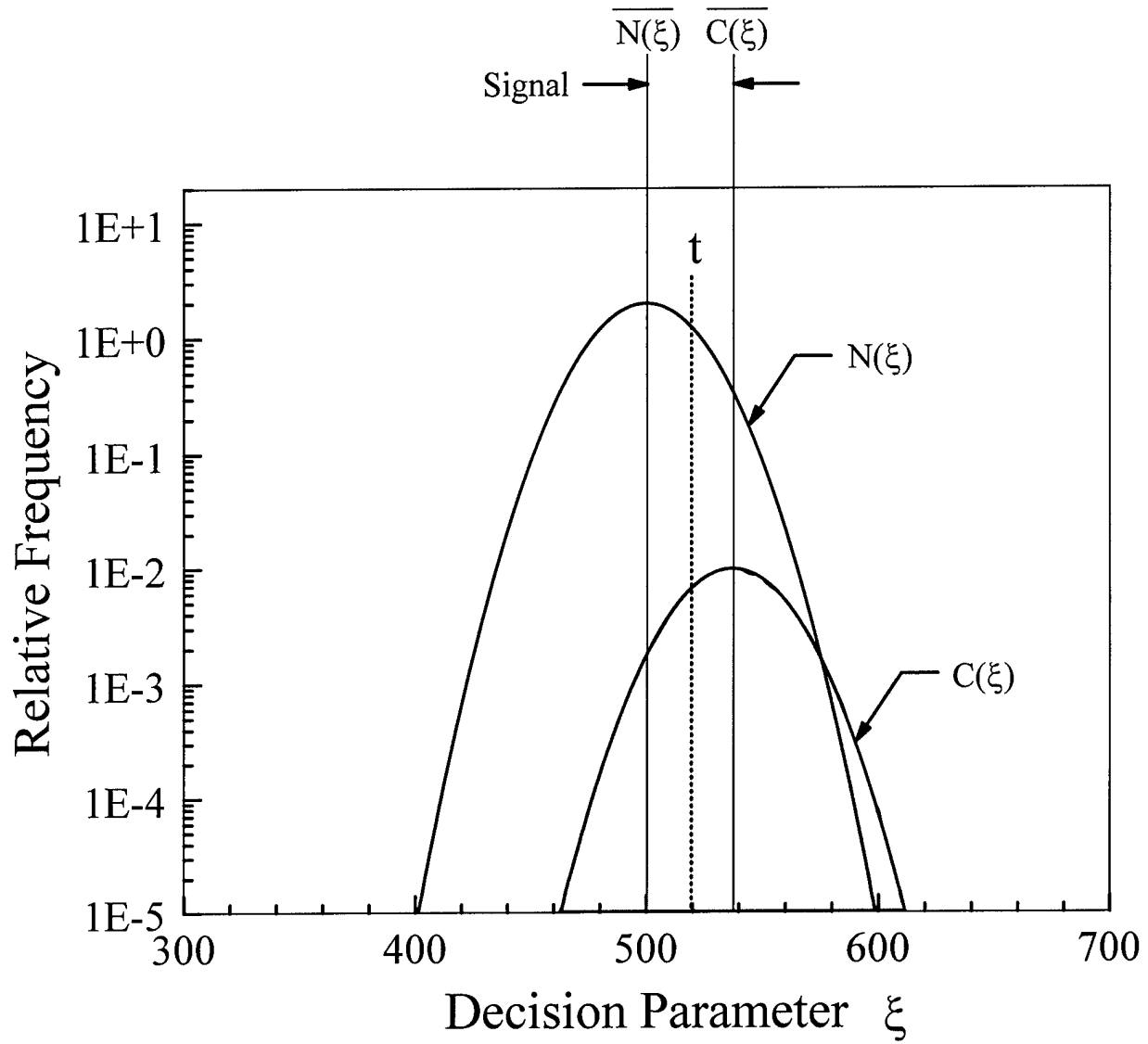


Figure 29

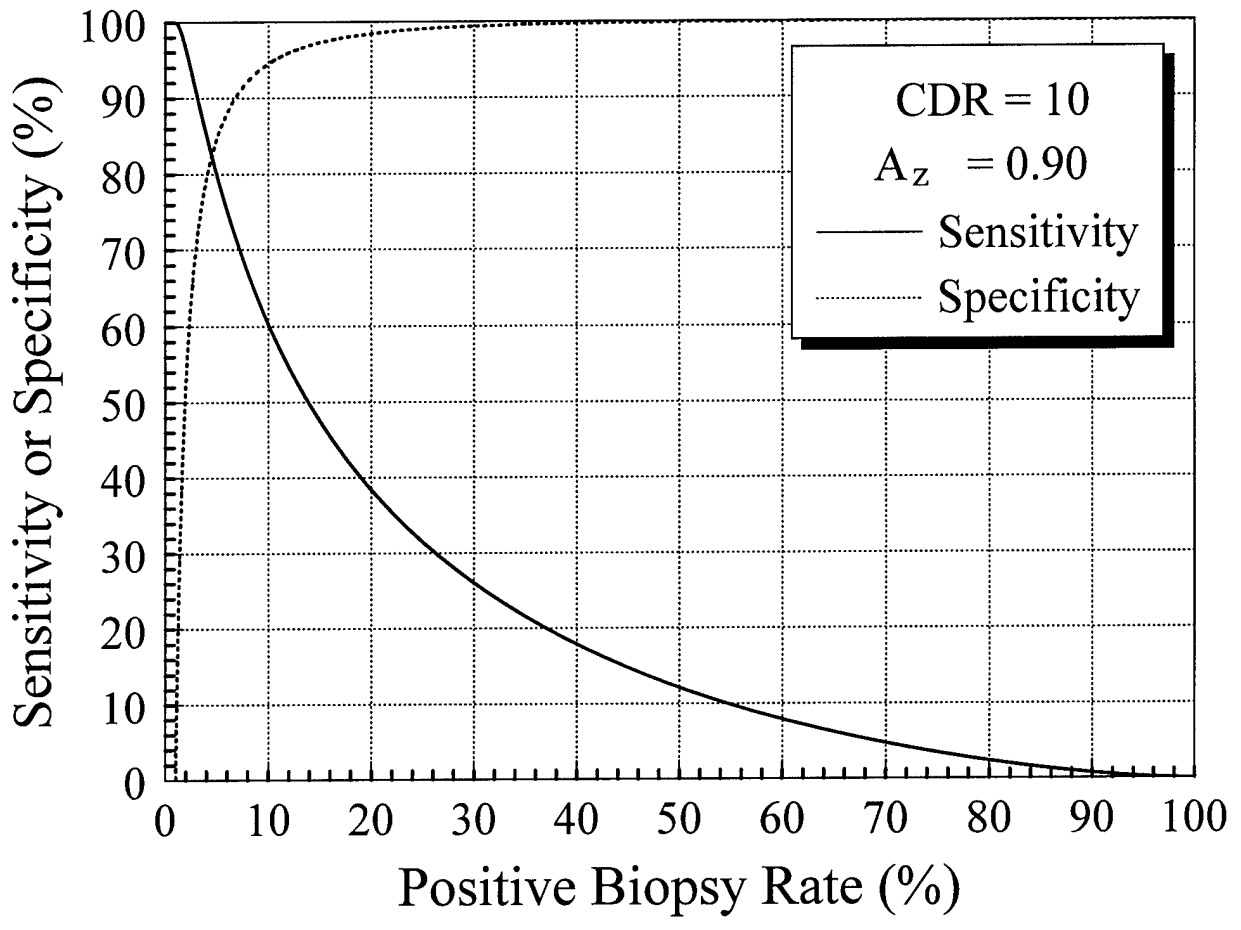


Figure 30

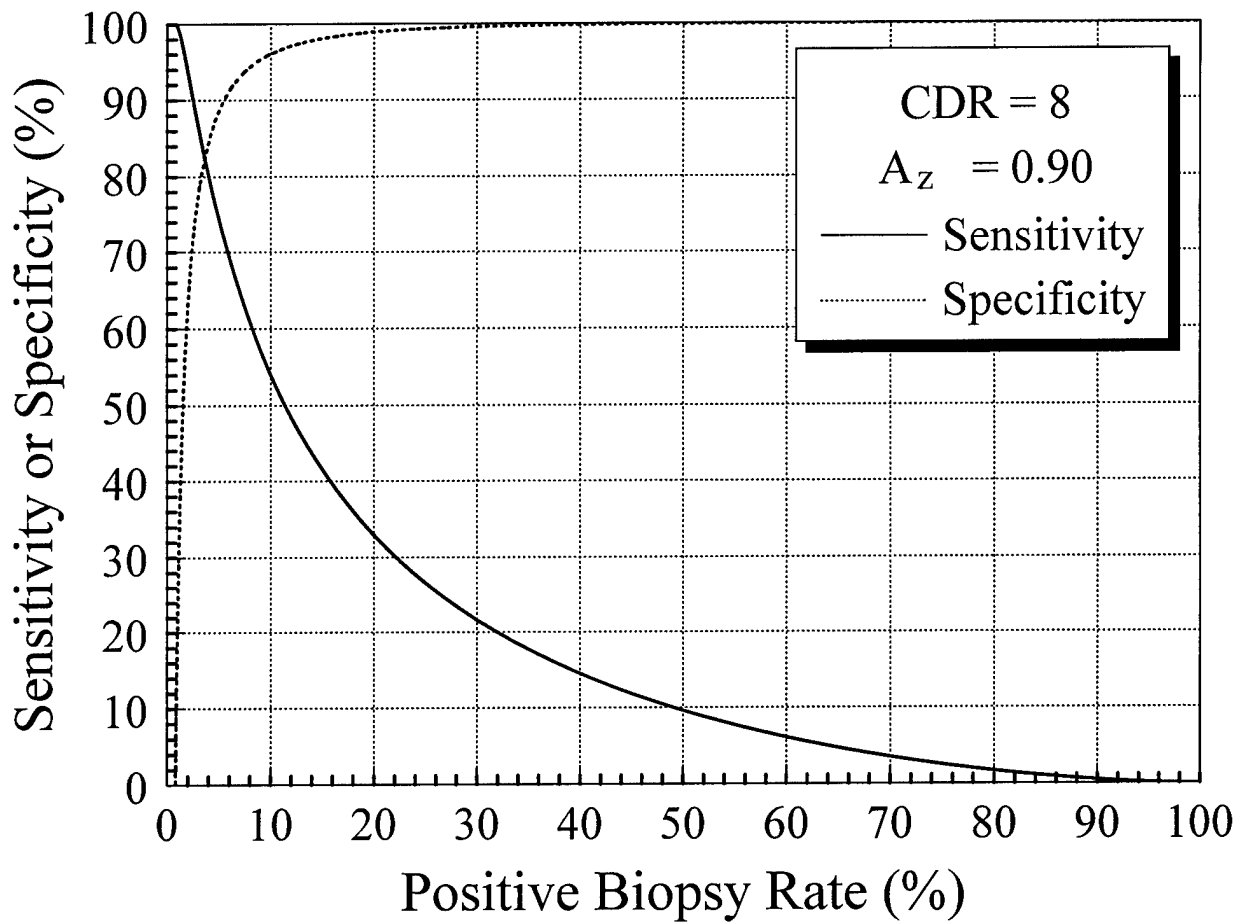


Figure 31

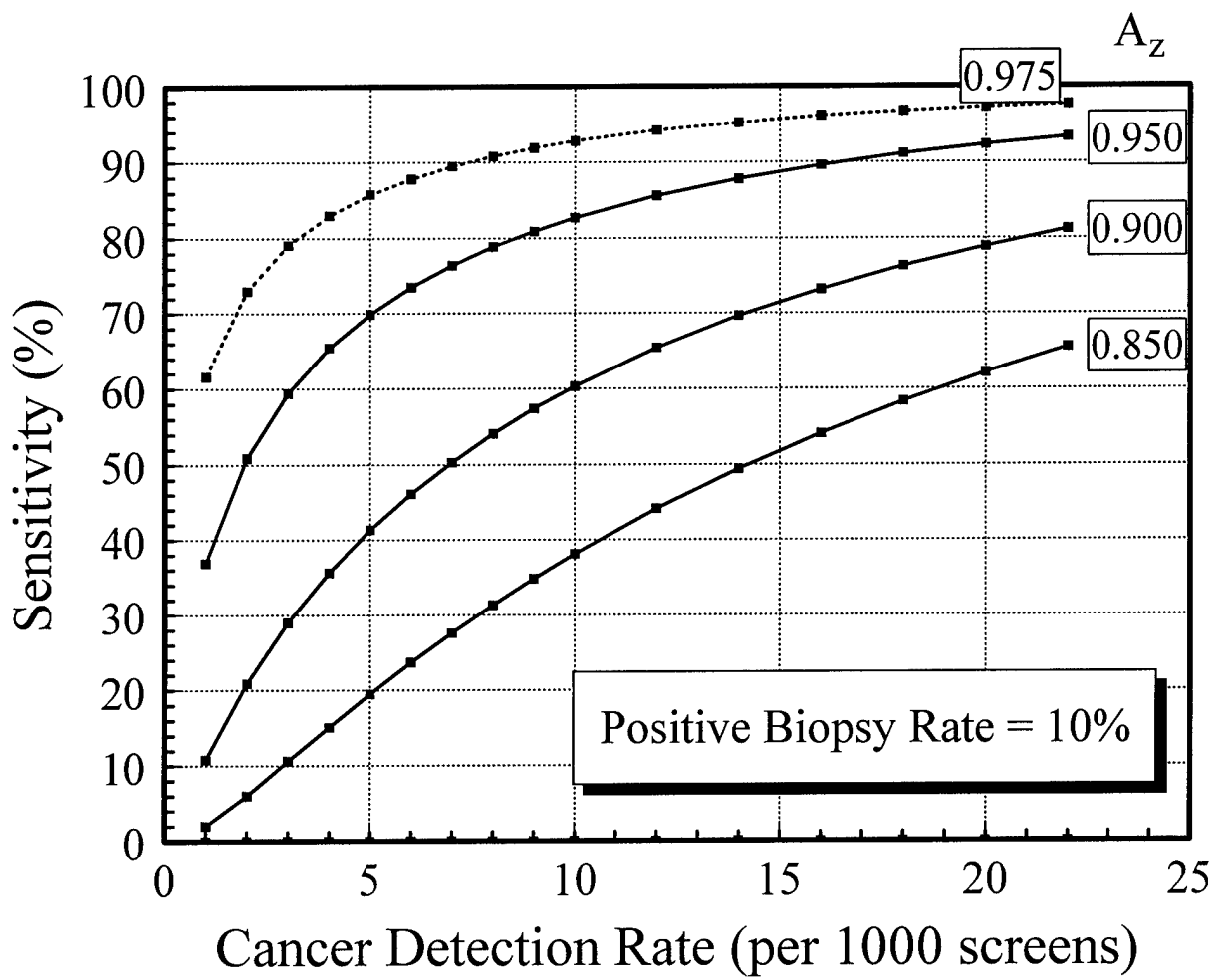


Figure 32

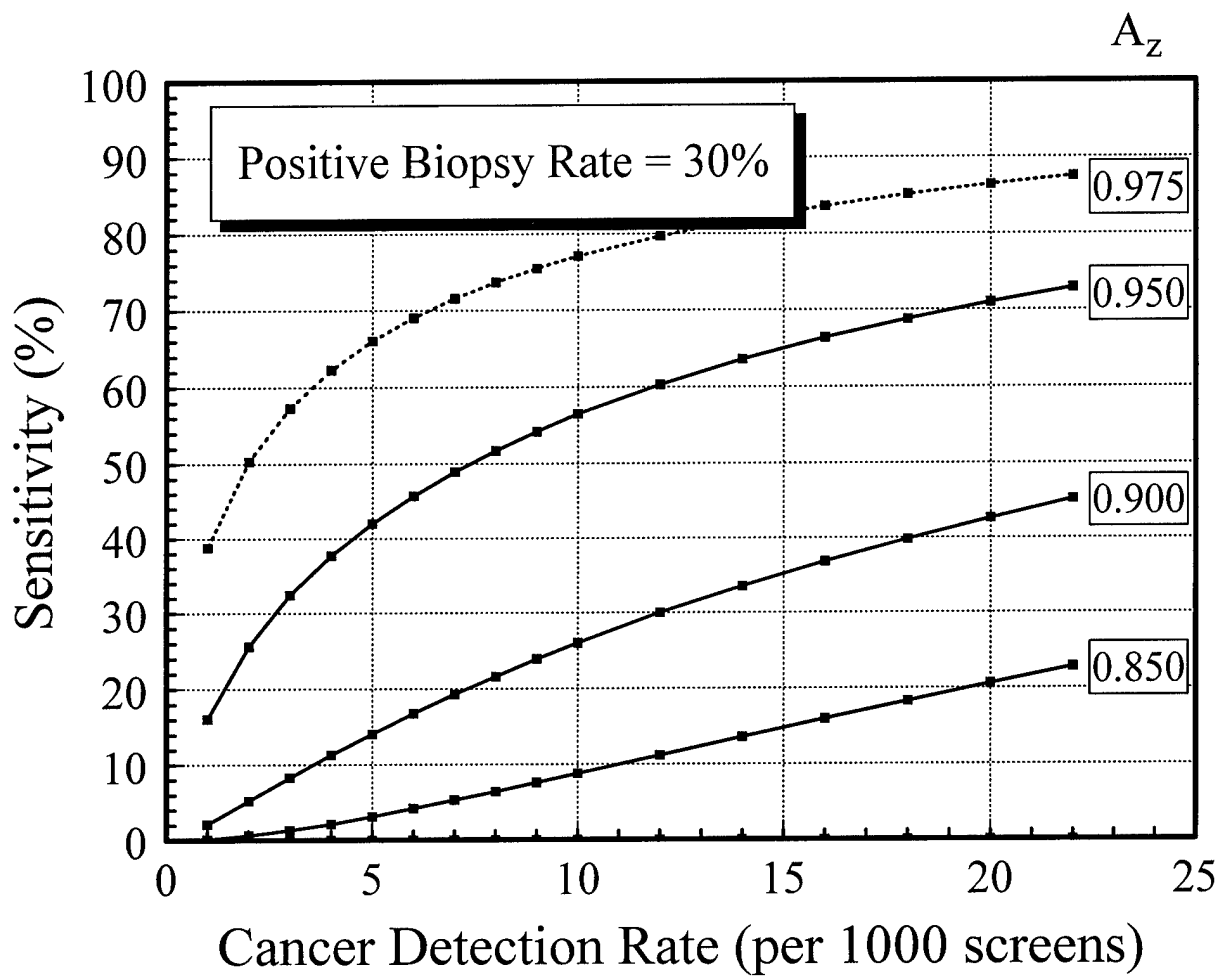


Figure 33

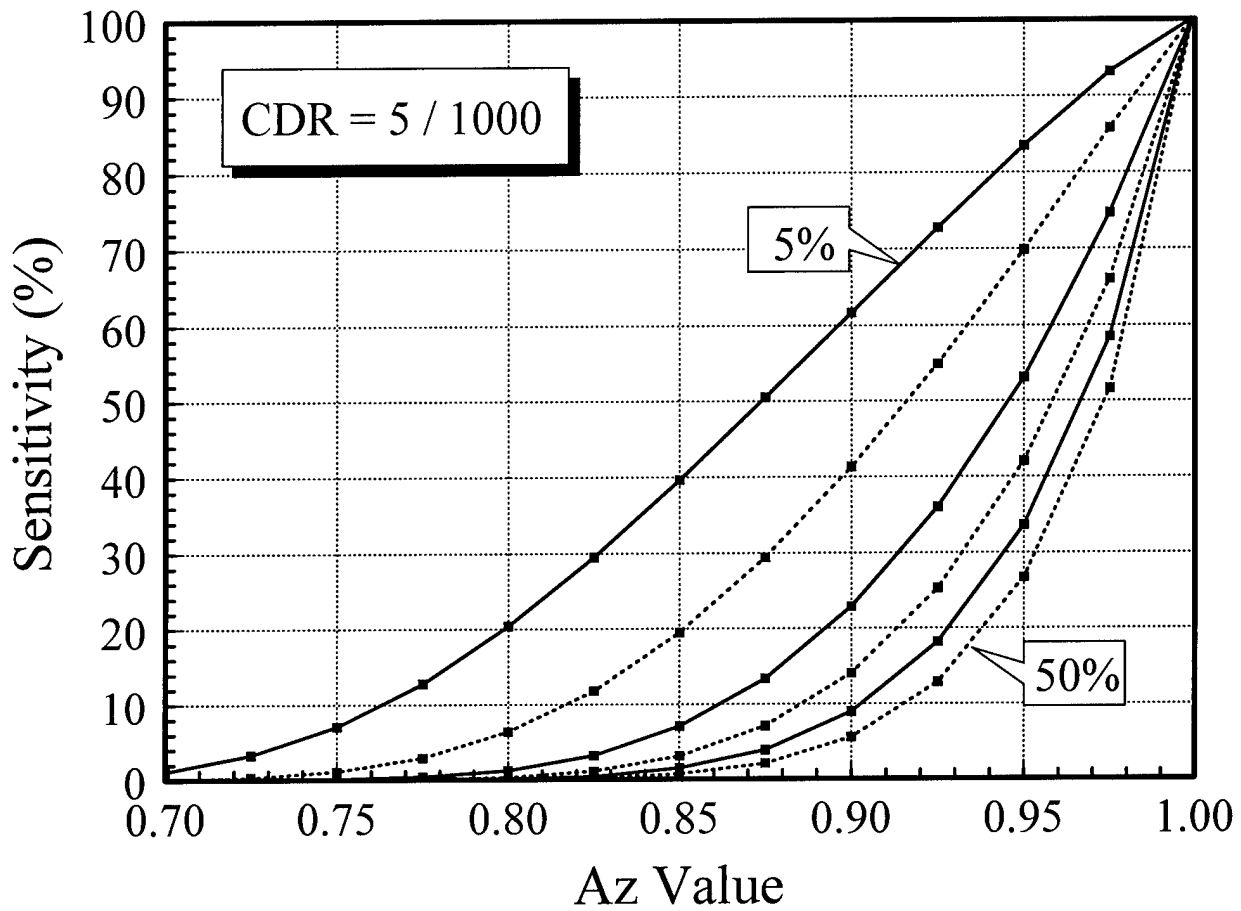


Figure 34

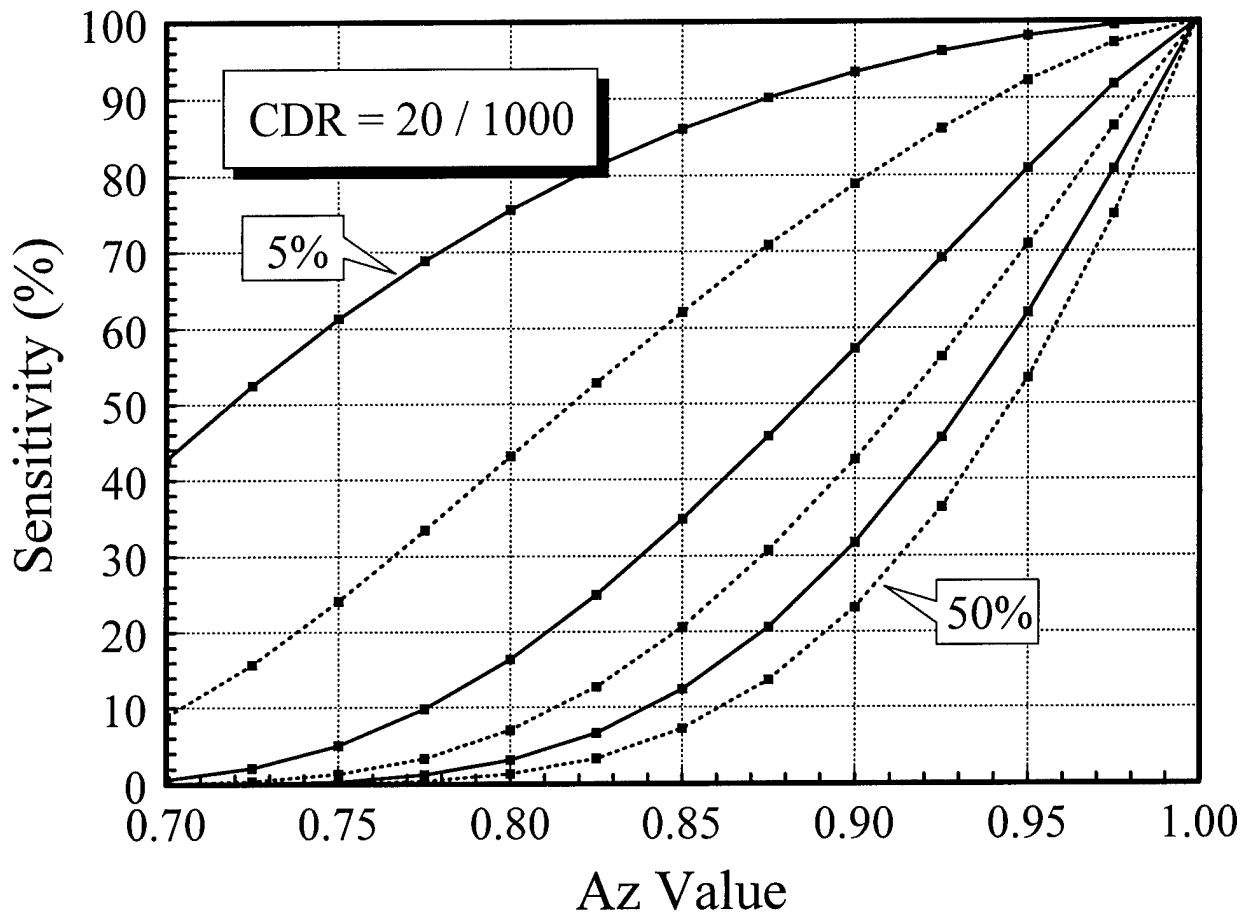


Figure 35

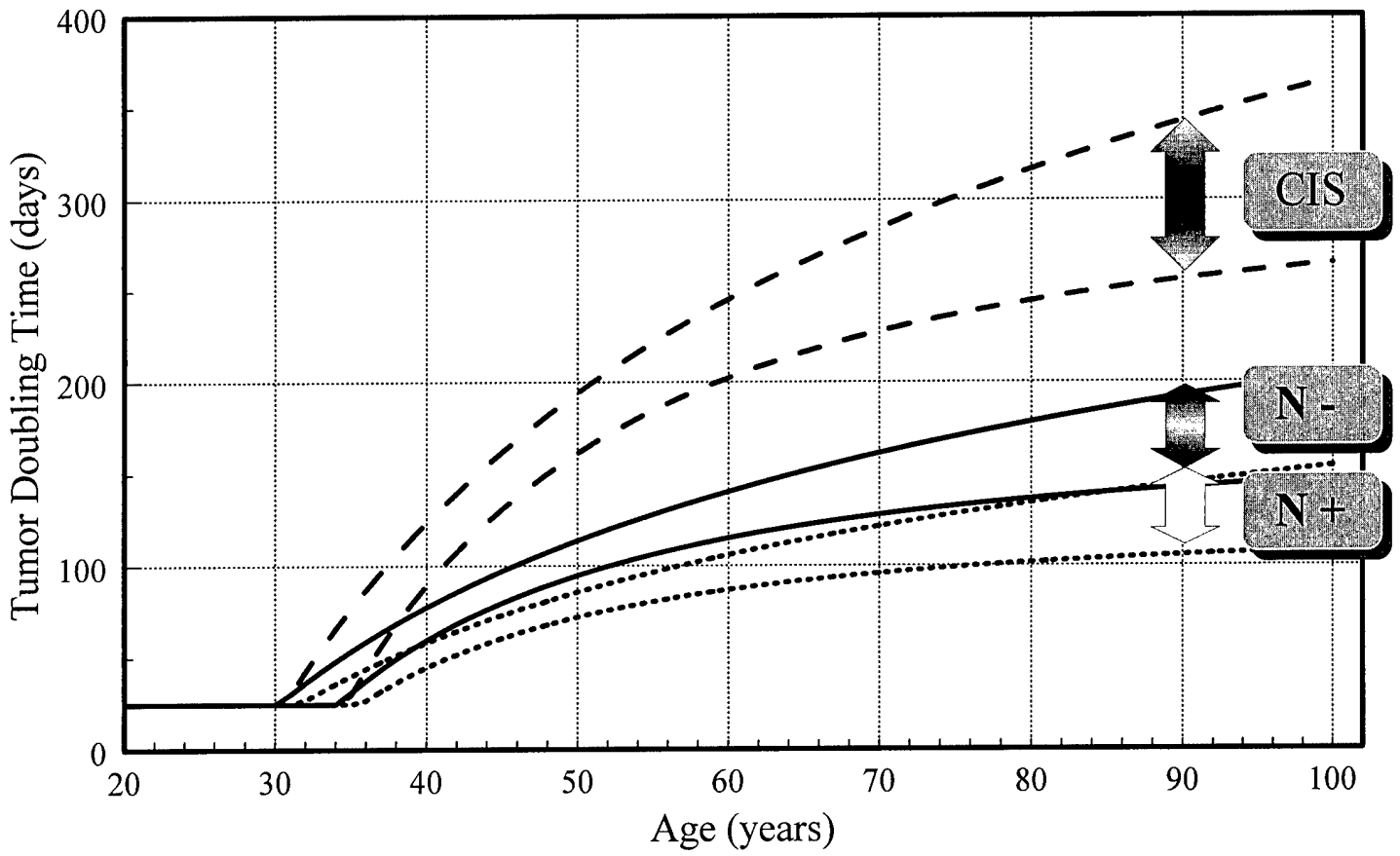


Figure 36

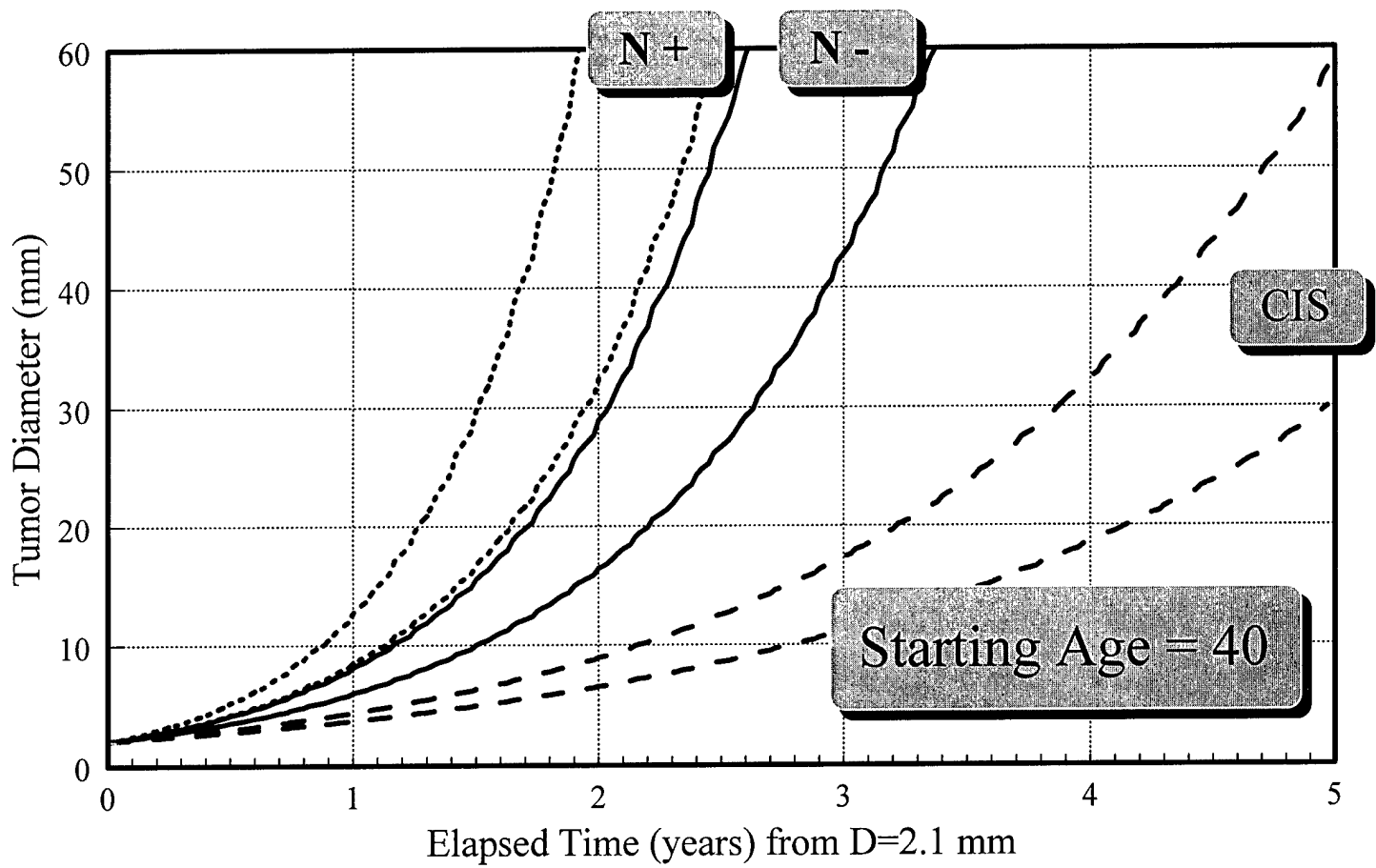


Figure 37

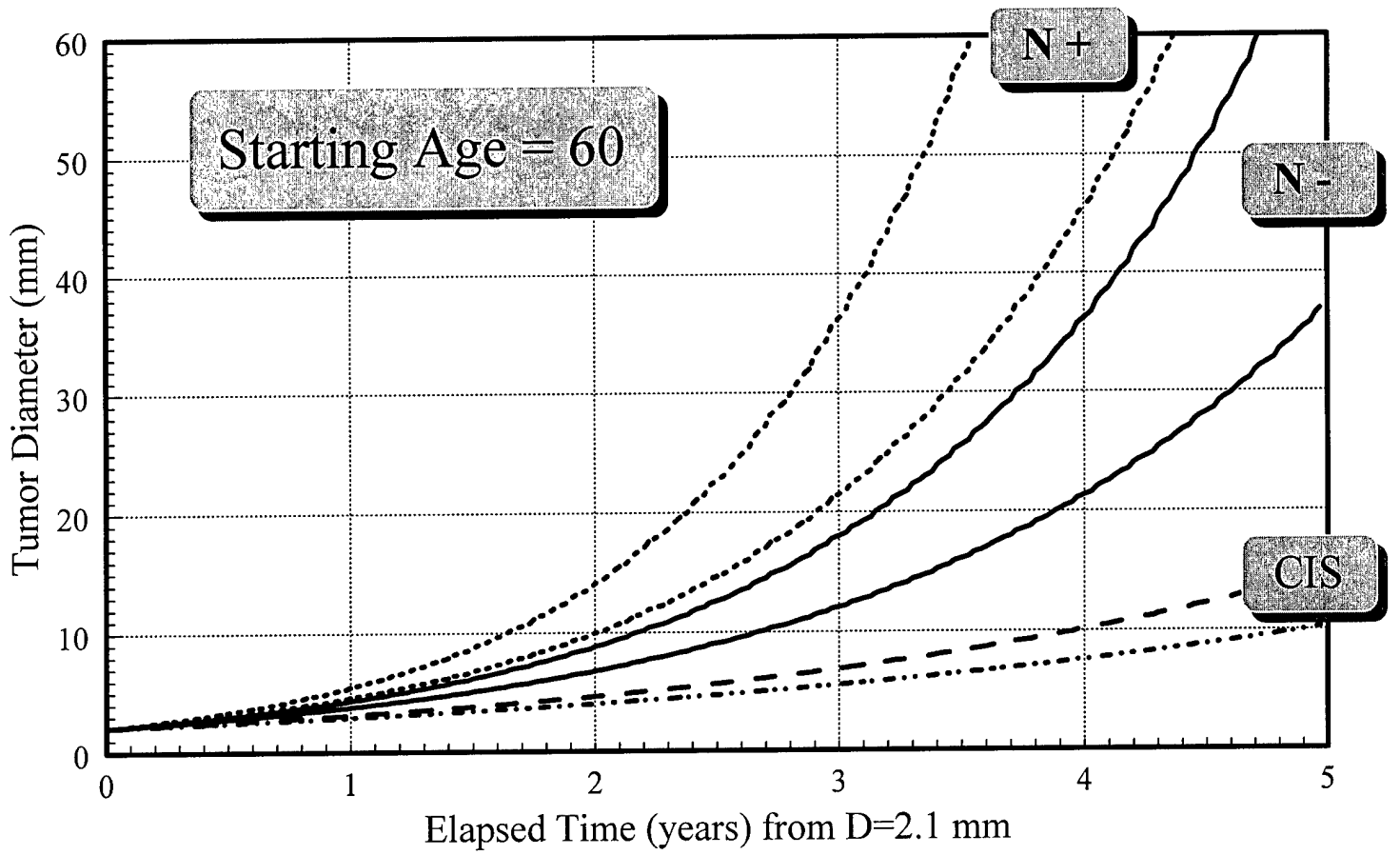


Figure 38

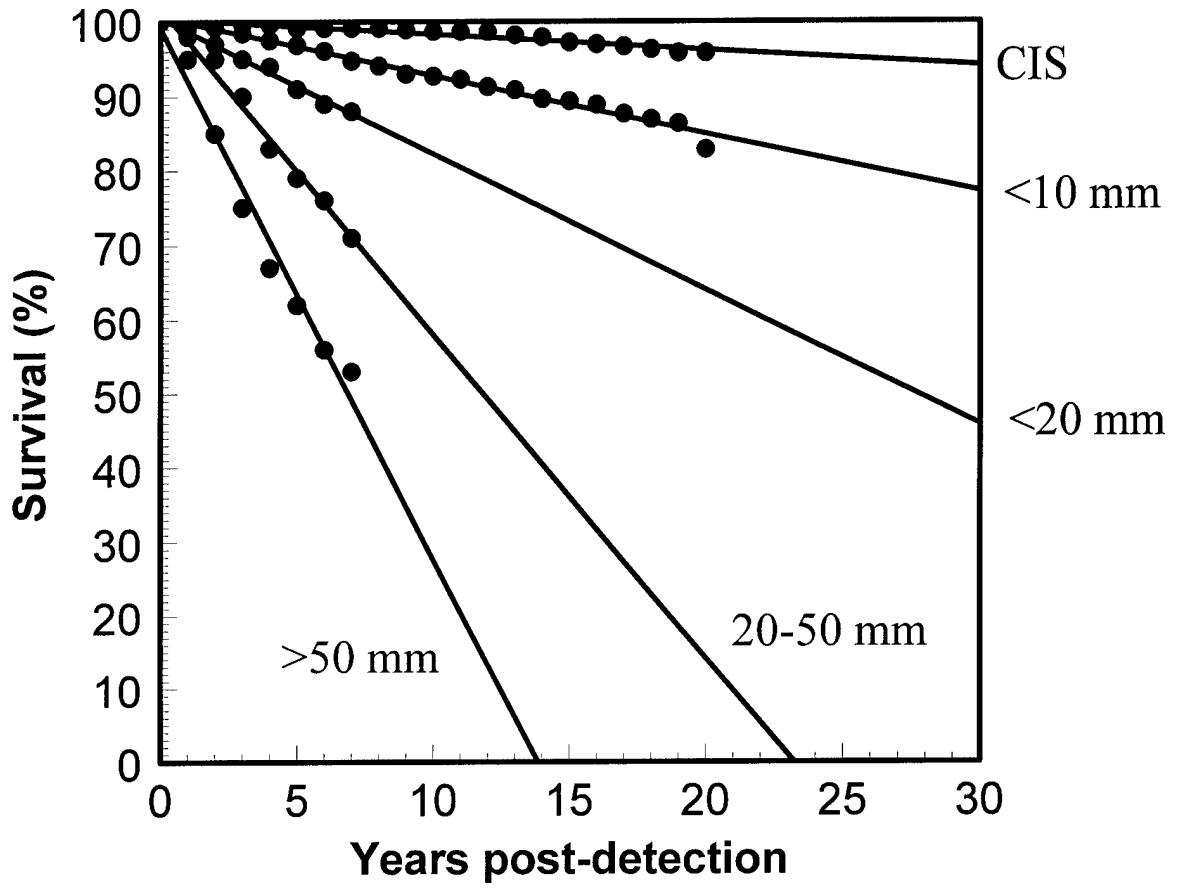


Figure 39

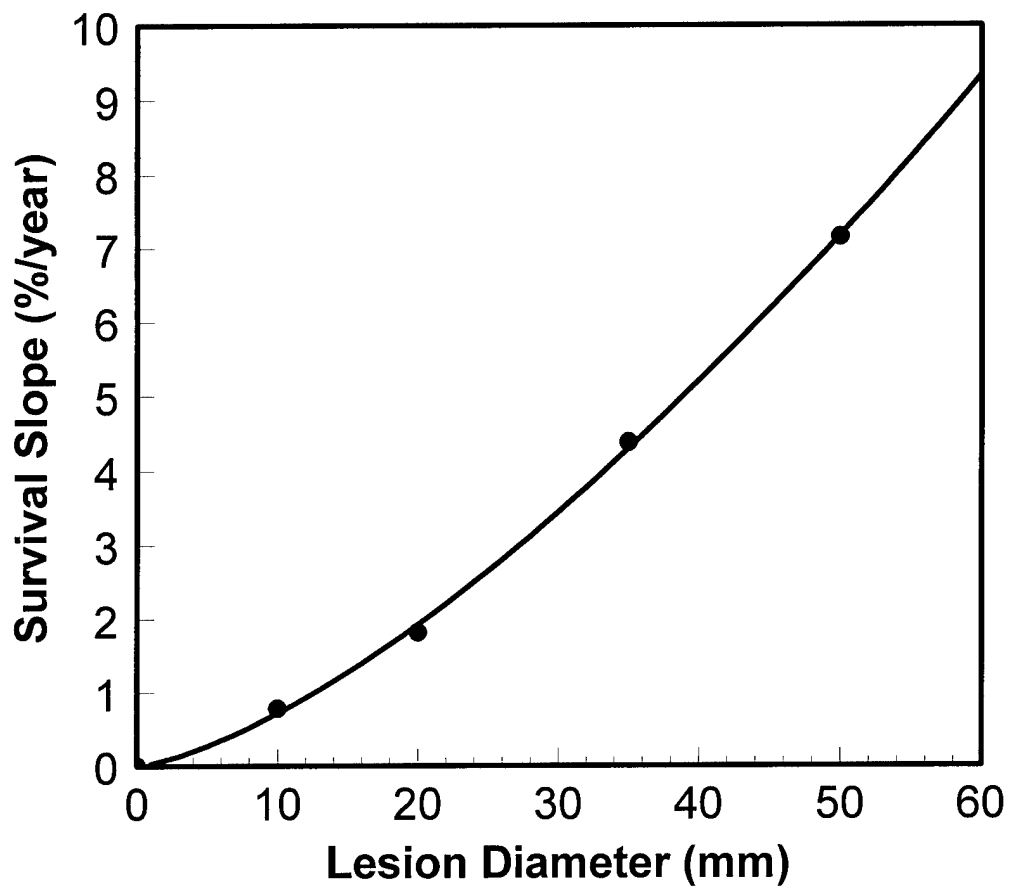


Figure 40

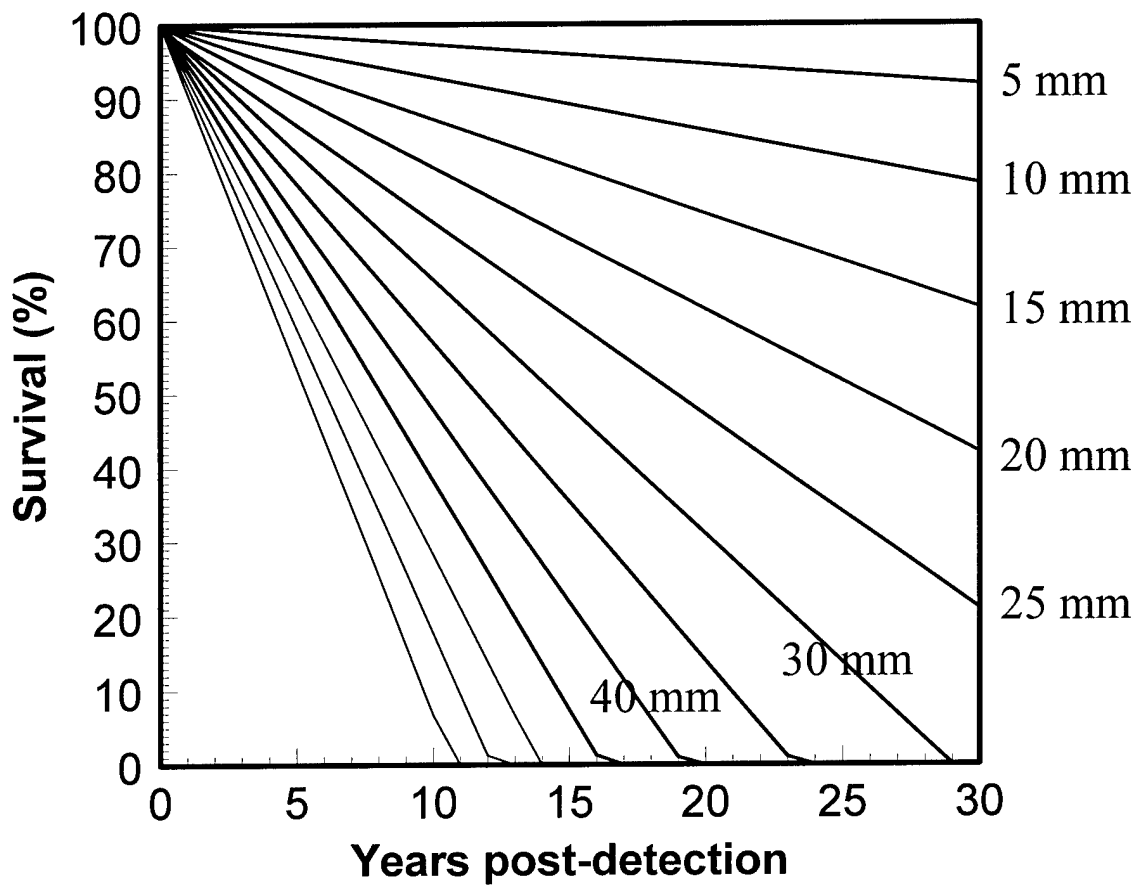


Figure 41

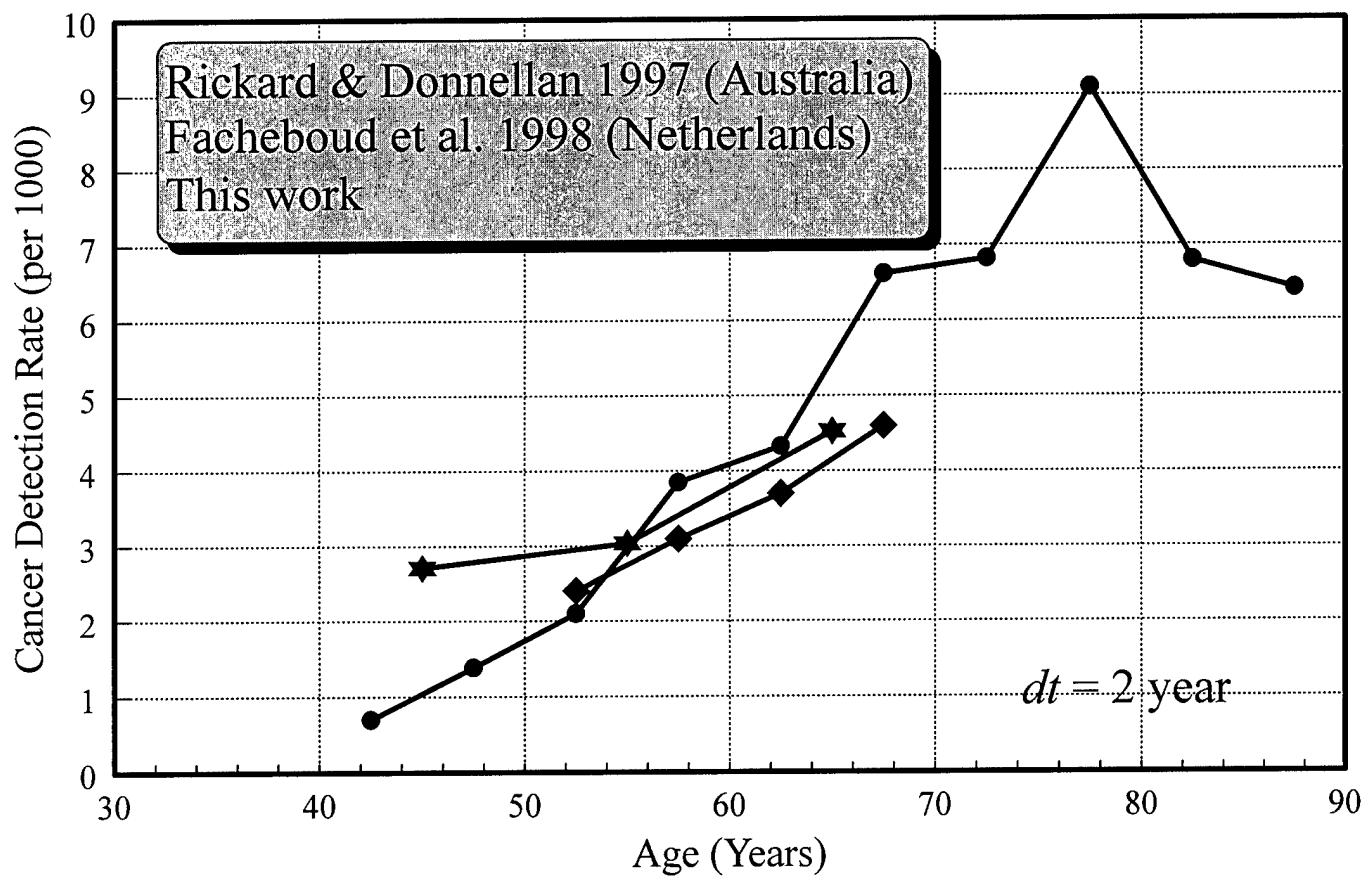


Figure 42

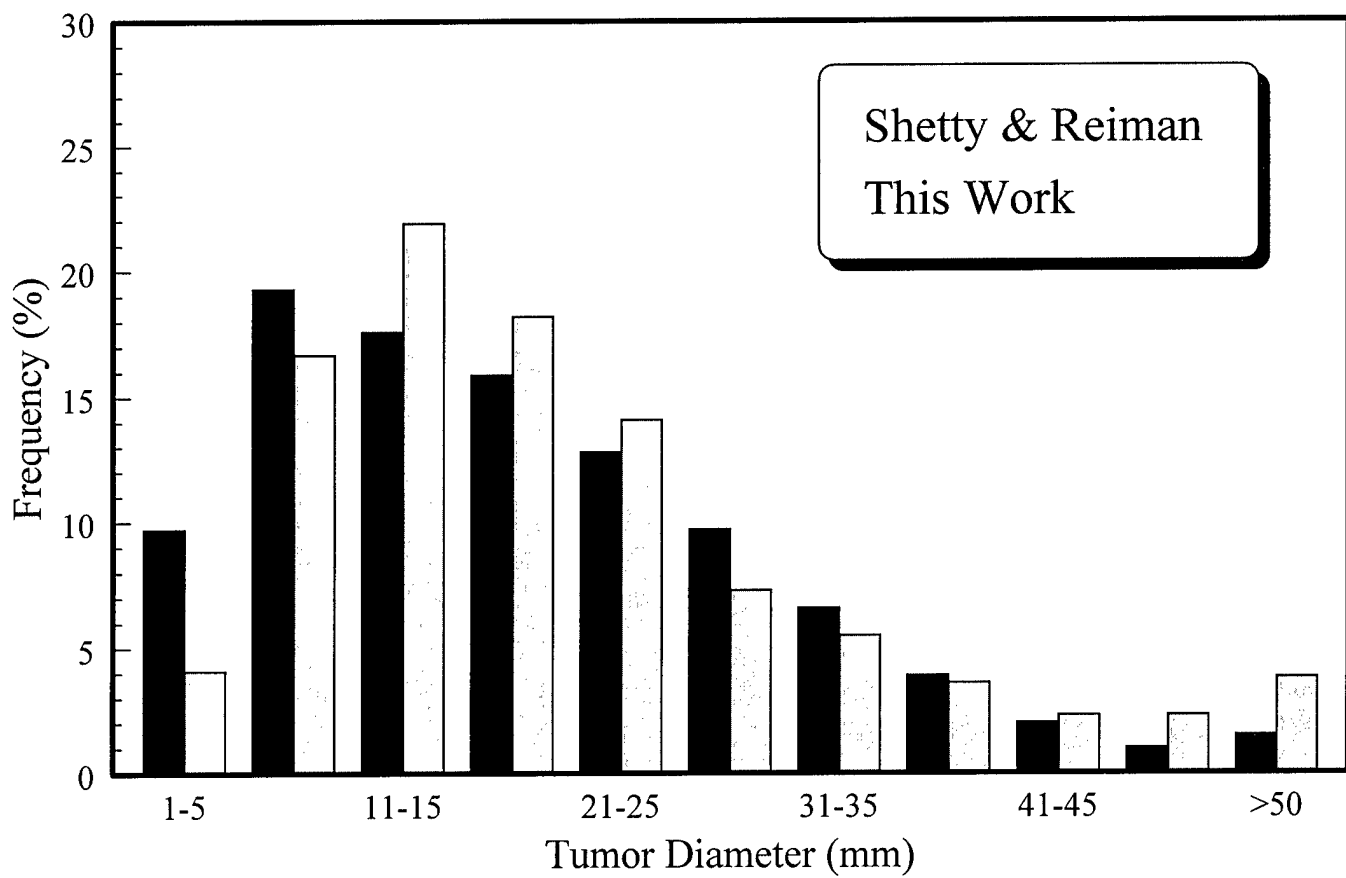


Figure 43

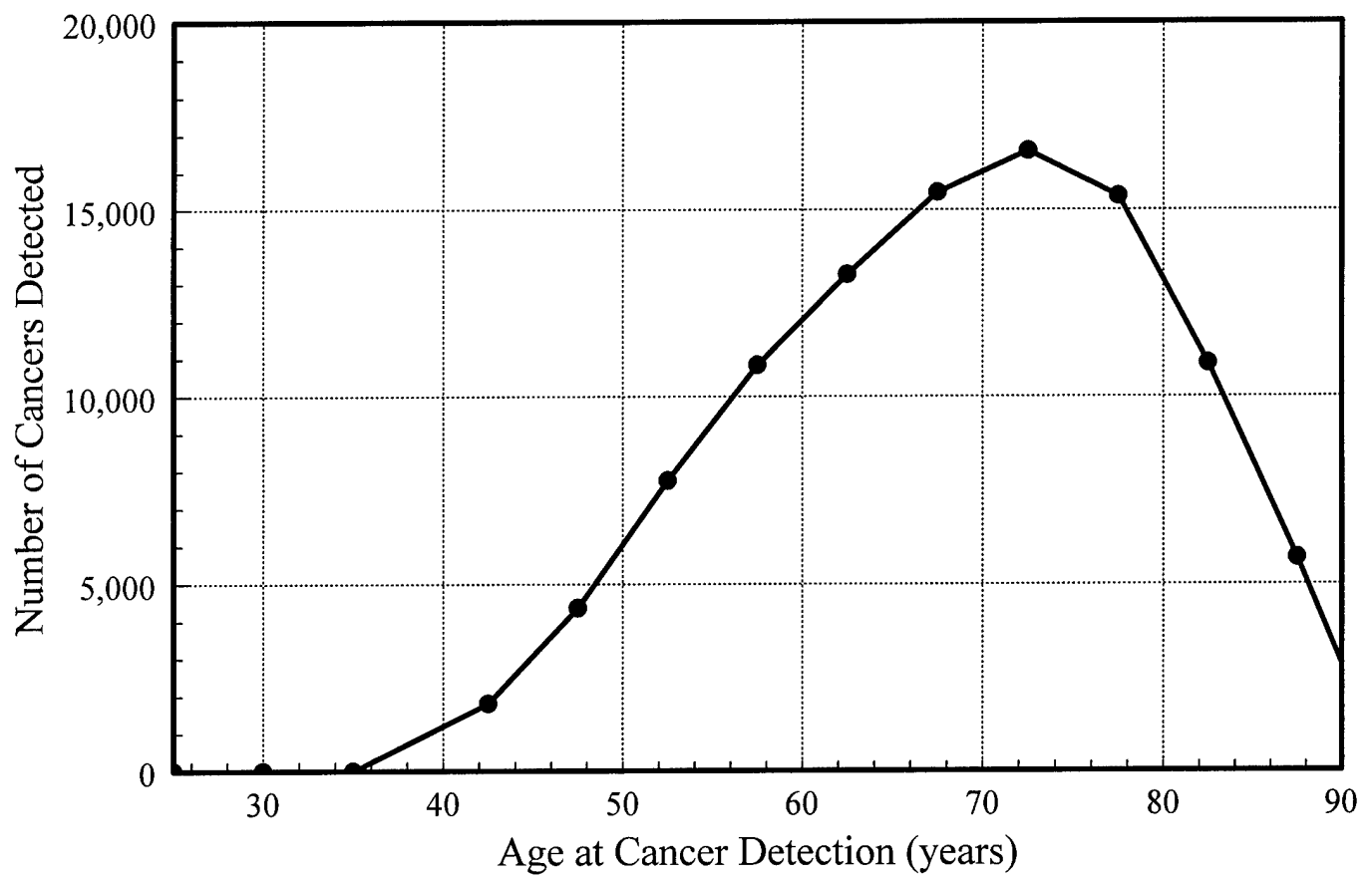


Figure 44

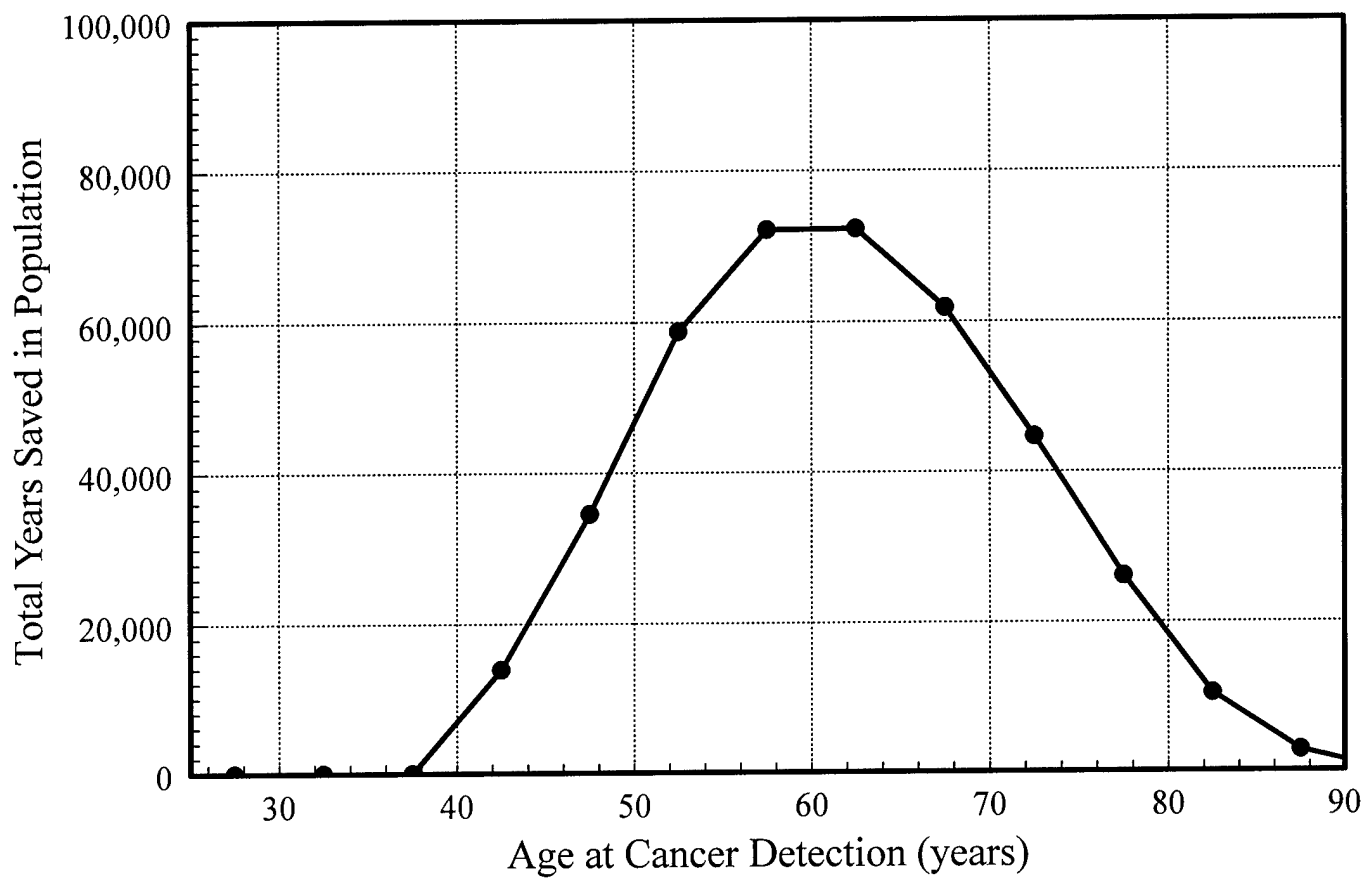


Figure 45

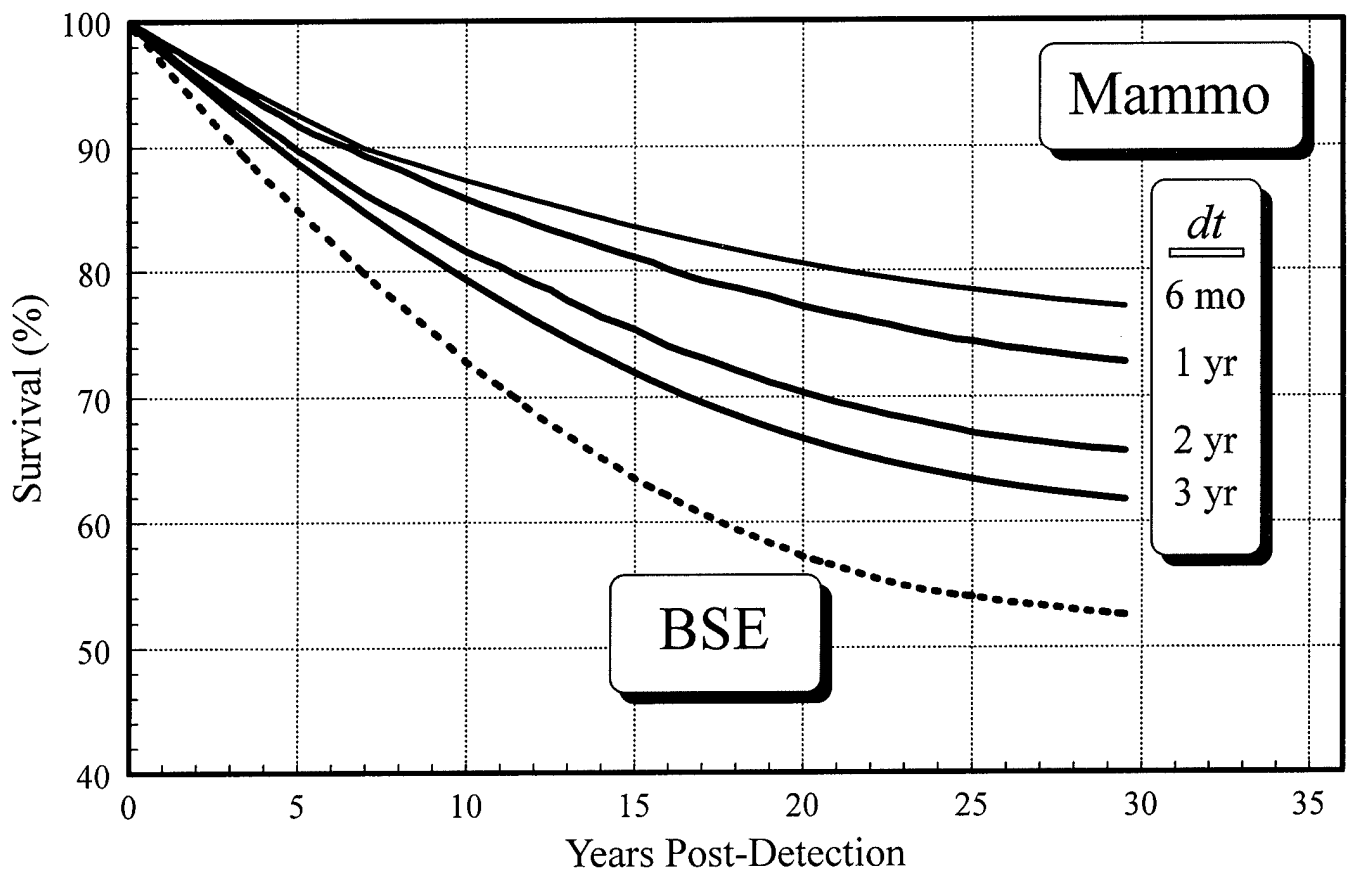


Figure 46

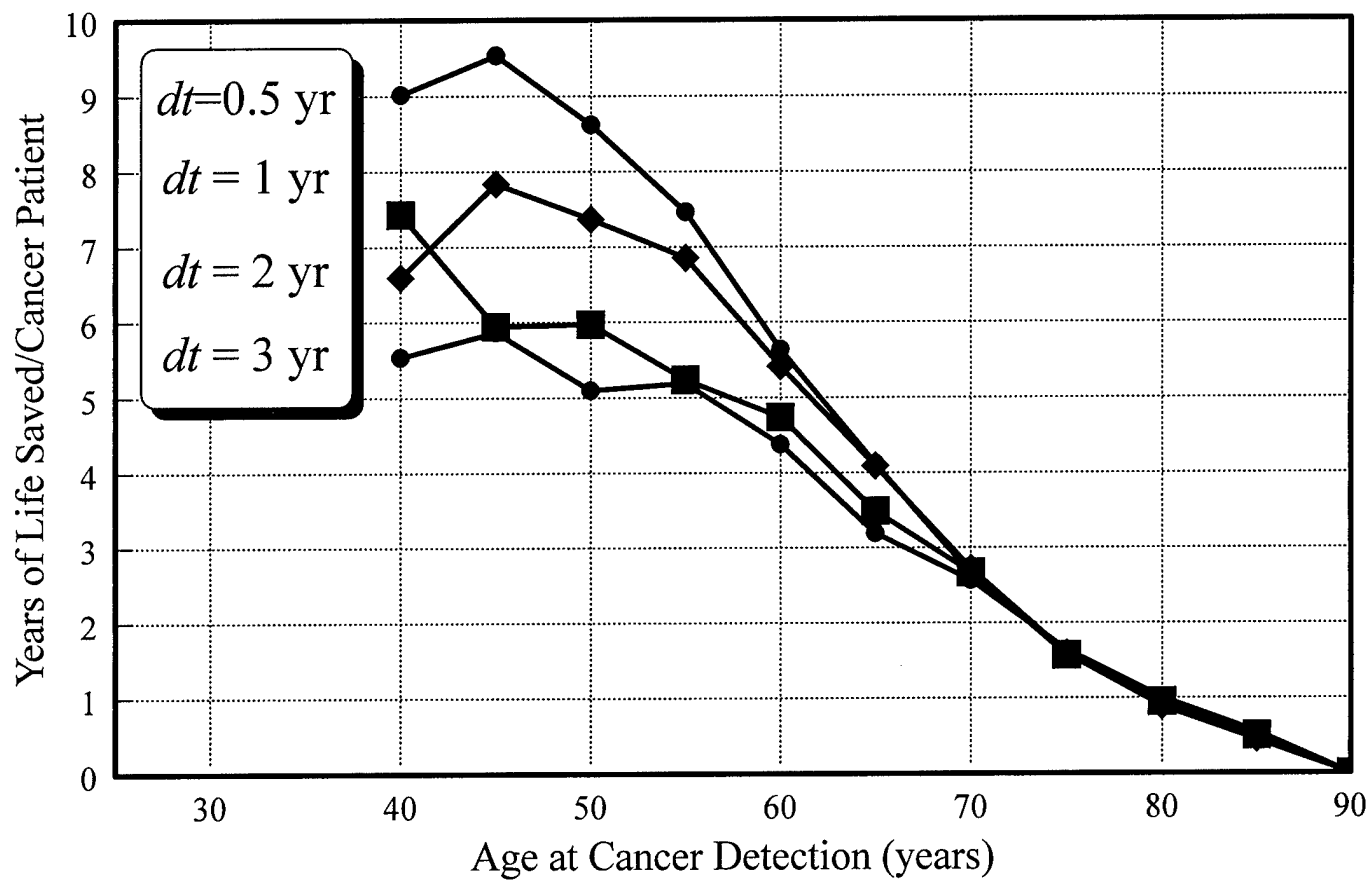


Figure 47

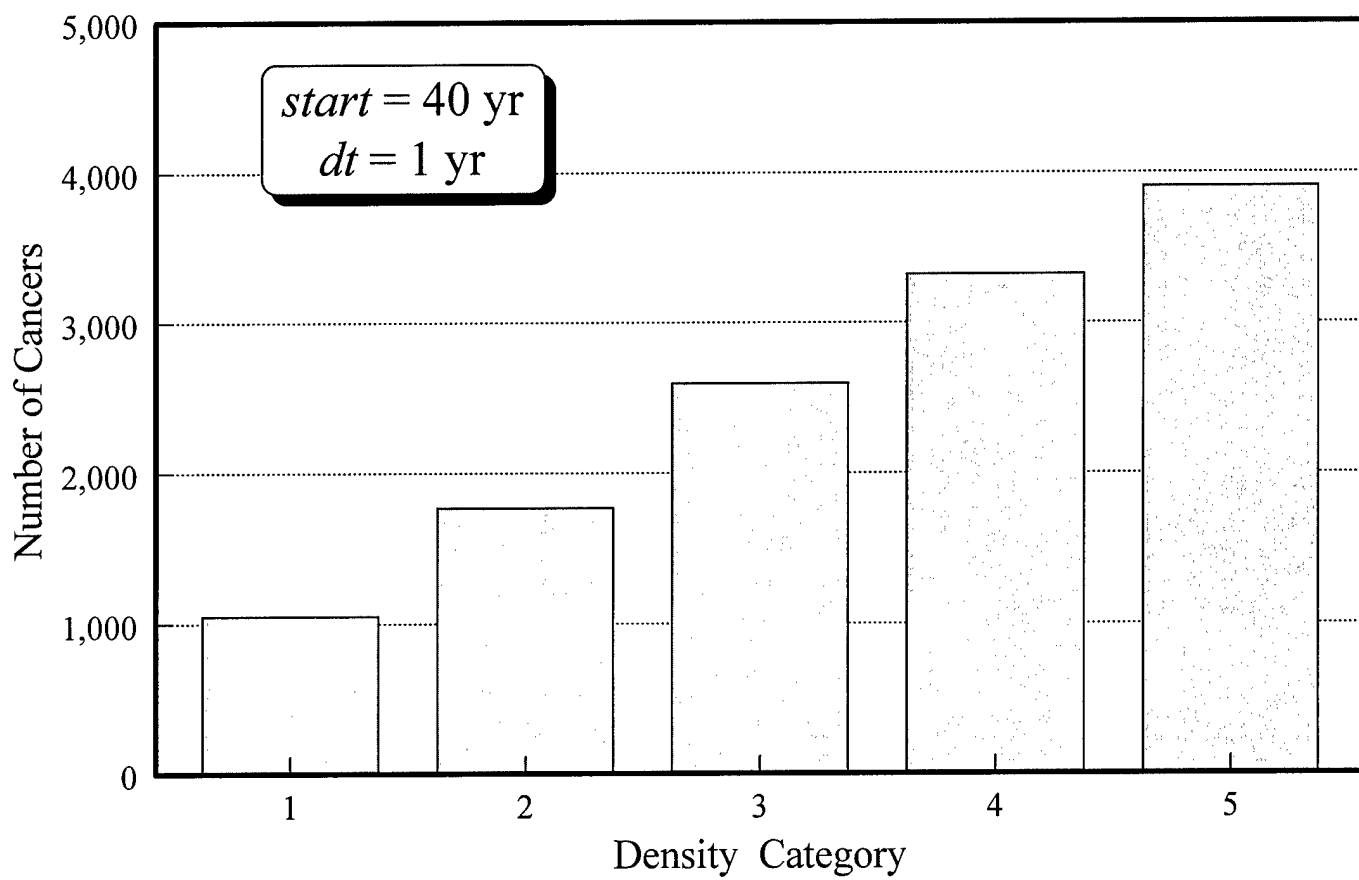


Figure 48

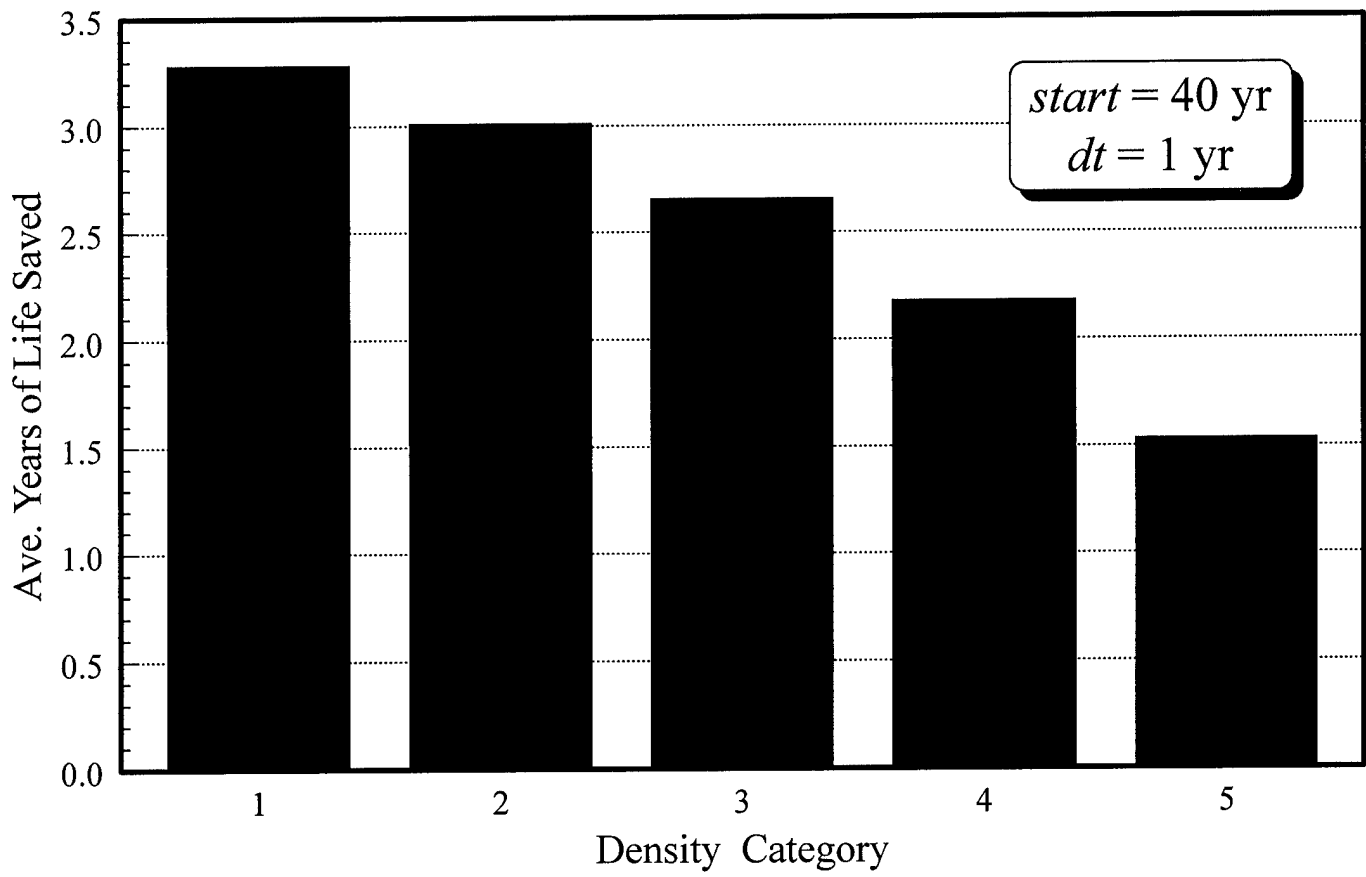


Figure 49

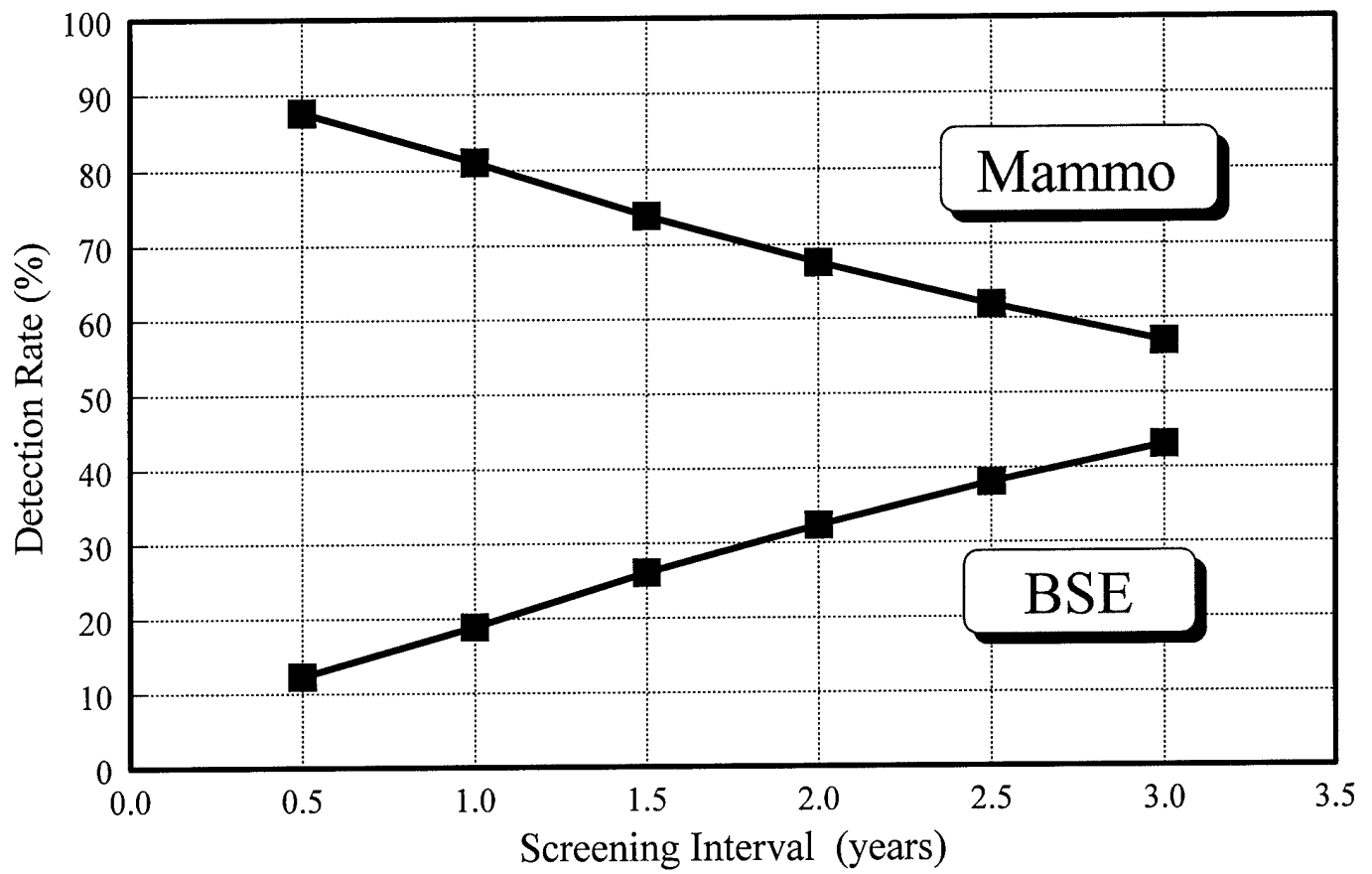


Figure 50

Page Blank